
α -TCAV: A Unified Framework for Testing with Concept Activation Vectors

Ekkehard Schnoor

Department of Computer Science
Aalto University
Espoo, Finland
ekkehard.schnoor@aalto.fi

Jawher Said

Department of Artificial Intelligence
Fraunhofer Heinrich Hertz Institute
Berlin, Germany
jawharsd@gmail.com

Malik Tiomoko

Huawei Noah's Ark Lab
Huawei Technologies
Paris, France
malik.tiomoko@huawei.com

Wojciech Samek

Department of Artificial Intelligence, Fraunhofer HHI
Department of EECS, Technische Universität Berlin
Berlin, Germany
wojciech.samek@hhi.fraunhofer.de

Alex Jung

Department of Computer Science
Aalto University
Espoo, Finland
alex.jung@aalto.fi

Abstract

Concept Activation Vectors (CAVs) are a fundamental tool for concept-based explainability in deep learning, yet their practical utility is limited by statistical instability. We analyze the stochastic nature of CAVs and the Testing with CAVs (TCAV) method, deriving the distributions of major CAV classes including Pattern-CAV, FastCAV, and ridge regression-based CAVs. We then identify a fundamental flaw in the standard TCAV score: its reliance on a discontinuous indicator function induces non-decaying variance in critical regimes. To address this, we introduce α -TCAV, a generalized framework that replaces the indicator with a parameterized smooth function, yielding a unified probabilistic formulation that subsumes both TCAV and Multi-TCAV. We characterize the induced distributions of sensitivity scores and different TCAV variants, showing that established state-of-the-art choices lack theoretical justification. We provide principled guidance on tuning the parameter in α -TCAV — either to imitate Multi-TCAV at substantially lower computational cost, or to obtain a calibrated Bayes-optimal probabilistic measure of a concept's influence. Finally, our analysis yields practical recommendations that challenge established routines: most notably, allocating the full sampling budget to a single CAV rather than splitting it across several.

1 Introduction

Explainable AI: from Feature Attribution to Concept-based Explanations. As deep neural networks have achieved impressive performance across diverse domains, understanding their decision-making has become critical, particularly in high-stakes applications such as medical diagnosis or autonomous driving; explanations of AI systems are also increasingly required by law. Traditional explainability methods focus on low-level feature attribution (*heatmaps*) via techniques such as

Saliency Maps [Simonyan et al., 2013], *Grad-CAM* [Selvaraju et al., 2017], and *Integrated Gradients* [Sundararajan et al., 2017], highlighting key input regions for specific predictions. Yet such pixel-level maps diverge from human reasoning: they show *where* the model looks, but not *what* concepts it has detected, while humans naturally reason in terms of patterns, shapes, and colors (in a vision context). This gap motivates concept-based explanation methods, which decode internal representations in terms of human-understandable concepts. Among these, *Concept Activation Vectors (CAVs)* [Kim et al., 2018] have emerged as one of the most popular and influential techniques, and are the topic of this article. Concept-based XAI has been highly active in recent years: [Ghorbani et al., 2019] introduced *Automatic Concept Extraction* for unsupervised concept discovery, while *Concept Relevance Propagation (CRP)* [Achtibat et al., 2023] generalizes the feature-based *Layer-wise Relevance Propagation (LRP)* [Bach et al., 2015]; [Aysel et al., 2025] establish a benchmarking framework with novel metrics quantifying alignment between model explanations and human-annotated ground truth. We refer the reader to the survey [Poeta et al., 2023] and references therein.

Concept Activation Vectors. [Kim et al., 2018] introduced CAVs and Testing with CAVs (TCAV), representing human-understandable concepts as directions in latent space. Using linear classifiers (e.g., SVMs) and directional derivatives, TCAV quantifies concept importance (e.g., *stripes* for *zebras*). Various CAV computation methods exist [Dreyer et al., 2024], including *PatternCAV* [Pahde et al., 2022, Haufe et al., 2014, Martin and Weller, 2019], and *FastCAV* [Schmalwasser et al., 2025] for improved efficiency. Originally framed within computer vision, CAVs have proven useful in other domains, e.g. for analyzing large policy-value networks in deep reinforcement learning such as chess [Pálsson and Björnsson, 2023] and *AlphaZero* [McGrath et al., 2022, Schut et al., 2023]. Several related extensions have appeared: *Concept Bottleneck Models (CBMs)* [Koh et al., 2020] enforce human-defined concepts as intermediate representations, enabling test-time interventions; [Yuksekgonul et al., 2022] extend this to post-hoc CBMs without retraining; *Visual-TCAV* [De Santis et al., 2024] bridges local saliency and global concept-based explanations via a generalization of *Integrated Gradients*; and *Concept Activation Regions (CARs)* [Crabbé and van der Schaar, 2022] represent concepts as regions rather than single vectors. For large language models, recent work focuses on *steering* and control: [Zhao et al., 2026] use sparse autoencoders to denoise concept vectors, [Zhang et al., 2025] steer behavior controlling toxicity (GCAV), [Sun et al., 2024] route activations through concept bottlenecks for text generation, and [Postmus and Abreu, 2024] employ *Conceptors* (ellipsoids). [Fel et al., 2023] provide a unified pipeline bridging automatic concept extraction and TCAV-based importance estimation, and *CoCoX* [Akula et al., 2020] uses TCAV to identify “fault-lines” (minimal concept-importance changes flipping a prediction) for conceptual and counterfactual explanations. A critical challenge in XAI is *stability*—producing consistent explanations for the same model and input across multiple applications [Sundararajan et al., 2017, Alvarez Melis and Jaakkola, 2018]. Inconsistent results erode user trust [Krishna et al., 2022], a problem especially prevalent in TCAV due to its stochastic nature.

Related Work. Despite intensive research efforts on CAVs over the last years, the theoretical and particularly the statistical properties of CAVs have only recently begun to receive attention. Most notably, [Wenkman and Garreau, 2025, Schnoor et al., 2026] have initiated a more rigorous investigation of the stochastic nature of CAVs, aiming to describe their distributions and variability. Our paper continues this line of work, and we will make extensive references to those two articles throughout. A key idea in our paper is the smooth approximation of the indicator function in an expression of the type $\mathbb{E}[\mathbb{1}_{X>0}]$ which can be traced back to fundamental results in probability theory, most prominently perhaps Lindeberg’s classical proof of the central limit theorem [Lindeberg, 1922] and its non-asymptotic variante, the *Berry-Esseen theorem* [Vershynin, 2026], or in applications of *Stein’s method* [Stein, 1972]. Surprisingly, to our best knowledge this classical technique has been missed out so far in the context of TCAV. On a higher level, our paper is similar to other efforts aiming for a theoretical analysis of XAI methods such as [Garreau and Luxburg, 2020, Garreau and von Luxburg, 2020] for *Local Interpretable Model Agnostic Explanation (LIME)* [Ribeiro et al., 2016], or [Chen et al., 2025] for *Shapley Values* [Shapley et al., 1953] and their adaption to XAI [Lundberg and Lee, 2017]. Despite the theoretical nature of our work, we also provide concrete practical recommendations, partly proposing fundamental changes, while partly we complementing previous advice for working with CAVs (multi-layer analysis, concept dependencies and entanglement) [Nicolson et al.].

Summary of Contributions. This paper provides a unified theoretical treatment of CAVs, significantly extending on previous recent work [Wenkmann and Garreau, 2025, Schnoor et al., 2026].

- We derive the distributions of *PatternCAV*, *FastCAV* and *Ridge Regression*, enabling to investigate their *classification accuracy* and induced distribution of *sensitivity scores*. We consider both classical ($d \ll n$) and modern ($d \asymp n$) regimes, for dimension d and sample size n ; see Sec. 2 and Sec. B.
- We introduce α -TCAV in the end of Sec. 3.2, a parameterized generalization of the TCAV score. We show that α -TCAV is a *unified framework* that recovers existing approaches while offering computational and statistical advantages that we investigate in detail in Sec. 4.
- In particular, we show analytically and empirically that α -TCAV can reduce variance by roughly 50% compared to Multi-TCAV in Sec. 3 (especially Sec. 4.2) Crucially, it achieves this stability at a fraction of the computational cost, effectively *breaking the traditional trade-off between compute and reliability*.
- In Sec. 4.2, we discuss the question of fine-tuning α , and argue that TCAV is *overconfident*, and the state-of-the-art method of Multi-TCAV is *underconfident*. We propose a Bayes-optimal choice of α , a *calibrated probability that the concept contributes to the model’s prediction*.
- We challenge the established practical recommendation of averaging multiple TCAV scores as it is statistically sub-optimal. We propose a drastically different *single-run strategy* allocating the entire sample budget into computing a single CAV. This is discussed in Sec. 4.4.

On a higher level, this paper helps to more rigorously address the following two questions, both of which can be answered by studying (random) inner products $\langle z, w_{\text{CAV}} \rangle$ for CAVs (random vectors) w_{CAV} , where the meaning of z differs (firstly, latent activations of (non-)concept data, and secondly, gradients of the predictions). Both are crucial questions in concept-based XAI, and underline the importance of a rigorous analysis of the distributional properties of CAVs studied in detail Sec. 2.

1. *Is a concept encoded in the neural network?* This can be answered by the *classification accuracy* of a CAV-based classifier separating the latent concept and non-concept distributions; see Sec. 5.
2. *Is a concept being used for the model’s prediction?* This is answered by *sensitivity scores* (inner products of the type $\langle z, w_{\text{CAV}} \rangle$; see (14)) and the *TCAV* method, addressed in detail in Sec. 3.1.

The main part of this paper is structured as follows. Sec. 2 introduces the theoretical background and presents several methods for computing CAVs, together with characterizations of their distributions; these in turn make the *variability* of CAVs—a measure of their stochastic nature—straightforward to study. Sec. 3 recalls sensitivity scores and the (Multi-)TCAV technique, and reinterprets them probabilistically as expectations of random variables. We identify shortcomings of the current approach and introduce α -TCAV as a remedy. Building on our findings, we develop a mathematical model associating each TCAV variant with a classical probability distribution, enabling a rigorous comparison of their properties. Building on these findings, Sec. 4 introduces a mathematical model that characterizes the various TCAV approaches in terms of corresponding classical probability distributions, from which their means and variances can be derived. While the most direct application of this model concerns the sensitivity scores, the framework enables a qualitative comparison of TCAV variants in the general case as well; we discuss the relations between the different approaches in detail and provide numerical simulations that show excellent agreement with our theoretical predictions. Sec. 4.2 then addresses the practical question of how to choose the sharpness parameter α together with the corresponding normalization of the sensitivity scores. In Sec. 4.3 we provide experiments on real data and conclude with practical recommendations in Sec. 4.4. Finally, while the main paper focuses on the TCAV technique — asking whether a concept is *used* for the model’s prediction — and in particular on our novel α -TCAV approach, Sec. 5 additionally provides a detailed treatment of the *classification accuracy*, i.e. whether a concept is *encoded* in the network at all. This is possible because both questions can be phrased in terms of (different) inner products of the form $\langle z, w_{\text{CAV}} \rangle$ that recur throughout the paper: interpreting w_{CAV} as a random vector and studying its distribution (cf. Sec. 2 and Sec. B) lets us address both topic. More technical details are provided in the appendix.

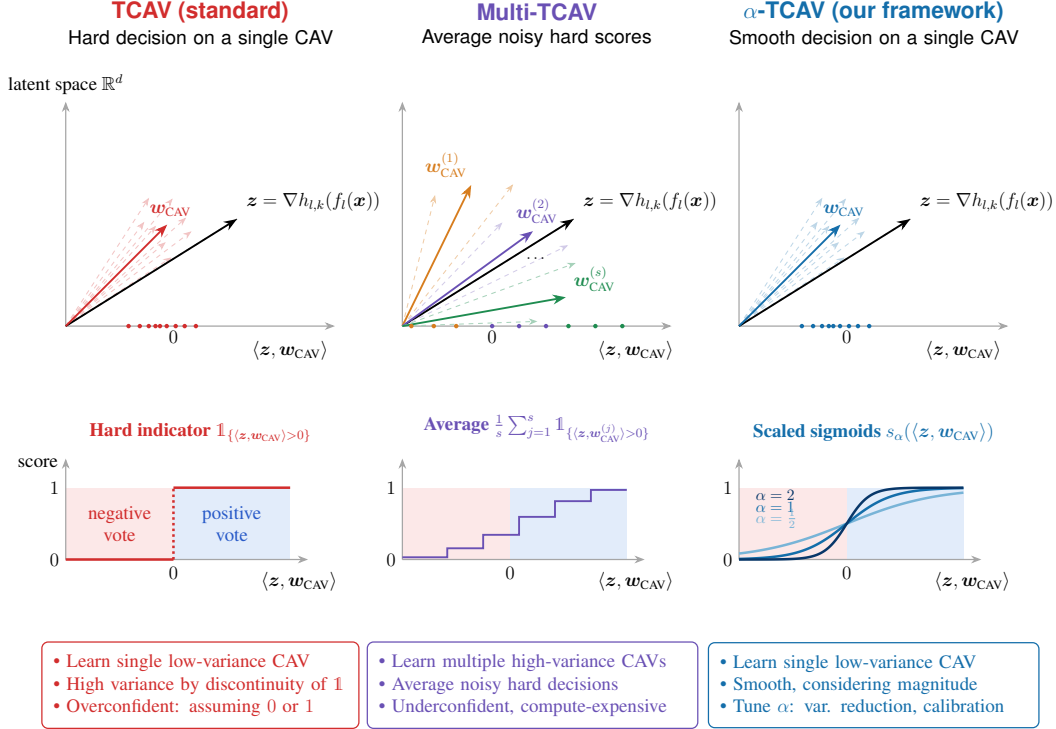


Figure 1: TCAV, Multi-TCAV and α -TCAV (our proposed framework). For input \mathbf{x} , the gradient $\mathbf{z} = \nabla h_{l,k}(f_l(\mathbf{x}))$ of logit k at layer l is projected onto a (random) CAV $\mathbf{w}_{\text{CAV}} \in \mathbb{R}^d$ (at layer l), yielding the sensitivity scores $\langle \mathbf{z}, \mathbf{w}_{\text{CAV}} \rangle$. Next, different TCAV scores are computed, where **TCAV** (left) uses a hard indicator on a single CAV, potentially leading to large (or even non-vanishing) variance. **Multi-TCAV** (middle) averages several such indicators using several (more noisy) CAVs $\mathbf{w}_{\text{CAV}}^{(j)}$. Finally, **α -TCAV (ours)** (right) replaces the discontinuous indicator function with a smooth sigmoid family s_α whose temperature α controls the steepness, using the full budget to learn a single CAV. Note that we consider two notions of *variance*: firstly, for a (random) CAV \mathbf{w}_{CAV} in the sense of Definition 2.5; secondly, for the sensitivity scores $\langle \mathbf{z}, \mathbf{w}_{\text{CAV}} \rangle$ in the usual sense of a real-valued random variable.

2 Concept Activation Vectors

Neural Network Architecture and CAVs. Consider a (pretrained) L -layer neural network for a K -class classification task, represented by the composition $f_l \circ h_l$. Here, $f_l : \mathbb{R}^{d_0} \rightarrow \mathbb{R}^{d_l}$ maps inputs to layer l activations, and $h_l : \mathbb{R}^{d_l} \rightarrow \mathbb{R}^{d_L}$ maps these to the output (where $d_L = K$). We denote the mapping to the k -th class logit as $h_{l,k} : \mathbb{R}^{d_l} \rightarrow \mathbb{R}$. Concept Activation Vectors (CAVs) are derived by training a linear classifier to separate activations of a concept C from non-concept examples. The resulting CAV, $\mathbf{v}_C \in \mathbb{R}^{d_l}$, is the vector orthogonal to the separating hyperplane pointing toward the concept region (we also write \mathbf{w}_{CAV} to denote generic CAVs). We consider a general binary setup with classes \mathcal{C}_ℓ for $\ell \in \{1, 2\}$, where \mathcal{C}_1 (label -1) represents non-concept data and \mathcal{C}_2 (label 1) represents the concept class; labels are thus written as $(-1)^\ell$. We assume both classes consist of i.i.d. samples from unknown distributions, where N denotes the effective number of random samples (see Rem. 2.1). Finally, \mathcal{X}_k the dataset for class k for the neural network classification sampled from a distribution \mathcal{D}_k . We interpret CAVs as random vectors with distribution \mathcal{D}_{CAV} . $\mathbb{1}_A$ the indicator function of set A . We adopt a compact generic notation for the binary classification problem using a data matrix $\mathbf{X} = [\mathbf{x}_1, \dots, \mathbf{x}_n] \in \mathbb{R}^{d \times n}$ with labels $\mathbf{y} \in \{-1, 1\}^n$. Let $\mathbf{X} = [\mathbf{X}^{(1)}, \mathbf{X}^{(2)}]$, where $\mathbf{X}^{(\ell)} \in \mathbb{R}^{d \times n_\ell}$ gathers n_ℓ vectors for class \mathcal{C}_ℓ . The total size is $n = n_1 + n_2$, with class probabilities $c_\ell = n_\ell/n$. Each class is characterized by a mean $\boldsymbol{\mu}_\ell \in \mathbb{R}^d$, covariance $\boldsymbol{\Sigma}_\ell \in \mathbb{R}^{d \times d}$, and generalized covariance $\mathbf{C}_\ell = \boldsymbol{\Sigma}_\ell + \boldsymbol{\mu}_\ell \boldsymbol{\mu}_\ell^\top$. We write $\mathbf{x} \in \mathcal{C}_\ell$ to indicate \mathbf{x} follows the distribution of class \mathcal{C}_ℓ .

Remark 2.1 (Sample Sizes and Asymptotics). In the CAV setting, a *balanced* regime ($n_1 = n_2$) is plausible since, given n_2 concept examples, matching n_1 non-concept examples is typically cheap.

As it is cheap and CAV training may benefit from more of it, one may also consider n_2 fixed and $n_1 \rightarrow \infty$ —the imbalanced setting (based on [Owen, 2007]) for logistic-regression CAVs studied in [Wenkman and Garreau, 2025]; unlike this paper which treats concept data as deterministic (all CAV randomness stems from non-concept data), we consider CAV distributions induced by *both* concept and non-concept data. We write N for the *effective (random) sample size*, i.e., $N = n_1 + n_2$ in the general case, and $N = n_2$ in the setting of [Wenkman and Garreau, 2025]. This uniformly describes variance decay in N without distinguishing between the two data sources. Despite its appeal, the imbalanced setting also poses difficulties—e.g., the trivial majority-class classifier achieves asymptotic zero error; see [He and Garcia, 2009] for a survey and [Buda et al., 2018] for a systematic neural-network study.

Methods for CAV Computations. We discuss several methods to compute CAVs and characterize their distributions. While formulated as general binary classification problems, recall that for an application to CAVs the data matrix \mathbf{X} contains the collection of the latent representations of the (*non-*)*concept* input examples. One approach to obtaining the CAV is by solving the classical *ridge regression* problem (A.20), an ℓ_2 -regularized least-squares problem. The explicit solution - if it exists - is given in (A.21) in Sec. B.2 in the appendix, which provides more mathematical details. In particular, to describe how the data distribution over \mathbf{X} induces a distribution over $\mathbf{w}_{\text{ridge}}$, we follow the framework in [Tiomoko, 2021, Chapter 2.3]; see also [Cherkaoui et al.]. The *PatternCAV* [Pahde et al., 2022, Martin and Weller, 2019] is based on an objective proposed in [Haufe et al., 2014], aiming at modeling the data as a function of the labels. As shown in [Pahde et al., 2022, Appendix B.3], for a binary classification problem such as for CAVs, the *PatternCAV* $\mathbf{w}_{\text{pat}} \in \mathbb{R}^d$ is given by the difference of the empirical class means (pointing towards the concept region),

$$\mathbf{w}_{\text{pat}} = \frac{1}{n_2} \sum_{i=1}^{n_2} \mathbf{x}_i^{(2)} - \frac{1}{n_1} \sum_{i=1}^{n_1} \mathbf{x}_i^{(1)} = \hat{\boldsymbol{\mu}}_2 - \hat{\boldsymbol{\mu}}_1. \quad (1)$$

the *FastCAV* [Schmalwasser et al., 2025] are another efficient alternative to optimization-based classifiers. Aggregating all (non-)concept activations, the joint empirical mean $\hat{\boldsymbol{\mu}}_{1,2}$ is

$$\hat{\boldsymbol{\mu}}_{1,2} = \frac{1}{n_1 + n_2} \sum_{\ell=1}^2 \sum_{i=1}^{n_i} \mathbf{x}_i^{(\ell)} \in \mathbb{R}^d. \quad (2)$$

The *FastCAV*, denoted as \mathbf{w}_{fast} , is defined as the vector originating from this global centroid $\hat{\boldsymbol{\mu}}_{1,2}$ and pointing toward the mean $\boldsymbol{\mu}_2$ of the concept class \mathcal{C}_2 . Formally, it is given as

$$\mathbf{w}_{\text{fast}} = \frac{1}{n_2} \sum_{i=1}^{n_2} \left(\mathbf{x}_i^{(2)} - \hat{\boldsymbol{\mu}}_{1,2} \right) = \hat{\boldsymbol{\mu}}_2 - \hat{\boldsymbol{\mu}}_{1,2} \in \mathbb{R}^d, \quad (3)$$

where $\hat{\boldsymbol{\mu}}_2$ represents the empirical mean of the concept class.

Characterizing CAV Distributions. We characterize the distribution of \mathbf{w}_{fast} , \mathbf{w}_{pat} in terms of the data distribution, generalizing [Schnoor et al., 2026, Prop. 1]; the proof is given in the appendix.

Proposition 2.2 (Distribution of \mathbf{w}_{fast} and \mathbf{w}_{pat}). *Mean and covariance of \mathbf{w}_{fast} and \mathbf{w}_{pat} can be expressed in terms of the data distribution (class-specific mean $\boldsymbol{\mu}_\ell$ and covariance $\boldsymbol{\Sigma}_\ell$, $\ell = 1, 2$) as*

$$\mathbb{E}[\mathbf{w}_{\text{pat}}] = \boldsymbol{\mu}_2 - \boldsymbol{\mu}_1 \in \mathbb{R}^d, \quad (4)$$

$$\text{Cov}(\mathbf{w}_{\text{pat}}) = \frac{1}{n_1} \boldsymbol{\Sigma}_1 + \frac{1}{n_2} \boldsymbol{\Sigma}_2 \in \mathbb{R}^{d \times d}. \quad (5)$$

The *PatternCAV* \mathbf{w}_{pat} is a scaled version of the *FastCAV* \mathbf{w}_{fast} ; for general $n_1, n_2 \in \mathbb{N}$ it holds that

$$\mathbf{w}_{\text{fast}} = \frac{n_1}{n_1 + n_2} \mathbf{w}_{\text{pat}}. \quad (6)$$

Therefore, mean and covariance of \mathbf{w}_{fast} are given as appropriately scaled versions of 4 and (5),

$$\mathbb{E}[\mathbf{w}_{\text{fast}}] = \frac{n_1}{n_1 + n_2} (\boldsymbol{\mu}_2 - \boldsymbol{\mu}_1) \in \mathbb{R}^d, \quad (7)$$

$$\text{Cov}(\mathbf{w}_{\text{fast}}) = \left(\frac{n_1}{n_1 + n_2} \right)^2 \left(\frac{1}{n_1} \boldsymbol{\Sigma}_1 + \frac{1}{n_2} \boldsymbol{\Sigma}_2 \right). \quad (8)$$

The next corollary follows immediately as a special case by assuming classes of equal size.

Corollary 2.3 (Balanced case). *In the case of $n_1 = n_2$, the relation (6) simplifies to $\mathbf{w}_{fast} = \frac{1}{2}\mathbf{w}_{pat}$, when (7) and (8) now become (note that n_1, n_2 in the covariance term can be used interchangeably)*

$$\mathbb{E}[\mathbf{w}_{fast}] = \frac{\boldsymbol{\mu}_2 - \boldsymbol{\mu}_1}{2} \in \mathbb{R}^d, \quad \text{Cov}(\mathbf{w}_{fast}) = \frac{1}{4n_1}\boldsymbol{\Sigma}_1 + \frac{1}{4n_2}\boldsymbol{\Sigma}_2 \in \mathbb{R}^{d \times d}. \quad (9)$$

Further, [Schnoor et al., 2026, Remark 1] pointed out a close relation of \mathbf{w}_{fast} (and, in the balanced case as in Corollary (2.3), also \mathbf{w}_{fast}) to the case of ridge regression \mathbf{w}_{ridge} — see (A.20) — with a large regularization parameter $\lambda > 0$. Finally, let us also consider the case of a fixed number of *concept* samples n_2 , while taking the limit $n_1 \rightarrow \infty$ for the *non-concept* data, which is the scenario studied in [Wenkman and Garreau, 2025]. Interestingly, in this setup limiting mean and covariance \mathbf{w}_{pat} and \mathbf{w}_{fast} coincide, showing a similar behavior to the balanced case $n_1 = n_2$.

Corollary 2.4 (Asymmetrically asymptotic: $n_1 \rightarrow \infty$). *For a fixed number n_2 of concept samples, and $n_1 \rightarrow \infty$ for the number of non-concept samples, we obtain for \mathbf{w}_{pat} and \mathbf{w}_{fast} that*

$$\mathbb{E}[\mathbf{w}_{pat}] = \boldsymbol{\mu}_2 - \boldsymbol{\mu}_1 \in \mathbb{R}^d, \quad \text{Cov}(\mathbf{w}_{pat}) \rightarrow \frac{1}{n_2}\boldsymbol{\Sigma}_2 \in \mathbb{R}^{d \times d}, \quad (10)$$

$$\mathbb{E}[\mathbf{w}_{fast}] \rightarrow \boldsymbol{\mu}_2 - \boldsymbol{\mu}_1 \in \mathbb{R}^d, \quad \text{Cov}(\mathbf{w}_{fast}) \rightarrow \frac{1}{n_2}\boldsymbol{\Sigma}_2 \in \mathbb{R}^{d \times d}. \quad (11)$$

Here, by \rightarrow we denote convergence w.r.t. to any vector or matrix norm on \mathbb{R}^d or $\mathbb{R}^{d \times d}$, respectively.

Informally, as $n_1 \rightarrow \infty$, randomness w.r.t. to the *non-concept* data vanishes, and the covariance matrices in (11) depend solely on the variability of the *concept* data. A corresponding result for the ridge regression (A.21) is given in the supplementary material in Theorem B.6.

Variability of CAVs. A measure to quantify the stochastic nature of CAVs is their (total) variance, the sum of the variances of the individual entries, or equivalently, the trace of their covariance. Let us introduce this formally, as already proposed before in [Wenkman and Garreau, 2025, Definition 1].

Definition 2.5. We define the variance of a CAV $\mathbf{w}_{CAV} \in \mathbb{R}^d$ (assuming its covariance exists) as

$$\text{Var}(\mathbf{w}_{CAV}) := \text{Tr}(\text{Cov}(\mathbf{w}_{CAV})). \quad (12)$$

Of course, this definition is possible for any random vector with existing covariance; this definition only highlights its use in the context of CAVs. It has been shown that $\text{Var}(\mathbf{w}_{pat}) = \mathcal{O}(n_1^{-1})$ both for the *PatternCAV* (there, referred to as the *Difference of Means* [Martin and Weller, 2019]) and the logistic-regression CAV (under mild assumption) in [Wenkman and Garreau, 2025, Thm. 2 & Cor. 4]

Thanks to the expressions for the covariances of several CAVs provided above, we are immediately able to recover the variance behavior. For instance, assuming the *concept* data to be fixed (deterministic) as in [Wenkman and Garreau, 2025], we have $\boldsymbol{\Sigma}_2 = \mathbf{0}$; then, for the covariance of the *PatternCAV* as in (5), and by Definition (2.5), we find that

$$\text{Tr}(\text{Cov}(\mathbf{w}_{pat})) = \frac{1}{n_1} \text{Tr}(\boldsymbol{\Sigma}_1) = \mathcal{O}(n_1^{-1}), \quad (13)$$

simply treating $\text{Tr}(\boldsymbol{\Sigma}_1)$ as a constant. In this way, we can recover the corresponding aforementioned result from [Wenkman and Garreau, 2025] as a consequence of more generally describing the distribution of *PatternCAV*; similar results can be derived for *FastCAV* (even with smaller constants). By the conventions in Remark 2.1, this would correspond to the case $N = n_1$. In case of $N = n_1 + n_2$ (concept and non-concept data are both non-deterministic), we obtain similarly, as $n_\ell / (n_1 + n_2) = c_\ell$, i.e., $1/n_\ell = c_\ell / (n_1 + n_2)$ for $\ell = 1, 2$, then $\text{Tr}(\text{Cov}(\mathbf{w}_{pat})) \leq (\text{Tr}(\boldsymbol{\Sigma}_1)/c_1 + \text{Tr}(\boldsymbol{\Sigma}_2)/c_2) / (n_1 + n_2)$, i.e., $\text{Tr}(\text{Cov}(\mathbf{w}_{pat})) = \mathcal{O}(1/N)$. This variance decay seems to hold quite universally for different realistic approaches to compute CAVs, as already suggested by [Wenkman and Garreau, 2025], and we will make use of it for our investigations in this paper. For the ridge regression, we refer to B.2.

3 Testing with Concept Activation Vectors

3.1 Sensitivity Scores, TCAV and Multi-TCAV

To quantify the contribution of a concept C to the prediction of class k for a single input $\mathbf{x} \in \mathbb{R}^{d_0}$, [Kim et al., 2018] proposed the following sensitivity score $S_{C,k,l}(\mathbf{x})$, based on a CAV \mathbf{v}_C^l at layer l ,

$$S_{C,k,l}(\mathbf{x}) = \lim_{h \rightarrow 0} \frac{h_{l,k}(f_l(\mathbf{x}) + h \cdot \mathbf{v}_C^l) - h_{l,k}(f_l(\mathbf{x}))}{h} = \langle \nabla h_{l,k}(f_l(\mathbf{x})), \mathbf{v}_C^l \rangle. \quad (14)$$

The equivalence of the directional derivative of $h_{l,k}$ along \mathbf{v}_C^l to the inner product holds under appropriate smoothness assumptions, which we assume to hold thereafter. For the remainder of this work, we primarily utilize the inner product formulation for its computational convenience, or simply use the generic expression $S_{C,k,l}(\mathbf{x})$ itself. To emphasize the dependence on the (random) CAV, we may also write $S_{C,k,l}(\mathbf{x}, \mathbf{v}_C^l)$ or $S_{C,k,l}(\mathbf{x}, \mathbf{w}_{\text{CAV}})$. While $S_{C,k,l}(\mathbf{x})$ considers only a single input \mathbf{x} , [Kim et al., 2018] also introduced the $\text{TCAV}_{Q_{C,k,l}}$ score to measure the overall importance of a concept C to class \mathcal{X}_k , dubbed *Testing with Concept Activation Vectors (TCAV)*. It quantifies the fraction of inputs $\mathbf{x} \in \mathcal{X}_k$ for which the sensitivity score is positive (for a given CAV realization),

$$\text{TCAV}_{Q_{C,k,l}} = \frac{|\{\mathbf{x} \in \mathcal{X}_k : S_{C,k,l}(\mathbf{x}) > 0\}|}{|\mathcal{X}_k|} \quad (15)$$

$$= \frac{1}{|\mathcal{X}_k|} \sum_{\mathbf{x} \in \mathcal{X}_k} \mathbb{1}_{\{S_{C,k,l}(\mathbf{x}) > 0\}}, \quad (16)$$

so that $\text{TCAV}_{Q_{C,k,l}} \in [0, 1]$. We comment on the practical interpretation of this quantity in Remark 3.1 below. The original formulation (15) was provided in Kim et al. [2018] and seems to be used exclusively until today in the literature. However, the equivalent reformulation (16) as an average of indicator functions turns out to be insightful: despite being a simple rephrasing, it highlights the mean-like character of this quantity. This will inspire us to formally define this approach in the language of probability theory as an expectation of a random variable containing the indicator function; we will then take the opportunity to propose a refined version employing a smooth variant below. Notably, both $S_{C,k,l}(\mathbf{x})$ and $\text{TCAV}_{Q_{C,k,l}}$ depend on the specific choice of the CAV \mathbf{w}_{CAV} , which in turn - even for fixed (*non-*)concept examples and a fixed layer l , still depends on a specific method and number of sample used to compute it. More formally, (15) and (16) could be interpreted as an estimator (using a single CAV realization and the available samples from \mathcal{X}_k from \mathcal{D}_k)

$$\overline{\text{TCAV}}(\mathbb{1}) := \mathbb{E}_{\substack{\mathbf{x} \sim \mathcal{D}_k \\ \mathbf{w}_{\text{CAV}} \sim \mathcal{D}_{\text{CAV}}}} [\mathbb{1}_{(S_{C,k,l}(\mathbf{x}, \mathbf{w}_{\text{CAV}})) > 0}] = \mathbb{P}_{\substack{\mathbf{x} \sim \mathcal{D}_k \\ \mathbf{w}_{\text{CAV}} \sim \mathcal{D}_{\text{CAV}}}} (S_{C,k,l}(\mathbf{x}, \mathbf{w}_{\text{CAV}}) > 0) \quad (17)$$

for simplicity dropping the subscript (assuming the concept C , class k and layer l to be clear from the context), and instead emphasizing the role of the indicator function $\mathbb{1}_{x>0}$ being used here. Similar to the “standard” version in (16), we may also use an alternative estimator of (17) that additionally performs an averaging over different realization of the CAV. This exactly is the idea of Multi-TCAV, which will be introduced below.

Remark 3.1 (Interpretation and Limitations of TCAV). TCAV quantifies the influence of concept C on the k th class by measuring the prevalence of positive directional derivatives. Values near 1 indicate a strong positive contribution, 0.5 suggests a neutral role (uncorrelated), and values near 0 imply the concept contradicts the prediction. Despite its intuitive appeal, the standard definition in (15) suffers from a significant flaw: only the sign matters and it is insensitive to magnitudes and exhibits problematic behavior at the decision threshold. Specifically, the metric fails to distinguish between a truly negative contribution ($S_{C,k,l}(\mathbf{x}) < 0$ for all \mathbf{x}) and a neutral, zero-gradient case ($S_{C,k,l}(\mathbf{x}) = 0$ for all \mathbf{x}) - in both scenarios, $\text{TCAV}_{Q_{C,k,l}}$ collapses to 0. This discontinuity is more than a theoretical curiosity, but the reason why TCAV’s variance may sometimes be non-decaying [Wenkman and Garreau, 2025, Sec. 4.4].

Remark 3.2 (Sources of Randomness). Note that the sensitivity score $S_{C,k,l}(\mathbf{x})$ in (14) is a random variable with several sources of randomness. While the model itself (specifically the functions $h_{l,k}$ and f_l) is assumed to be deterministic — thereby neglecting potential dependencies on the training data — the distribution of $S_{C,k,l}(\mathbf{x})$ originates from, firstly, \mathbf{x} being a random data vector, drawn from the input data distribution (mixture of several classes), and secondly, the CAV \mathbf{v}_C^l being a random vector, whose distribution is induced by both the (l th layer) *concept* and the *non-concept* distribution.

Remark 3.3. [Asymptotically Normal Distribution.] With deterministic *concept* data, and $n_1 \rightarrow \infty$ for the non-concept data, [Wenkmann and Garreau, 2025, Theorem 1 & Corollary 1] have shown (asymptotically) normal distributions of the CAV \mathbf{w}_{CAV} and the corresponding sensitivity scores $\langle \mathbf{z}, \mathbf{w}_{\text{pat}} \rangle$ (for deterministic \mathbf{z}), for imbalanced logistic regression [Owen, 2007]. With our findings in Sec. 2, it is straightforward to obtain a similar result for the *PatternCAV* (or *FastCAV*) obtaining an asymptotically normal distribution. We provide the precise result and its proof in Lemma B.1.

To decrease the variance via averaging, Multi-TCAV was already proposed in the seminal paper [Kim et al., 2018] and is considered the state of the art until now [Wenkmann and Garreau, 2025]. It partitions the total number $N = s \cdot n$ of (non-)concept examples into s disjoint subsets of size n . For each subset $j \in \{1, \dots, s\}$, a separate CAV is trained, providing an individual TCAV score T_j ,

$$T_j = \text{TCAV}_{Q_{C,k,l}}(\mathbf{w}_{\text{CAV}}^{(j)}) = \frac{\left| \{ \mathbf{x} \in \mathcal{X}_k : S_{C,k,l}(\mathbf{x}, \mathbf{w}_{\text{CAV}}^{(j)}) > 0 \} \right|}{|\mathcal{X}_k|}. \quad (18)$$

The final multi-run TCAV score, T_{multi} , is defined as the empirical average of these individual scores,

$$T_{\text{multi}} = \frac{1}{s} \sum_{j=1}^s T_j = \frac{1}{s \cdot |\mathcal{X}_k|} \sum_{j=1}^s \sum_{\mathbf{x} \in \mathcal{X}_k} \mathbb{1}_{\{ \langle \mathbf{x}, \mathbf{w}^{(j)} \rangle > 0 \}}. \quad (19)$$

Typically $\mathbf{w}_{\text{CAV}}^{(1)}, \dots, \mathbf{w}_{\text{CAV}}^{(s)}$ have the same mean as a single global CAV computed with the identical method using all samples, but this is generally *not* true for the covariance (see e.g. Proposition 2.2). Naturally, recalling Definition 2.5 and generally the discussion in Sec. 2, we typically have a stronger variance decay $\text{Var}(\mathbf{w}_{\text{CAV}}) = \text{Tr}(\text{Cov}(\mathbf{w}_{\text{CAV}})) = \mathcal{O}(1/N)$ for the single CAV, in contrast to the larger variance $\text{Var}(\mathbf{w}_{\text{CAV}}^{(j)}) = \text{Tr}(\text{Cov}(\mathbf{w}_{\text{CAV}}^{(j)})) = \mathcal{O}(1/n)$ in the multi-CAV approach for $j = 1, \dots, s$. Regarding the variance of Multi-TCAV, [Wenkmann and Garreau, 2025, Conjecture 1] states that $\text{Var}(T_{\text{multi}}) = \mathcal{O}(1/s)$, which indeed is a straightforward consequence of Lemma A.1 for independent T_j and assuming $\text{Var}(T_j) = \mathcal{O}(1)$ for all j . While this scaling with respect to s seems overall correct, it misses a mild dependency on n . Given a fixed sampling budget $N = s \cdot n$, increasing s necessarily leads to a larger n , thus typically increases the above-mentioned $\text{Var}(\mathbf{w}_{\text{CAV}}^{(j)})$ of the individual CAVs, and thus variances of T_j . Thus, increasing s also increases the variances of T_j over which we average in (19). This subtle tradeoff suggests that Multi-TCAV may not be optimal.

3.2 α -TCAV

As a novel alternative to the standard TCAV procedure, and as a generalized framework, we introduce α -TCAV. Its fundamental idea is to replace the indicator fct. in (17) (similar for its empirical versions (16) and (19)) for Multi-TCAV, by the *scaled sigmoid function* $s_\alpha(x) = \frac{1}{1 + \exp(-\alpha x)}$, $\alpha > 0$; see also (A.1) and Sec. A.1 in the appendix. Thus, as an alternative TCAV definition to (17) we propose

$$\overline{\text{TCAV}}(\alpha) := \mathbb{E}_{\substack{\mathbf{x} \sim \mathcal{D}_k \\ \mathbf{w}_{\text{CAV}} \sim \mathcal{D}_{\text{CAV}}}} [s_\alpha(S_{C,k,l}(\mathbf{x}, \mathbf{w}_{\text{CAV}}))]. \quad (20)$$

While the proposed α -TCAV may be regarded as a smooth approximation of (16) - e.g., similar to the sigmoid function being employed for adversarial TCAV [Schnoor et al., 2026] - we think it is a refined definition in first place. It is better at capturing the neutral behavior around the origin $S_{C,k,l}(\mathbf{x}) = 0$, by discounting sensitivity scores close to zero, thus not only taking the sign of $S_{C,k,l}(\mathbf{x})$ into account, but also its magnitude. It can help to drastically reduce the variance *without* the need for a multi-run CAV (computing several CAVs); see also Figure 1. The definition of α -TCAV as given in (20) is quite generic as it considers an expectation with respect to the underlying data distribution $\mathbf{x} \sim \mathcal{D}_k$ as well as the distribution of the CAV \mathbf{w}_{CAV} . It is straightforward to consider specific variants of this, like assuming a fixed (deterministic) set of concept examples, and sampling only from the non-concept distribution [Wenkmann and Garreau, 2025]. We may also consider a *conditional* version (conditionally on the random CAV \mathbf{w}_{CAV}), by just taking the expectation with respect to $\mathbf{x} \in \mathcal{X}_k$, making the (conditional) expectation in (20) a random variable (or vice versa).

Remark 3.4 (Role of α). Larger values of α in s_α drive the definition of α -TCAV closer to the original one, while retaining smoothness and, and showing a favourable behavior around $S_{C,k,l}(\mathbf{x}) = 0$. For $\alpha \rightarrow \infty$, the pointwise limit yields the *Heaviside step function* s_∞ - see (A.2) in the appendix for the

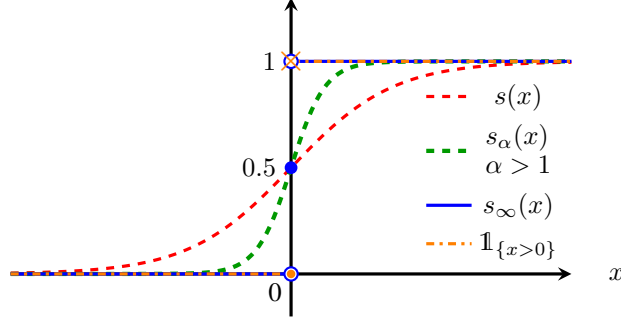


Figure 2: The indicator function $\mathbb{1}_{\{x>0\}}$ and approximations by the sigmoid function s , the scaled sigmoid function s_α , as well as the pointwise limit $s_\infty(x) := \lim_{\alpha \rightarrow \infty} s_\alpha(x)$, the *Heaviside function*.

formal definition - that differs from the originally used indicator function only in the origin; compare also Figure 2. Even though s_∞ is no longer continuous in the origin (similar to the indicator function $\mathbb{1}_{\{x>0\}}$) - which is even also the only point where it differs from $\mathbb{1}_{\{x>0\}}(0)$; see again Figure 2 - it shows a superior behavior by clearly reflecting the “neutral” behavior $s_\infty(0) = 0.5$ at the origin, opposed to the indicator function with $\mathbb{1}_{\{x>0\}}(0) = 1$, as discussed in Remark 3.1.

As seen in Rem. 3.3, sensitivity scores $S_{C,k,l}(\mathbf{x}) = \langle \nabla h_{l,k}(f_l(\mathbf{x})), \mathbf{w}_{\text{CAV}} \rangle$ as defined in (14) tend to be normally distributed for fixed input \mathbf{x} with $\nabla h_{l,k}(f_l(\mathbf{x})) \neq \mathbf{0}$, and sufficiently large sample size to compute the (random) CAV \mathbf{w}_{CAV} (this is not necessarily the case for the *joint* distribution; determining the distribution of $S_{C,k,l}(\mathbf{x}) = \langle \nabla h_{l,k}(f_l(\mathbf{x})), \mathbf{w}_{\text{CAV}} \rangle$ for $\mathbf{x} \sim \mathcal{D}_k$ may be intractable). Therefore, $s_\alpha(S_{C,k,l}(\mathbf{x}))$ follows the so-called *logit-normal distribution* over the open interval $(0, 1)$, *i.e.*, a normal distribution passed through a (scaled) sigmoid function s_α (or equivalently, a standard sigmoid function $s = s_1$, with appropriately scaled mean and variance); see also A.2. It turns out this distribution arises not only due to the Gaussian nature of $S_{C,k,l}(\mathbf{x})$ and the desire to smoothly approximate the indicator function $\mathbb{1}_{x>0} \approx s_\alpha(x)$, but has other another remarkable feature [Johnson, 1949]: depending on its parameters, it can be either *bimodal* (Bernoulli-like, and thus resembling TCAV) or *uni-modal* (Binomial like, resembling the Multi-TCAV); see also Fig. 3. Thus, α -TCAV provides a generalized framework combining standard TCAV and Multi-TCAV, while being more flexible and conceptually clearer, statistically more robust and clearly computationally more efficient (by avoiding multiple runs as in Multi-TCAV). We discuss the statistical aspects in the next section.

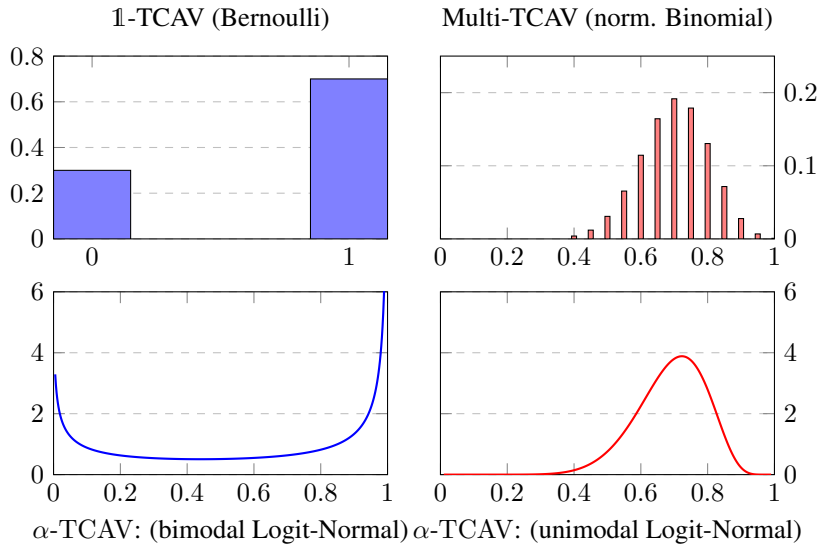


Figure 3: Schematic illustration: $\mathbb{1}$ -TCAV corresponds to a Bernoulli distribution, while Multi-TCAV is associated to a (normalized) Binomial distribution. α -TCAV follows a logit-normal distribution, that can either be bimodal (Bernoulli-like; left), or unimodal (Binomial-like; right).

4 Distribution of TCAV Scores and Numerical Experiments

A key theme of this paper is the stochastic nature of CAVs, which carries over to the various variants of TCAV scores. The high variance of the classical TCAV definition (15) was already noted in the seminal work Kim et al. [2018] and motivated Multi-TCAV. A trivial yet instructive upper bound,

$$\text{Var}(\text{TCAV}) \leq \frac{1}{4}, \quad (21)$$

holds for any random variable TCAV taking values in $[0, 1]$, by the classical *Popoviciu's Inequality* [Popoviciu, 1935]; see Theorem A.2. It is attained by a symmetric Bernoulli distribution placing all mass on $\{0, 1\}$. Although elementary, this observation highlights a key shortcoming: $\text{TCAV}_{Q_{C,k,l}}$ in (16) uses the indicator $\mathbb{1}_{\{x>0\}}$ and thus follows a Bernoulli distribution, which is prone to high variance when (near-)symmetric and attains low variance only by concentrating most mass on 0 or 1 (see Fig. 4).

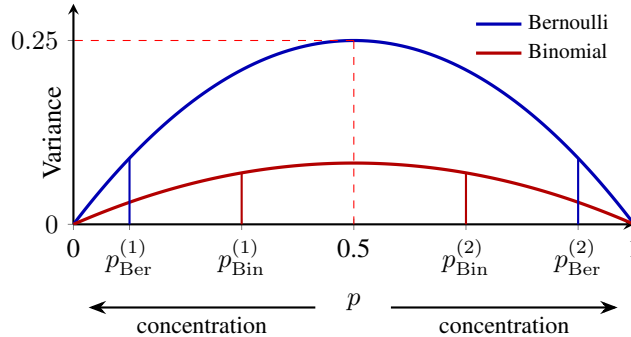


Figure 4: Comparison of the variance between a Bernoulli distribution and a scaled (average of i.i.d. Bernoullis) Binomial distribution ($s = 3$) with a probability of success p , *i.e.*, with variances $p(1 - p)$ (Bernoulli) and $p(1 - p)/s$ (normalized Binomial). The figure also illustrates a finding of Table 1: as a side-effect of averaging we are not comparing variances corresponding to the same value of p , but “more neutral” ones for the Binomial. More precisely (recall Φ from (26)), for TCAV and Multi-TCAV, the underlying reason is that $\Phi(\sqrt{N}\mu/\sigma)$ is “more neutral (closer to 0.5)” than $\Phi(\sqrt{n}\mu/\sigma)$ and therefore shifts the success probability slightly *against* a variance reduction (e.g. $p_{\text{Bin}}^{(1)}$ vs. $p_{\text{Ber}}^{(1)}$, and $p_{\text{Bin}}^{(2)}$ vs. $p_{\text{Ber}}^{(2)}$ as schematic illustration), - despite an overall variance reduction thanks to the averaging.

4.1 Modelling different TCAV approaches

Let us lay out a mathematical model describing the sensitivity scores $S_{C,k,l}(\mathbf{x}) = \langle \nabla h_{l,k}(f_l(\mathbf{x})), \mathbf{w}_{\text{CAV}} \rangle = \langle \mathbf{z}, \mathbf{w}_{\text{CAV}} \rangle$ (for a fixed but arbitrary input \mathbf{x}) based on their asymptotically normal distribution (assuming $\mathbf{z} = \nabla h_{l,k}(f_l(\mathbf{x})) \neq \mathbf{0}$) — recall Rem. 3.3 — and their variance decay as described in Section 2. Let $X \sim \mathcal{N}(\mu, \sigma^2)$ and i.i.d. copies X_1, \dots, X_N defined on the same probability space $(\Omega, \mathcal{E}, \mathbb{P})$. Assume we split it up into s batches of size n (*i.e.*, with $s \cdot n = N$), which we write as

$$X_1, \dots, X_N = X_1^{(1)}, \dots, X_n^{(1)}, X_1^{(2)}, \dots, X_n^{(2)}, \dots, X_1^{(s)}, \dots, X_n^{(s)}, \quad (22)$$

$$N = s \cdot n. \quad (23)$$

By averaging them (all, or batch-wise), we can model the variance decay of the different TCAV approaches. By properties of the normal distribution (see also the basic Lemma A.1), we easily obtain the distributions of their averages. In particular,

$$\frac{1}{N} \sum_{j=1}^N X_j \sim \mathcal{N}(\mu, \sigma^2/N), \quad \text{and} \quad \frac{1}{n} \sum_{j=1}^n X_j^{(r)} \sim \mathcal{N}(\mu, \sigma^2/n) \quad \forall r = 1, \dots, s, \quad (24)$$

for the overall and batch-wise average. We use this approach for modeling the different TCAV approaches analyzed in this paper. More precisely, it is based firstly on assuming that $\langle \mathbf{z}, \mathbf{w}_{\text{CAV}} \rangle$

is normally distributed for deterministic fixed \mathbf{z} (playing the role of $h_{l,k}(f_l(\mathbf{x}))$ for any fixed input \mathbf{x}) and random vector \mathbf{w}_{CAV} (playing the role of the CAV in the sensitivity score $S_{C,k,l}(\mathbf{x}) = \langle \nabla h_{l,k}(f_l(\mathbf{x})), \mathbf{w}_{\text{CAV}} \rangle$). This assumption is well-justified by standard *CLT*-based arguments indicating an (asymptotically) normal distribution; recall our detailed discussion in Rem. 3.3, notably also Lemma B.1 and [Wenkman and Garreau, 2025, Theorem 1 & Corollary 1]. Secondly, it is a convenient way to model the appropriate variance decay of the random variable $\langle \mathbf{z}, \mathbf{w}_{\text{CAV}} \rangle$. Recalling Sec. 2 and notably Definition of 2.5 $\text{Var}(\mathbf{w}_{\text{CAV}}) = \text{Tr}(\text{Cov}(\mathbf{w}_{\text{CAV}}))$, and this (total) variance consistently decays at a rate of $\mathcal{O}(N^{-1})$ when using N i.i.d. samples to compute the CAV. Note that [Wenkman and Garreau, 2025] considers N to be the number of non-concept samples ($N = n_1$ in our notation) and the concept data to be fixed; nevertheless, while this is plausible as non-concept data is cheaper to generate, this restriction is not necessary and we find the same decay for $N = n_1 + n_2$, assuming a distribution over both the concept *and* non-concept data; recall also Remark 2.1. Note that this variance decay of \mathbf{w}_{CAV} naturally carries over to the inner product $\langle \mathbf{z}, \mathbf{w}_{\text{CAV}} \rangle$ as (with $\lambda_{\max}(\mathbf{A})$ denoting the largest eigenvalue of a matrix \mathbf{A}) we have

$$\text{Var}(\langle \mathbf{z}, \mathbf{w}_{\text{CAV}} \rangle) = \mathbf{z}^\top \text{Cov}(\mathbf{w}_{\text{CAV}}) \mathbf{z} \leq \|\mathbf{z}\|^2 \text{Tr}(\text{Cov}(\mathbf{w}_{\text{CAV}})) = \mathcal{O}(N^{-1}).$$

Thus, our setup is clearly the appropriate way to model (for any \mathbf{x}) the sensitivity scores $S_{C,k,l}(\mathbf{x}) = \langle \nabla h_{l,k}(f_l(\mathbf{x})), \mathbf{w}_{\text{CAV}} \rangle = \langle \mathbf{z}, \mathbf{w}_{\text{CAV}} \rangle$ using N samples to compute \mathbf{w}_{CAV} (or batch-wise for s batches of size m for modeling several instances $\langle \mathbf{z}, \mathbf{w}_{\text{CAV}} \rangle$ with random CAVs $\mathbf{w}_{\text{CAV}}^{(r)}$ for $i = 1, \dots, s$) by Gaussian averages as in (24). This however makes it possible to systematically study from a mathematical viewpoint the properties of the different TCAV methods, leading to interesting novel insights. It turns out that each TCAV approach is associated to a corresponding classical probability distribution, namely the *Bernoulli distribution* for the (standard) TCAV, the *Binomial distribution* (normalized to $\{0, \frac{1}{s}, \frac{2}{s}, \dots, 1\}$, rather than $\{1, \dots, s\}$) in case of Multi-TCAV, and finally the *Logit-Normal distribution* for the α -TCAV. Despite its simplicity, this approach has straightforward consequences to the more general case. For instance, showing that a TCAV method has a lower variance than another method (e.g., Multi-TCAV has a lower variance than TCAV) for any fixed realization of $\mathbf{z} = \nabla h_{l,k}(f_l(\mathbf{x})) \neq \mathbf{0}$, it must also hold in expectation for probability distribution over \mathbf{x} , including the (unknown) distribution of class \mathcal{X}_k . Thus, exploiting the Gaussianity of the conditional distributions is a powerful approach that enables us to compare the different TCAV approaches more rigorously. We summarize our findings in the table below, followed by a detailed derivation and discussion of our results. Thus, for a CAV $\mathbf{w}_{\text{CAV}} = \mathbf{w}_{\text{CAV}}(N)$ computed using N random samples the sensitivity scores are modeled the normal distribution as

$$\langle \mathbf{z}, \mathbf{w}_{\text{CAV}} \rangle \sim \frac{1}{N} \sum_{j=1}^N X_j \sim \mathcal{N}(\mu, \sigma^2/N), \quad (25)$$

This makes sense as we expect the mean to be the same when increasing the sample size, but the variance to reduce at order of $\mathcal{O}(1/N)$. Modeling this using a sequence/sum makes sense as we have a on-to-one correspondence with the sample size used for computing a CAV, and fits well in the Multi-TCAV framework. Intuitively, this model describes the following situation where μ is the *signal* (indicating the concept’s relevance) and σ^2/N is the *noise* (due to the randomness of the CAV \mathbf{w}_{CAV}). In particular, it can model the following situations.

- For $\mu > 0$, the concept has a positive influence on the prediction of the class. With higher probability $\langle \mathbf{z}, \mathbf{w}_{\text{CAV}} \rangle$ are positive, but due to the randomness of \mathbf{w}_{CAV} , with lower probability (increasing as N grows) some will be negative.
- For $\mu < 0$, the concept has a negative influence on the prediction of the class. With higher probability $\langle \mathbf{z}, \mathbf{w}_{\text{CAV}} \rangle$ are negative, but due to the randomness of \mathbf{w}_{CAV} , with lower probability (increasing as N grows) some will be positive.
- For $\mu = 0$, the concept is neutral regarding the prediction of the class. The scores $\langle \mathbf{z}, \mathbf{w}_{\text{CAV}} \rangle$ are concentrated around the origin, but due to the randomness of \mathbf{w}_{CAV} , it fluctuates around zero (however, it becomes more concentrated as N grows).

Later we cover all three situations in experiments in Fig. 6. Before that, let us elaborate on the different properties of the TCAV approaches.

Method Distribution	Random Variable	Mean	Variance
TCAV Bernoulli	$\mathbb{1}_{\left\{\frac{1}{N} \sum_{j=1}^N X_j > 0\right\}}$	$\Phi\left(\frac{\sqrt{N}\mu}{\sigma}\right)$	$\Phi\left(\frac{\sqrt{N}\mu}{\sigma}\right)\left(1 - \Phi\left(\frac{\sqrt{N}\mu}{\sigma}\right)\right)$
T_{multi} (norm.) Binomial	$\frac{1}{s} \sum_{i=1}^s \mathbb{1}_{\left\{\frac{1}{n} \sum_{j=1}^n X_j^{(i)} > 0\right\}}$	$\Phi\left(\frac{\sqrt{n}\mu}{\sigma}\right)$	$\frac{\Phi\left(\frac{\sqrt{n}\mu}{\sigma}\right)\left(1 - \Phi\left(\frac{\sqrt{n}\mu}{\sigma}\right)\right)}{s}$
α -TCAV Logit-Normal	$s_\alpha\left(\frac{1}{N} \sum_{j=1}^N X_j\right)$	$m := m\left(\mu, \frac{\sigma^2}{N}, \alpha\right)$	$m(1 - m)\left(1 - \frac{1}{\sqrt{1 + \tau_2 \alpha^2 \sigma^2 / N}}\right)$

Table 1: Characterization of the three TCAV variants under the Gaussian model for the sensitivity score $\langle z, w_{\text{CAV}} \rangle$ modeled as in (25). Each variant corresponds to a classical probability distribution — Bernoulli, (normalized) Binomial, and Logit-Normal — with closed-form mean and variance (approximate for α -TCAV). Here Φ denotes the standard normal cdf (26), $N = sn$ is the total sample budget split into s batches of size n , $\tau_2 \approx 0.358$ is the constant from (A.10), and $m = m(\mu, \sigma^2/N, \alpha)$ is the logit-normal mean approximation discussed in more detail in Sec. A.2.

Before we continue, let us briefly recall the *cumulative distribution function (cdf)* Φ of the standard normal distribution $X \sim \mathcal{N}(0, 1)$,

$$\mathbb{P}(X \leq t) = \Phi(t) = \int_{-\infty}^t \frac{1}{\sqrt{2\pi}} \exp\left(-\frac{x^2}{2}\right) dx. \quad (26)$$

The two constants $\tau_1 = \frac{\pi}{8}$ and $\tau_2 = 0.358$ from (A.10), and the function $m(\mu, z, \alpha)$, defined as in (A.7) with $\mu \in \mathbb{R}, z > 0, \alpha > 0$,

$$m := m(\mu, z, \alpha) := s \left(\frac{\alpha\mu}{\sqrt{1 + \tau_1 \alpha^2 z}} \right). \quad (27)$$

TCAV. Note that the distribution of interest is a Bernoulli distribution, whose “success” probability is related to the underlying Gaussian distribution $\mathcal{N}(\mu, \sigma^2/N)$. Thus, we obtain the for the mean that

$$\mathbb{E}\left[\mathbb{1}_{\left\{\frac{1}{N} \sum_{j=1}^N X_j > 0\right\}}\right] = \mathbb{P}\left(\frac{1}{N} \sum_{j=1}^N X_j > 0\right) = \Phi\left(\frac{\mu}{\sigma/\sqrt{N}}\right) = \Phi\left(\frac{\sqrt{N}\mu}{\sigma}\right). \quad (28)$$

Next, recall that $Y = Y^2$ for any Bernoulli random variable Y , such that $\mathbb{E}[Y] = \mathbb{E}[Y^2]$. Therefore,

$$\text{Var}\left(\mathbb{1}_{\left\{\frac{1}{N} \sum_{j=1}^N X_j > 0\right\}}\right) = \Phi\left(\frac{\sqrt{N}\mu}{\sigma}\right)\left(1 - \Phi\left(\frac{\sqrt{N}\mu}{\sigma}\right)\right), \quad (29)$$

showing the claimed expression for the variance. Let us comment on our findings.

- If $\mu = 0$, both mean $\Phi(0) = \frac{1}{2}$ and variance $\Phi(0)(1 - \Phi(0)) = \frac{1}{2}(1 - \frac{1}{2}) = \frac{1}{4}$ are constant.
- If $\mu > 0$, then $N \rightarrow \infty$ will push $\Phi\left(\frac{\sqrt{N}\mu}{\sigma}\right) \rightarrow 1$, and the variance vanishes.
- If $\mu < 0$, then $N \rightarrow \infty$ will push $\Phi\left(\frac{\sqrt{N}\mu}{\sigma}\right) \rightarrow -1$, and the variance vanishes.

T_{multi} . As a (normalized) sum of s i.i.d. Bernoulli random variables, the random variable describing T_{multi} follows a (normalized) Bernoulli distribution taking values in $\{0, \frac{1}{s}, \frac{2}{s}, \dots, 1\}$. Similar to (28), for any batch $r_0 \in \{1, \dots, s\}$ with n samples, by the we find that

$$\begin{aligned}
\mathbb{E} \left[\frac{1}{s} \sum_{i=1}^s \mathbb{1}_{\left\{ \frac{1}{n} \sum_{j=1}^n X_j^{(r)} > 0 \right\}} \right] &= \mathbb{E} \left[\mathbb{1}_{\left\{ \frac{1}{n} \sum_{j=1}^n X_j^{(i)} > 0 \right\}} \right] \\
&= \mathbb{P} \left(\frac{1}{n} \sum_{j=1}^n X_j^{(r_0)} > 0 \right) = \Phi \left(\frac{\sqrt{n}\mu}{\sigma} \right). \tag{30}
\end{aligned}$$

For a “success” probability p (i.e., the probability of 1, which is also the expectation of the Bernoulli distribution), the variance of a general Bernoulli distribution is $p(p-1)$. Taking the normalization into account and due to the independence, by Lemma A.1 and using (30), we find immediately that

$$\text{Var} \left(\frac{1}{s} \sum_{i=1}^s \mathbb{1}_{\left\{ \frac{1}{n} \sum_{j=1}^n X_j^{(i)} > 0 \right\}} \right) = \frac{\Phi \left(\frac{\sqrt{n}\mu}{\sigma} \right) \left(1 - \Phi \left(\frac{\sqrt{n}\mu}{\sigma} \right) \right)}{s}. \tag{31}$$

- Let us point out that in the special case of $s = 1$ and $n = N$ (a single batch of size N), T_{multi} collapses to the (standard) TCAV, consistently with our findings for the corresponding means and variances.
- Furthermore, it is worth mentioning that the mean (30) of T_{multi} is independent of s and controlled by n , the number sample per batch (used for one of the CAV computations).
- In contrast, the expression (31) for the variance is mainly governed by s and scales like $\mathcal{O}(1/s)$; while the numerator depends on n , it is lower bounded by 0 and upper bounded by 0.25. This has interesting consequences in practice, as the user faces some tradeoff when given a limited sampling budget of N samples: On the one hand, as a low variance is desirable, we may want to choose a large number of batches s ; however (apart from computational aspects), this enforces a smaller batch size n (when $N = s \cdot n$ is fixed) and will result in a smaller mean (less decisive, more tending towards a neutral assessment, perhaps underestimating). On the other hand, a small value of s (in the extreme case, obtaining (standard) TCAV for $s = 1$) may lead to a larger variance and, as n becomes larger, a more decisive mean closer to the extreme values 1 (overwhelming concept influence; if $\mu > 0$) and 0 (negligible concept influence; if $\mu < 0$). We explicitly state this next.
- Compare mean of TCAV and T_{multi} : for $\mu = 0$ they are the same of course, and they are always bounded as $0 \leq \Phi \leq 1$. For $\mu > 0$ note that TCAV mean is pushed more towards one, while as $n \ll N$, T_{multi} is more moderate. Similar for $\mu < 0$ TCAV mean is pushed more towards zero, while as $n \ll N$, T_{multi} is more moderate.
- Given a large sampling budget, a user can increase s , while keeping n fixed, to reduce the variance. By the *CLT*, the distribution will become Gaussian-like for $s \rightarrow \infty$. However, increasing the number s requires a large sampling budget, and is computationally expensive.

α -TCAV. Finally, let us comment on α -TCAV, which by assumptions clearly follows a logit-normal distribution, whose means and variance do not have closed-form solutions. However, we use the highly accurate approximations for its mean and variance, i.e., the well-established estimates provided in (A.7) and (A.9) in Sec. A.2. α -TCAV provides a parameterized general framework aimed at superior statistical robustness and computational efficiency. However, this flexibility also leaves the user with choice of α . On the one hand, by convergence to the *Heaviside step function* s_∞ - see (A.2) - for $\alpha \rightarrow \infty$; thus, for sufficiently large values of α , α -TCAV will resemble the (standard) TCAV approach (highly decisive by taking either 0 or 1, with a high variance). On the other hand, as $\alpha \rightarrow 0$, the sigmoid flattens out and the score will be highly indecisive (around 0.5) with a vanishing variance. By arguments based on the intermediate value theorem, by choosing an appropriate α we can obtain any behavior in-between. In particular, we comment on two specific interesting choices of α . Firstly, we comment on the possibility of imitating Multi-TCAV using α -TCAV, while drastically reducing the variance. *Still, this does not mean that - and in which sense - this choice is objectively optimal; Multi-TCAV is considered the state-of-the-art approach, but based on heuristics itself.* Secondly, we suggest a choice of α that is statistically sound and can be interpreted as a *calibrated probability that the concept contributes to the model’s prediction*. Before that, let us point out that in the limit $\alpha \rightarrow \infty$, once again with the approximation $s(z) \approx \Phi(\sqrt{\tau_1}z)$,

$\tau_1 = \pi/8$, we obtain

$$\lim_{\alpha \rightarrow \infty} s \left(\frac{\alpha\mu}{\sqrt{1 + \tau_1\alpha^2\sigma^2/N}} \right) = s \left(\frac{\sqrt{N}\mu}{\sqrt{\tau_1}\sigma} \right) \approx \Phi \left(\frac{\sqrt{N}\mu}{\sigma} \right), \quad (32)$$

again confirming the consistency of the framework as the mean of α -TCAV collapses to the mean of TCAV in this limit. Further, the case of a large sample size when $N \gg \tau_1\alpha^2\sigma^2$ is instructive, when

$$s \left(\frac{\alpha\mu}{\sqrt{1 + \tau_1\alpha^2\sigma^2/N}} \right) \approx s(\alpha\mu). \quad (33)$$

4.2 Choosing α and Normalizing the Sensitivity Scores

Matching α -TCAV with Multi-TCAV. Interestingly, α -TCAV can be used to imitate Multi-TCAV in the following sense. In this paragraph, we investigate how to choose α such that the means of α -TCAV and Multi-TCAV — as provided in Table 1 — agree, and compare the corresponding variances. Therefore, we make the *ansatz*

$$\Phi \left(\frac{\sqrt{n}\mu}{\sigma} \right) \approx s \left(\frac{\alpha\mu}{\sqrt{1 + \tau_1\alpha^2\sigma^2/N}} \right) \stackrel{\text{def}}{=} m(\mu, z, \alpha). \quad (34)$$

Using (A.13), *i.e.*, $s(z) \approx \Phi(\sqrt{\tau_1}z)$ where $\tau_1 = \pi/8$, equating the corresponding arguments yields

$$\frac{\sqrt{n}\mu}{\sigma} = \frac{\sqrt{\tau_1}\alpha\mu}{\sqrt{1 + \tau_1\alpha^2\sigma^2/N}}. \quad (35)$$

A straightforward computation solving for α using from (23) that $N = s \cdot n$, such that $n/N = 1/s$, yields the condition (assuming $s \geq 2$; we comment below on the case $s = 1$ corresponding to TCAV)

$$\alpha^* = \frac{1}{\sigma} \sqrt{\frac{n}{\tau_1(1 - 1/s)}} \quad (36)$$

for the means of both methods to approximately match. (As a side remark, note that when $s \rightarrow 1$ on the right-hand side of (36), we have $\alpha^* \rightarrow \infty$; once again illustrating the consistency of our framework as the case $s = 1$ corresponds to the (standard) TCAV setting, which corresponds to $\alpha = \infty$.) While matching the means with α^* , let us next compare the variances. To show that α -TCAV has a lower (or at least not worse) variance, we need to show that the fraction of the variances is bounded by 1, *i.e.*, we aim to show that

$$s \cdot \frac{m(\mu, z, \alpha^*)(1 - m(\mu, z, \alpha^*)) \left(1 - \frac{1}{\sqrt{1 + \tau_2\alpha^{*2}\sigma^2/N}} \right)}{\Phi \left(\frac{\sqrt{n}\mu}{\sigma} \right) \left(1 - \Phi \left(\frac{\sqrt{n}\mu}{\sigma} \right) \right)} \leq 1. \quad (37)$$

Recall that α^* was chosen in a way such that (34) holds with $\alpha = \alpha^*$. Using this fine-tuned value α^* and the above approximation in (37), the ratio on the left-hand-side of (37) considerably simplifies to become (where $\tau_2/\tau_1 \approx 0.9116$)

$$s \cdot \left(1 - \frac{1}{\sqrt{1 + \tau_2\alpha^{*2}\sigma^2/N}} \right) = s \cdot \left(1 - \frac{1}{\sqrt{1 + \frac{\tau_2/\tau_1}{s-1}}} \right) =: r(s). \quad (38)$$

Remarkably, the ratio $r(s)$ of the variances depends only on s . Note that $r(s)$ is not defined for $s = 1$ (which would correspond to (standard) TCAV), and — as pointed out above — as $s \rightarrow \infty$ we would have $\alpha^* \rightarrow \infty$, once again obtaining (standard) TCAV; as the methods coincide in this case, there obviously the variance gap vanishes. We may therefore, in the spirit of Multi-TCAV, assume $s \geq 2$ for our comparison. Consider the Taylor expansion around the origin $x \approx 0$ (note that as $s \rightarrow \infty$ we have $x = \frac{\tau_2/\tau_1}{s-1} \rightarrow 0$, justifying the Taylor expansion around the root point in the origin)

$$\frac{1}{\sqrt{1+x}} \approx 1 - \frac{1}{2}x + \frac{3}{8}x^2. \quad (39)$$

Next, we employ this Taylor expansion to investigate the asymptotic behavior of (38) as $s \rightarrow \infty$. Using the Taylor expansion and simplifying yields

$$r(s) \approx \frac{s}{s-1} \cdot \frac{\tau_2/\tau_1}{2} - \frac{3\tau_2^2/\tau_1^2 s}{8(s-1)^2} \xrightarrow{s \rightarrow \infty} \frac{\tau_2/\tau_1}{2} \approx 0.4558. \quad (40)$$

Thus, with the choice of $\alpha = \alpha^*$ as in (36), we can obtain a similar mean of α -TCAV and Multi-TCAV, while significantly reducing the variance by more than half already for moderately large values of s , which significantly improves over the state of the art.¹ We plot the variance ratio function in Figure 5, illustrating the variance reduction in a range of roughly 45% and 55%.

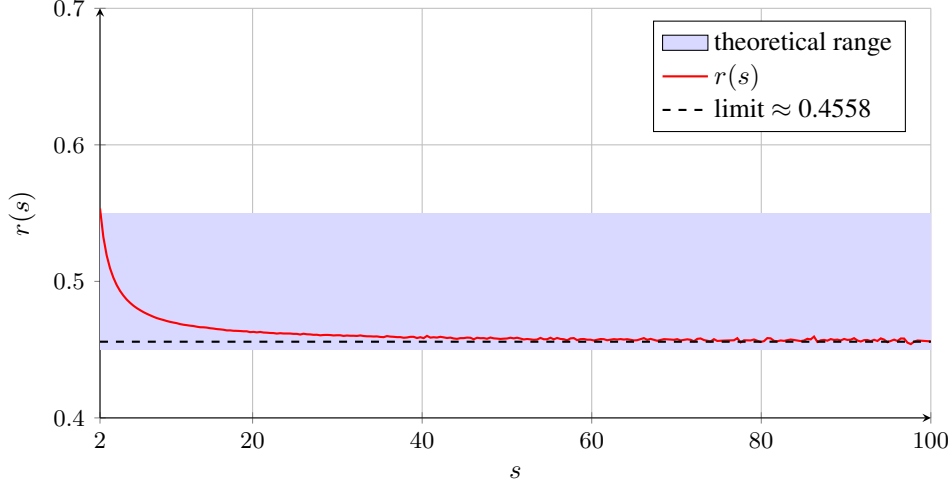


Figure 5: Numerical plot of the variance ratio function $r(s)$ for $s \in [2, 100]$, even though in practice of course $s \in \mathbb{N}$ takes discrete values, showing the theoretical range of $[0.45, 0.55]$, as approximately $r(2) \approx 0.55$ and $\lim_{s \rightarrow \infty} r(s) \approx 0.4558$.

A Bayesian Interpretation of α -TCAV. Under the running model of Sec. 4.1 simulating a CAV computed from N samples, let us shortly write $S_N := \langle \mathbf{z}, \mathbf{w}_{\text{CAV}} \rangle \sim \mathcal{N}(\mu, \sigma^2/N)$. For fixed \mathbf{z} and random CAV \mathbf{w}_{CAV} , whether the concept has a positive or negative influence on the model’s prediction is determined by the sign of the mean μ , *i.e.*, by $\theta := \mathbb{1}_{\{\mu > 0\}}$. Adopting a Bayesian viewpoint, we treat μ as random and place a *flat* (improper) prior $\pi(\mu) \propto 1$ on \mathbb{R} , encoding no prior belief (note that π does not integrate to one, but the resulting posterior does). Recall that a prior is *conjugate* to a likelihood if the posterior lies in the same family as the prior; for Gaussian likelihoods with known variance, Gaussians (and flat priors as their limit with increasing variance) are conjugate, see, e.g., [Gelman et al., 2013, Ch. 2]. By Bayes’ theorem (posterior \propto likelihood \times prior), the posterior over μ after observing S_N is given by

$$\pi(\mu | S_N) \propto \exp\left(-\frac{N}{2\sigma^2}(S_N - \mu)^2\right) \cdot 1 \propto \exp\left(-\frac{N}{2\sigma^2}(\mu - S_N)^2\right), \quad (41)$$

which we recognize as $\mu | S_N \sim \mathcal{N}(S_N, \sigma^2/N)$. Standardizing yields the posterior sign probability (analog to the derivation in (28), with the theoretical mean μ replaced by the observed mean S_N)

$$\mathbb{P}(\mu > 0 | S_N) = \Phi\left(\frac{\sqrt{N} S_N}{\sigma}\right), \quad (42)$$

which corresponds to the calibrated probability that the concept matters for \mathbf{z} . Next, let us connect this Bayesian view to α -TCAV; once again using the sigmoid-probit approximation (A.13), that is $s(z) \approx \Phi(\sqrt{\tau_1}z)$ with $\tau_1 = \pi/8$, we have $s(\alpha S_N) \approx \Phi(\sqrt{\tau_1}\alpha S_N)$, which matches (42) when

$$\alpha^\dagger := \frac{1}{\sigma} \sqrt{\frac{N}{\tau_1}}. \quad (43)$$

¹This is only the statistical benefits; note that the computational differences are not essential for this simulation using normally distributed synthetic data; note however, that for a practical computation of Multi-TCAV, an expensive computation of several CAVs is required; we report on experiments for real data in Fig. 7.

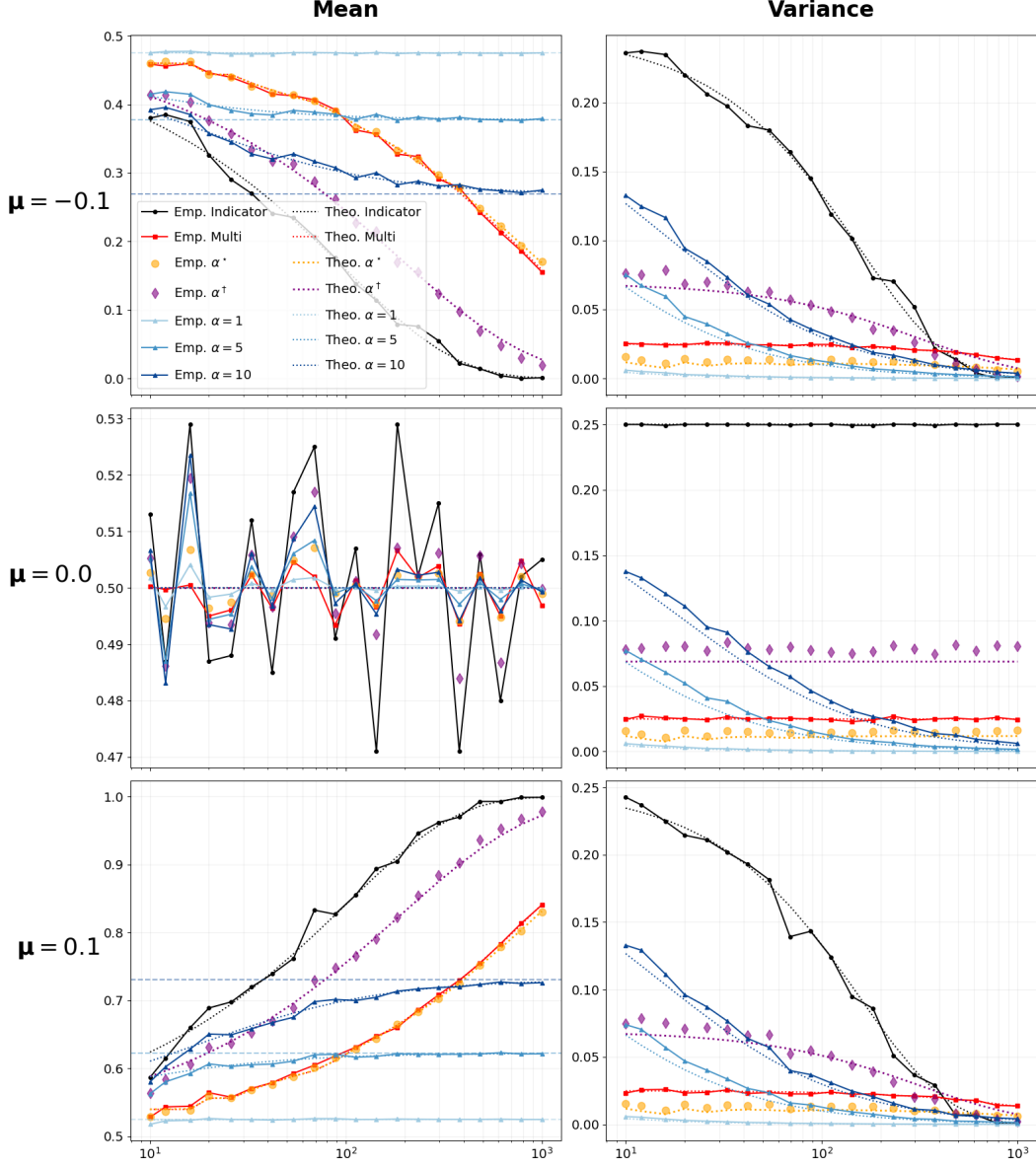


Figure 6: Numerical simulation of **mean and variance (columns)** of the different TCAV approaches in Table 1 according to the model explained in Sec. 4 with $\sigma = 1$ and different values for **different values of μ (rows)** and N on the x -axis (modeling the sample size), showing an excellent agreement between the theoretical prediction and the empirical simulation. Standard (*indicator*) TCAV (**black**) provides provides the most extreme mean (tending towards either 0 or 1), while clearly being biased (mean changes with the sample size), and having a large variance (notably large for small sample size), and even non-decaying variance for $\mu = 0$, with a constant variance of 0.25 as in the worst-case setting of *Popoviciu's Inequality* (Thm. A.2); also recall (21). Multi-TCAV (**red**), with fixed $s = 10$ and n matching each $N = s \cdot n$ can be well-matched using α^* -TCAV (**yellow**) with α^* from (36) with a significantly lower variance. (Notably, α^* depends on $N = s \cdot n$: as s is fixed and N grows, so does n , and therefore α^* .) For appropriate values of α -TCAV, the bias is much less pronounced compared to the other approaches. The Bayes-optimal α^\dagger -TCAV with α^\dagger from (43) is shown in **violet**, highlighting it is *between the over-confident TCAV and the under-confident Multi-TCAV*; it becomes more confident for growing N : by the interpretation of a probability (rather than some abstract score), the probability approaches zero ($\mu < 0$) or one ($\mu > 0$), respectively, as the sample size grows. We plot various other value α -TCAV for various values of α in **blue** together with the theoretical means (for large N) 33. The experiments have been performed in *GoogleColab*.

Thus, α -TCAV at $\alpha = \alpha^\dagger$ is (up to the sigmoid-probit approximation (A.13)) the Bayes-optimal estimator of θ under *squared loss* $\ell(\hat{\theta}, \theta) = (\hat{\theta} - \theta)^2$, and is calibrated by construction. This recasts α -TCAV not as a smooth surrogate but as a principled posterior estimator. The contrast with *standard TCAV* — the indicator $\mathbb{1}_{\{S_N > 0\}}$ — is instructive: standard TCAV is the Bayes-optimal estimator under *0–1 loss* $\ell(\hat{\theta}, \theta) = \mathbb{1}_{\{\hat{\theta} \neq \theta\}}$, which returns the posterior *mode* (the most probable value of θ , here either 0 or 1). Reporting only the mode discards the magnitude of the posterior probability and is therefore systematically *overconfident* when $|S_N|$ is small relative to σ/\sqrt{N} : in this regime the posterior $\Phi(\sqrt{N}S_N/\sigma)$ is close to $1/2$ (genuine uncertainty), yet standard TCAV outputs a definite 0 or 1. *Multi-TCAV*, on the other hand, is *underconfident*: each batch uses only N/s samples, so its effective signal-to-noise is \sqrt{n}/σ rather than \sqrt{N}/σ . The mean-matching choice (recall (36))

$$\alpha^* = \frac{1}{\sigma} \sqrt{\frac{n}{\tau_1(1-1/s)}} = \frac{1}{\sigma} \sqrt{\frac{N}{\tau_1(s-1)}} \quad (44)$$

leads to the ratio $\alpha^*/\alpha^\dagger = 1/\sqrt{s-1} < 1$ and is therefore a deliberately flatter sigmoid that reflects Multi-TCAV’s underconfidence, as it averages noisy estimates. Note that both α^* and α^\dagger from (36) and (43) depend on σ , which in practice is unknown and has to be estimated from the data. We comment on this below.

Normalizing Sensitivity Scores. The sensitivity magnitudes $|S| := |S_{C,k,\ell}(\mathbf{x})|$ vary across concepts and layers by orders of magnitude, e.g. $|S| \sim 10^{-3}$ in `layer2` vs. $|S| \sim 10^{-2}$ in `layer4` of *ResNet50*. Without normalization, a fixed value of α has completely different effects across settings when computing α -TCAV (recall (20))

$$\frac{1}{|\mathcal{X}_k|} \sum_{\mathbf{x} \in \mathcal{X}_k} s_\alpha(S_{C,k,\ell}(\mathbf{x})) = \frac{1}{|\mathcal{X}_k|} \sum_{\mathbf{x} \in \mathcal{X}_k} s(\alpha \cdot S_{C,k,\ell}(\mathbf{x})). \quad (45)$$

If $\alpha |S| \ll 1$, the sigmoid stays in its linear regime around the origin and the score collapses around 0.5; if $\alpha |S| \gg 1$, it saturates and recovers the indicator function. An advantage of α -TCAV is its flexibility to adapt to different typical magnitudes of sensitivity scores, and we comment on how to scale the sigmoid function adapting to the distribution of sensitivities. We propose the following normalization of sensitivity scores by the factor of $\gamma_{C,\ell}$ to allow for “natural” values of α and compute

$$\frac{1}{|\mathcal{X}_k|} \sum_{\mathbf{x} \in \mathcal{X}_k} s_\alpha\left(\frac{S_{C,k,\ell}(\mathbf{x})}{\gamma_{C,\ell}}\right) = \frac{1}{|\mathcal{X}_k|} \sum_{\mathbf{x} \in \mathcal{X}_k} s_{\alpha/\gamma_{C,\ell}}(S_{C,k,\ell}(\mathbf{x})), \quad (46)$$

by properties of the sigmoid function (A.2). Here, the normalization factor $\gamma_{C,\ell}$ is defined as the root-mean-square of the sensitivity score (typically for a *single* CAV realization \mathbf{w}_{CAV} in the spirit of α -TCAV, trained on the full reference set of random samples, or averaged over a small number of such high-sample CAVs for additional robustness),

$$\gamma_{C,\ell} = \sqrt{\mathbb{E}_{\mathbf{x} \sim \mathcal{D}_k} (S_{C,k,\ell}(\mathbf{x}, \mathbf{w}_{\text{CAV}})^2)} \quad (47)$$

$$\approx \sqrt{\frac{1}{|\mathcal{X}_k|} \sum_{\mathbf{x} \in \mathcal{X}_k} \langle \nabla h_{\ell,k}(f^\ell(\mathbf{x})), \mathbf{w}_{\text{CAV}} \rangle^2 + \varepsilon}, \quad (48)$$

with $\varepsilon = 10^{-8}$ in the practical computation (48) added for numerical stability. Recalling the inner-product form of the sensitivity score, $S_{C,k,\ell}(\mathbf{x}, \mathbf{w}_{\text{CAV}}) = \langle \nabla h_{\ell,k}(f^\ell(\mathbf{x})), \mathbf{w}_{\text{CAV}} \rangle$, note that

$$\gamma_{C,\ell}^2 = \text{Var}_{\mathbf{x} \sim \mathcal{D}_k} [S_{C,k,\ell}(\mathbf{x}, \mathbf{w}_{\text{CAV}})] + (\mathbb{E}_{\mathbf{x} \sim \mathcal{D}_k} [S_{C,k,\ell}(\mathbf{x}, \mathbf{w}_{\text{CAV}})])^2, \quad (49)$$

decomposing into a variance and a mean term. As the sigmoid behaves linearly around the origin (zero), for the normalization not only the variance of the sensitivity scores matters, but how far they are from the origin. After the normalization introduced in (46), the argument of the sigmoid is $\alpha \cdot S_{C,k,\ell}(\mathbf{x})/\gamma_{C,\ell}$, and by construction, the rescaled sensitivity $\tilde{S}(\mathbf{x}) := S_{C,k,\ell}(\mathbf{x})/\gamma_{C,\ell}$ satisfies $\mathbb{E}_{\mathbf{x} \sim \mathcal{D}_k} [\tilde{S}(\mathbf{x})^2] = 1$. Thus, typical values of \tilde{S} are of order unity rather than 10^{-3} or 10^{-2} (depending on layers), and α itself — not the product $\alpha \cdot |S|$ — becomes the effective sharpness of the sigmoid, and α trades off bias (distance from standard TCAV) against variance reduction.

Estimating σ in practice. The formula (36) requires knowledge of σ , the standard deviation parameter of the Gaussian model. On real data, we estimate σ from the observed sensitivities. Given a single CAV w_{CAV} trained on N samples, we compute the sensitivity scores $S_i = \langle \nabla h_{\ell,k}(f^\ell(\mathbf{x})), w_{\text{CAV}} \rangle$ for all test inputs $\mathbf{x} \in \mathcal{X}_k$, and define

$$\hat{\sigma}_{\text{eff}} = \sqrt{\text{Var}_x(S(\mathbf{x}, w_{\text{CAV}})) \cdot N}, \quad (50)$$

which recovers the population parameter σ from the observed variance $\text{Var}_x(S) = \sigma^2/N$ of the model. Combined with the γ -normalization from (48), the practical α^* on the normalized scale is

$$\alpha_{\text{norm}}^* = \frac{\gamma_{C,\ell}}{\hat{\sigma}_{\text{eff}}} \sqrt{\frac{n}{\tau_1 (1 - 1/s)}}, \quad (51)$$

and the score is computed as $\frac{1}{|\mathcal{X}_k|} \sum_{\mathbf{x} \in \mathcal{X}_k} s_{\alpha_{\text{norm}}^*}(S_{C,k,\ell}(\mathbf{x})/\gamma_{C,\ell})$. Since $\hat{\sigma}_{\text{eff}}/\gamma_{C,\ell}$ is of order unity by construction, α_{norm}^* takes values in the range 1–3 for typical choices of s , placing the sigmoid in the moderate smoothing regime regardless of layer or concept. Importantly, this estimation uses the *total* variance of sensitivities and does not require decomposing σ^2 into intrinsic and CAV-noise components, making it equally applicable to PatternCAV and logistic regression CAVs. The same estimate $\hat{\sigma}_{\text{eff}}$ is used to compute the Bayes-optimal α^\dagger from (43), replacing σ by $\hat{\sigma}_{\text{eff}}/\gamma_{C,\ell}$ on the normalized scale. Since both α^* and α^\dagger share the same $\hat{\sigma}_{\text{eff}}$, their ratio $\alpha^\dagger/\alpha^* = \sqrt{s-1}$ (cf. Eq. (43)) holds exactly in practice, regardless of the quality of the sigma estimate.

As a rule of thumb, we can describe the behavior with respect to α as follows:

- $\alpha \rightarrow 0$: the sigmoid collapses to the constant 1/2, and α -TCAV loses all discriminative power;
- $\alpha = 1$: gentle smoothing, with the sigmoid’s transition spanning the typical range of sensitivities; variance is strongly reduced, but borderline sensitivities are scored near 1/2, pulling the score away from the standard TCAV mean;
- $\alpha = 3$: moderate smoothing, still clearly discriminative and close to the standard TCAV mean;
- $\alpha = 5$: steep sigmoid, most sensitivities already in the saturated regime; nearly unbiased with respect to standard TCAV, with only a small variance benefit;
- $\alpha \rightarrow \infty$: recovers the indicator function, and thus standard TCAV exactly.

Experimental validation. Table 2 reports the computed α_{norm}^* values for ResNet-50 on DTD textures. For PatternCAV, α_{norm}^* ranges from 0.8 (at $s = 10$) to 2.4 (at $s = 2$), confirming that after normalization the effective sharpness falls in the natural range described above. Figure 8 (right) summarizes variance reduction across all methods; α^* -TCAV consistently achieves lower variance than Multi-TCAV across all concepts and values of s , confirming that the automatic calibration reliably reduces variance.

Layer	Concept	$\alpha^* (s=2)$	$\alpha^* (s=5)$	$\alpha^* (s=10)$
layer2	dotted	2.35	1.18	0.78
layer2	striped	2.26	1.13	0.75
layer2	zigzagged	2.30	1.15	0.77
layer3	dotted	2.15	1.08	0.72
layer3	striped	2.08	1.04	0.69
layer3	zigzagged	1.92	0.96	0.64

Table 2: α_{norm}^* values from (51) for PatternCAV on ResNet-50. Values are in the range 0.6–2.4, confirming that γ -normalization places the sigmoid in the moderate smoothing regime.

4.3 Numerical Experiments on Real Data

We validate our theoretical findings on a pretrained ResNet-50 [He et al., 2016] using the Describable Textures Dataset (DTD) [Cimpoi et al., 2014] with three texture concepts (dotted, striped, zigzagged). Concept images are taken from DTD; non-concept (random) images are drawn from a held-out subset of ImageNet [Deng et al., 2009] not containing texture-related classes.

Sensitivity scores $S_{C,k,\ell}(\mathbf{x}) = \langle \nabla h_{\ell,k}(f^\ell(\mathbf{x})), \mathbf{w}_{\text{CAV}} \rangle$ are computed at layers 2 and 3 using PatternCAV (Difference of Means). We compare: (i) Multi-TCAV with $s \in \{2, 5, 10, 20, 50\}$ subsets; (ii) α -TCAV with fixed $\alpha \in \{1, 3\}$ using the γ -normalization from Sec. 4.2; (iii) α^* -TCAV with α^* from (51); and (iv) α^\dagger -TCAV (Bayes-optimal) with α^\dagger from (43). Each configuration is repeated $E = 50$ times with total budget $R = 1000$. All experiments on real data (in this section and in Sec. 5) were conducted on a single NVIDIA Quadro RTX 5000 (16 GB VRAM). The vary- s and vary- N experiments (ResNet-50, DTD, PatternCAV, $E = 50$ repeats, $R = 1000$) required approximately 3 hours and 1.5 hours respectively. A single α -TCAV estimate takes approximately 2 seconds, compared to approximately 11 seconds for Multi-TCAV at $s = 50$.

Computational efficiency. α -TCAV requires training only a single CAV on the full sample budget, versus s CAVs for Multi-TCAV. Figure 7 shows that a single α -TCAV estimate achieves a 5–8 \times wall-clock speedup over Multi-TCAV at $s = 50$, with no loss in stability.

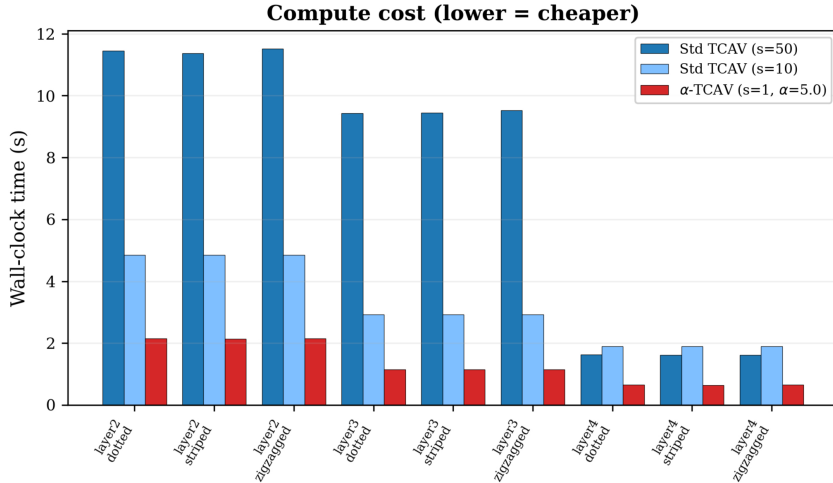


Figure 7: Wall-clock time per TCAV estimate on ResNet-50/DTD (PatternCAV, 6 layer \times concept configurations). α -TCAV ($s = 1$, single full-budget CAV, red) achieves a 5–8 \times speedup over Multi-TCAV at $s = 50$ and $\approx 2.3\times$ over $s = 10$, since it requires only one CAV training regardless of s .

Vary- s results. Figure 8 shows results for layer 2 as a function of the number of subsets s . α^\dagger -TCAV (purple) consistently produces the most decisive mean — above Multi-TCAV across all concepts and values of s — at the cost of higher variance, confirming its role as the overconfident Bayes-optimal posterior estimator under squared loss (Eq. (43)). $\alpha = 1$ (blue) achieves the strongest variance reduction (ratios 0.08–0.13 relative to Multi-TCAV) across all settings, at the cost of mean shrinkage toward 0.5. $\alpha = 3$ (green) offers a practical compromise: close to Multi-TCAV’s mean with moderate variance benefit. α^* -TCAV (red) adapts to the noise structure of each concept, with performance varying by regime (see Table 2 for calibrated values).

Vary- N results. Figure 9 shows the effect of increasing the total sample budget N , with a fixed per-subset size $m_{\text{ind}} = 50$ for the indicator and each Multi-TCAV subset. The indicator (black) maintains an approximately *constant* variance floor as N grows — the $\mathcal{O}(1)$ behavior identified in [Wenkman and Garreau, 2025, Sec. 4.4] due to borderline points at the fixed per-subset budget. By contrast, all α -TCAV variants, which use the full budget N for a single CAV, exhibit clear $\mathcal{O}(1/N)$ decay. α^\dagger -TCAV (purple) sits between the indicator and Multi-TCAV in both mean and variance, consistent with the theoretical ratio $\alpha^\dagger/\alpha^* = \sqrt{s - 1}$ from Eq. (43).

4.4 Practical Recommendations for TCAV

The theoretical unification and empirical results presented in this work provide a clear roadmap for practitioners seeking to improve the reliability of concept-based interpretability. To move beyond heuristic methods toward statistically grounded explanations, we propose the following guidelines:

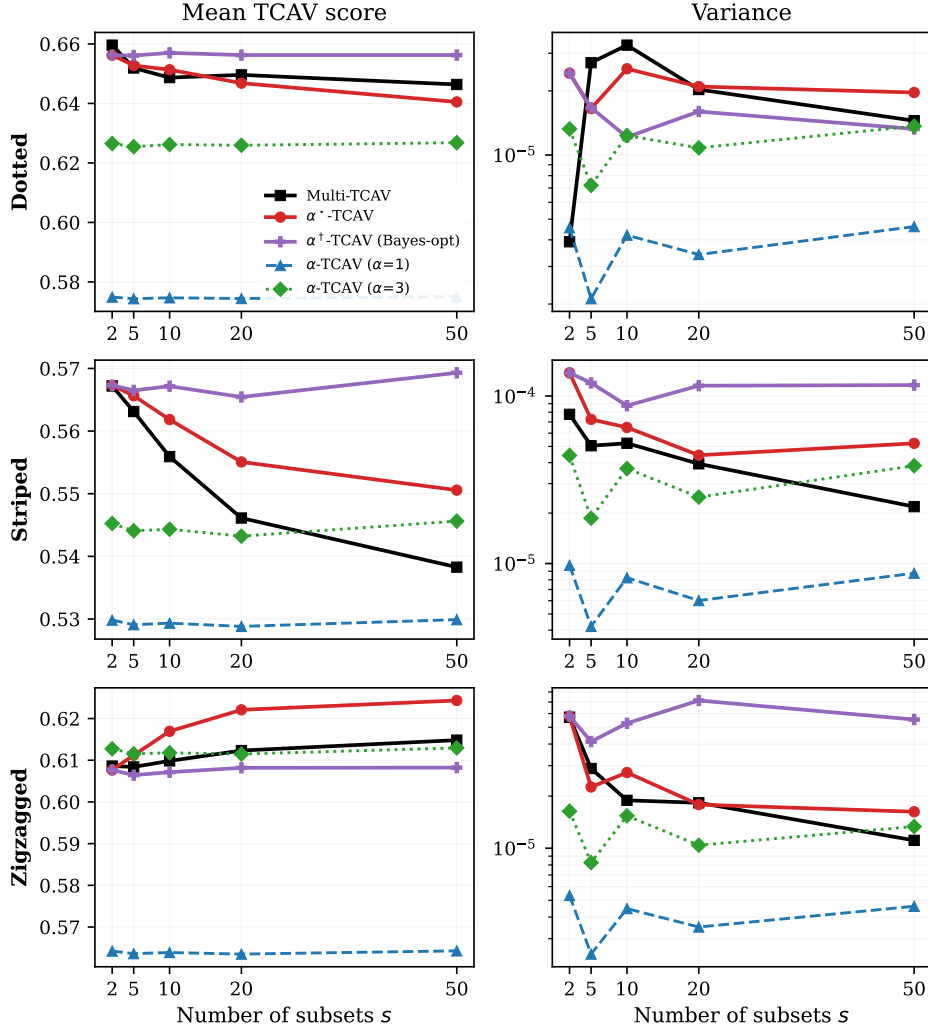


Figure 8: Comparison of TCAV methods on ResNet-50 (layer 2, PatternCAV; DTD textures, $R = 1000$, $E = 50$ repeats). **Left:** Mean TCAV score vs. number of subsets s . **Right:** Variance (log scale). α^\dagger -TCAV (purple) produces the most decisive mean across all concepts and values of s , consistent with its Bayesian interpretation (Eq. (43)), at the cost of higher variance. $\alpha = 1$ (blue) achieves the strongest variance reduction; $\alpha = 3$ (green) tracks the Multi-TCAV mean with moderate benefit. α^* -TCAV (red) adapts to the noise structure of each concept (see Table 2 for calibrated values). All α -TCAV variants require only a single CAV training on the full budget R , versus s CAVs for Multi-TCAV.

- 1. Optimal use of the sampling budget:** The common practice of Multi-TCAV means to partition a sample budget of N into s subsets to average multiple noisy estimates. Our analysis demonstrates that this approach is statistically suboptimal. Instead, we recommend using the **entire sample budget** N to estimate a single, high-fidelity CAV w_{CAV} . The desired robustness is more efficiently achieved by the smooth α -TCAV framework than by redundant ensemble averaging.
- 2. Selection of α :** The sharpness parameter α should be chosen based on the interpretative goals, rather than being treated as a hyperparameter to be tuned. Specifically:
 - **Stability objective (α^*):** To imitate Multi-TCAV (*i.e.*, to match the mean) while gaining superior stability, use the data-driven estimator α^* from (51). This method consistently reduces variance by more than 50% compared to standard averaging techniques.
 - **Bayesian objective (α^\dagger):** In cases where it is desirable that the TCAV score is the *calibrated probability that the concept contributes to the model's prediction*, choose α^\dagger from (43). This

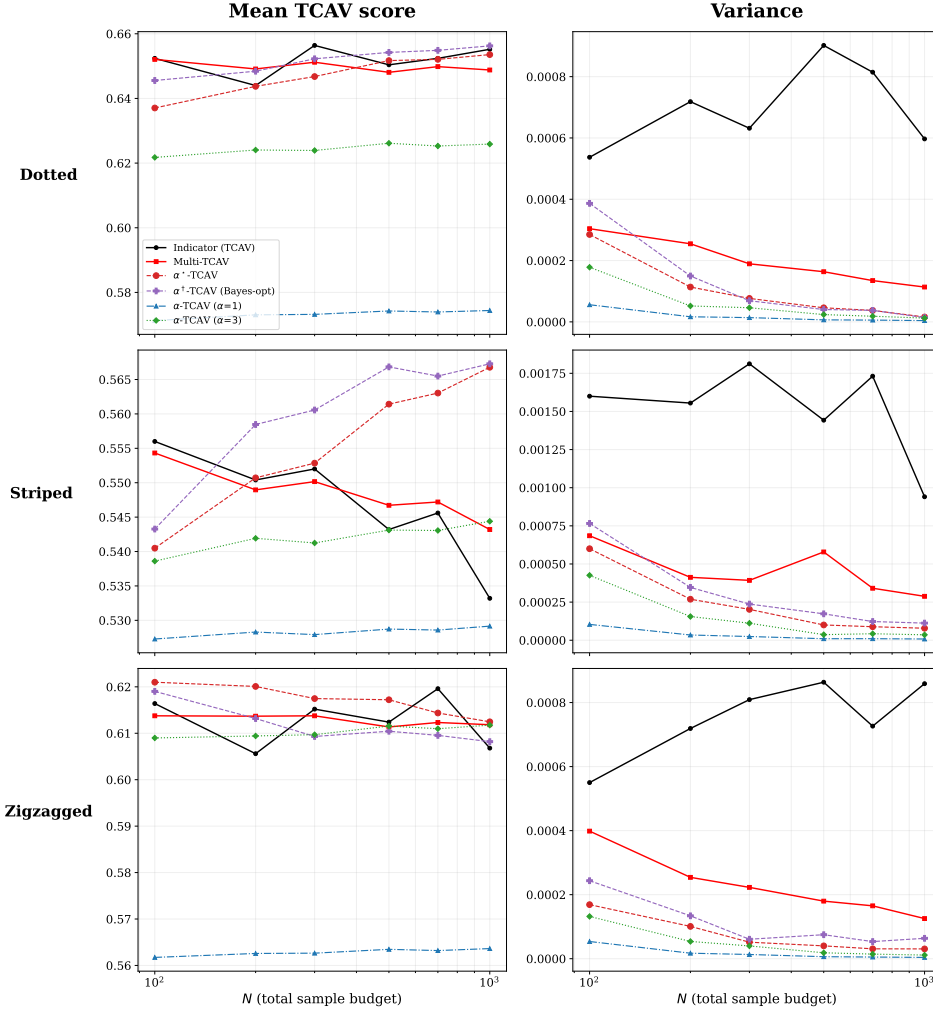


Figure 9: Effect of total sample budget N on TCAV scores (ResNet-50, layer 2, PatternCAV; fixed per-subset size $m_{\text{ind}} = 50$). **Left:** Mean TCAV score vs. N . **Right:** Variance vs. N . The indicator (black) exhibits a constant variance floor — the $\mathcal{O}(1)$ behavior of [Wenkmann and Garreau, 2025, Sec. 4.4]. All α -TCAV variants use the full budget for a single CAV and achieve $\mathcal{O}(1/N)$ decay. α^\dagger -TCAV (purple) lies between the indicator and Multi-TCAV, consistent with $\alpha^\dagger/\alpha^* = \sqrt{s-1}$ (Eq. (43)).

approach recasts the score as the posterior probability that a concept exerts a positive influence, providing a principled measure of epistemic uncertainty.

- 3. Scale normalization:** Sensitivity magnitudes can vary significantly across different layers of the network. To maintain a consistent interpretation of α , we recommend the normalization procedure described in Sec. 4.2. By rescaling sensitivities to unit root-mean-square, α becomes an absolute measure of sigmoid sharpness. For most architectures, $\alpha \in [1, 3]$ serves as a robust default.
- 4. Beyond scalar scores:** Since α -TCAV is computationally efficient once the CAV is fixed, practitioners are encouraged to evaluate scores across a range of α values. This "sensitivity profile" helps distinguish between concepts that are marginally influential (highly sensitive to α) and those that are robustly detected by the model across all smoothing scales.

Summary for the Practitioner: Avoid splitting your data to average multiple CAVs. Instead, train a single high-quality CAV on all data and apply the calibrated α -TCAV framework to obtain a score that is both statistically meaningful and significantly more stable than the current state-of-the-art.

5 Classification Accuracy

5.1 Preliminaries

We are interested in determining the asymptotically precise classification accuracy of a (normalized) linear classifier with weight vector $\mathbf{w} \in \mathbb{R}^d$ (such as a CAV $\mathbf{w}_{\text{CAV}} \in \mathbb{R}^{d_\ell}$ at the ℓ th layer) and threshold (or bias) $\eta \in \mathbb{R}$,

$$g(\mathbf{x}) = \frac{1}{\sqrt{n}} \mathbf{w}^\top \mathbf{x} \underset{\mathcal{C}_1}{\overset{\mathcal{C}_2}{\gtrless}} \eta, \quad (52)$$

applied to any data point $\mathbf{x} \in \mathbb{R}^d$. (Note that for an appropriate data preprocessing, simply $\eta = 0$ is optimal; compare Lemma 5.5.) Our derivation is based on the assumption of normally distributed classification scores, that for test data $\mathbf{x} \in \mathcal{C}_\ell$ from either class, the classification score $g(\mathbf{x}) = n^{-1/2} \mathbf{w}^\top \mathbf{x}$ follows a normal distribution $\mathcal{N}(\mu_\ell, \sigma_\ell^2)$, $\ell = 1, 2$. In this case, the optimal (in the sense of maximizing the classification accuracy) value for the threshold η^* is given by the intersection of the two density functions that is in-between the two means; in case of $\sigma_1^2 = \sigma_2^2$, it is simply given by $\eta = (\mu_1 + \mu_2)/2$. Schematically, this is illustrated in Figure 10. In Lemma 5.5, we will provide more technical details regarding the intersections of the density functions of normal distributions and optimal thresholds. This Gaussian behavior makes it possible to retrieve the precise classification accuracy with numerical integration. This behavior has been observed empirically in various works in experiments on real data; mathematically, the appearance of Gaussian distributions for inner products of the type $g(\mathbf{x}) = n^{-1/2} \mathbf{w}^\top \mathbf{x}$ is justified by the following result, which can be regarded as a variant of the *Central Limit Theorem* for concentrated random vectors. Originally, it is due to [Klartag, 2007, Fleury et al., 2007]; for the next result, we follow the presentation from [Seddik et al., 2021, Theorem 3.2].

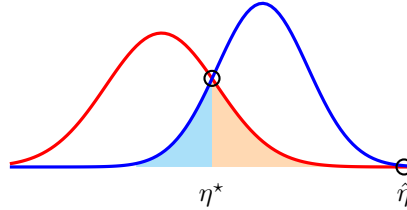


Figure 10: Illustration of the one-dimensional Gaussian distributions of the classification score $g(\mathbf{x}) = n^{-1/2} \mathbf{w}^\top \mathbf{x} \sim \mathcal{N}(\mu_\ell, \sigma_\ell^2)$ for $\mathbf{x} \in \mathcal{C}_\ell$, $\ell = 1, 2$, for both classes \mathcal{C}_1 (red) and \mathcal{C}_2 (blue). The smaller the “overlap” (cyan and orange area), for distant means and smaller variances, the higher is the classification accuracy. The optimal value of η^* is given at the intersection \circ of the density functions between the two means. A second intersection of the density functions is denoted as $\hat{\eta}$ (just for illustrational purposes).

Theorem 5.1 (Central Limit Theorem for Concentrated Random Vectors). *Let $\mathbf{x} \in \mathbb{R}^d$ be a random vector with $\mathbb{E}[\mathbf{x}] = \mathbf{0}$ and $\mathbb{E}[\mathbf{x} \mathbf{x}^\top] = \mathbf{I}_p$, satisfying the q -exponential concentration $\mathbf{x} \propto \mathcal{E}_2(1 | \mathbb{R}^d, \|\cdot\|_2)$ from B.2. Furthermore, let us denote by ν be the uniform measure on the sphere $S^{p-1} \subset \mathbb{R}^d$ of radius 1. Then, there exist two constants $C, c > 0$ and a set $\Omega \subset S^{p-1}$ such that $\nu(\Omega) \geq 1 - C\sqrt{p}e^{-c\sqrt{p}}$ and*

$$\sup_{t \in \mathbb{R}} |\mathbb{P}(\mathbf{w}^\top \mathbf{x} \geq t) - \Phi(t)| \leq p^{-1/4} \quad \forall \mathbf{w} \in \Omega. \quad (53)$$

where $\Phi(t) = \frac{1}{\sqrt{2\pi}} \int_{-\infty}^t e^{-x^2/2} dx$ is the cumulative distribution function of the standard normal distribution $\mathcal{N}(0, 1)$; see also (26).

The following result, Proposition 5.2, decomposes the classification score $g(\mathbf{x}) = n^{-1/2} \mathbf{w}^\top \mathbf{x}$ into terms based on data and model statistics - specifically the training data’s mean and covariance, and the weight vector’s mean and variance. Here, the weight vector $\mathbf{w} \in \mathbb{R}^d$ is treated as a random vector with a distribution induced by the training data \mathbf{X} . While the proposition is formulated generally for any two independent random vectors, it is primarily motivated by linear classifiers, where a new test

datum $\mathbf{x} \in \mathbb{R}^d$ is assumed to be independent of the training data \mathbf{X} , and therefore also independent of the learned parameters \mathbf{w} .

Proposition 5.2. *Consider two independent random vectors \mathbf{x}, \mathbf{w} taking values in \mathbb{R}^d , with means $\mathbb{E}[\mathbf{x}] = \bar{\mathbf{x}} \in \mathbb{R}^d$ and $\mathbb{E}[\mathbf{w}] = \bar{\mathbf{w}} \in \mathbb{R}^d$, and covariances $\text{Cov}(\mathbf{x}) = \boldsymbol{\Sigma}_x \in \mathbb{R}^{d \times d}$ and $\text{Cov}(\mathbf{w}) = \boldsymbol{\Sigma}_w \in \mathbb{R}^{d \times d}$, respectively. Then, for $g(\mathbf{x}) = \frac{1}{\sqrt{n}} \mathbf{x}^\top \mathbf{w}$, the following statements hold.*

$$\mathbb{E}_{\mathbf{w}, \mathbf{x}}[g(\mathbf{x})] = \frac{1}{\sqrt{n}} \mathbb{E}_{\mathbf{w}, \mathbf{x}}[\mathbf{w}^\top \mathbf{x}] = \frac{1}{\sqrt{n}} \bar{\mathbf{w}}^\top \bar{\mathbf{x}} \quad (54)$$

$$\text{Var}_{\mathbf{x}}(g(\mathbf{x})) = \mathbb{E}_{\mathbf{x}}[g(\mathbf{x})^2] - \mathbb{E}_{\mathbf{x}}[g(\mathbf{x})]^2 = \frac{1}{n} \text{Tr}(\boldsymbol{\Sigma}_x \mathbf{w} \mathbf{w}^\top) \quad (55)$$

$$\mathbb{E}_{\mathbf{w}}[\text{Var}_{\mathbf{x}}(g(\mathbf{x}))] = \frac{1}{n} \text{Tr}(\boldsymbol{\Sigma}_w \boldsymbol{\Sigma}_x) + \frac{1}{n} \text{Tr}(\boldsymbol{\Sigma}_x \bar{\mathbf{w}} \bar{\mathbf{w}}^\top), \quad (56)$$

$$\text{Var}_{\mathbf{w}, \mathbf{x}}(g(\mathbf{x})) = \mathbb{E}_{\mathbf{w}, \mathbf{x}}[g(\mathbf{x})^2] - \mathbb{E}_{\mathbf{w}, \mathbf{x}}[g(\mathbf{x})]^2 \quad (57)$$

$$= \frac{1}{n} \text{Tr}(\boldsymbol{\Sigma}_w \boldsymbol{\Sigma}_x) + \frac{1}{n} \text{Tr}(\boldsymbol{\Sigma}_w \bar{\mathbf{x}} \bar{\mathbf{x}}^\top) + \frac{1}{n} \text{Tr}(\boldsymbol{\Sigma}_x \bar{\mathbf{w}} \bar{\mathbf{w}}^\top) \quad (58)$$

Let us point out that in the situation of the above Proposition 5.2, there is a subtle difference between $\mathbb{E}_{\mathbf{w}}[\text{Var}_{\mathbf{x}}(g(\mathbf{x}))]$ from (56) and $\text{Var}_{\mathbf{w}, \mathbf{x}}(g(\mathbf{x}))$ from (57). For the first expression, note there is

$$\mathbb{E}_{\mathbf{w}}[\text{Var}_{\mathbf{x}}(g(\mathbf{x}))] = \mathbb{E}_{\mathbf{w}, \mathbf{x}}[g(\mathbf{x})^2] - \mathbb{E}_{\mathbf{w}}[\mathbb{E}_{\mathbf{x}}[g(\mathbf{x})]^2].$$

However, due to the mismatch in the second summand, this is generally *not* the same as the expression

$$\text{Var}_{\mathbf{w}, \mathbf{x}}(g(\mathbf{x})) = \mathbb{E}_{\mathbf{w}, \mathbf{x}}[g(\mathbf{x})^2] - \mathbb{E}_{\mathbf{w}, \mathbf{x}}[g(\mathbf{x})]^2,$$

It is the second the in (58), *i.e.*, the term $\frac{1}{n} \text{Tr}(\boldsymbol{\Sigma}_w \bar{\mathbf{x}} \bar{\mathbf{x}}^\top)$, that makes up for the difference between (56) and (57). Let us next prove Proposition 5.2.

Proof. Firstly, the expression (54) for the mean follows easily by linearity, and from the independence of the random vectors \mathbf{x} and \mathbf{w} . Secondly, for the variance conditionally on \mathbf{w} with respect to \mathbf{x} in (55) - note this is a random variable! - we obtain

$$\begin{aligned} \mathbb{E}_{\mathbf{x}}[g(\mathbf{x})^2] - \mathbb{E}_{\mathbf{x}}[g(\mathbf{x})]^2 &= \frac{1}{n} \mathbb{E}_{\mathbf{x}}[\mathbf{w}^\top \mathbf{x} \cdot \mathbf{w}^\top \mathbf{x}] - \frac{1}{n} \mathbf{w}^\top \bar{\mathbf{x}} \cdot \mathbf{w}^\top \bar{\mathbf{x}} \\ &= \frac{1}{n} \mathbb{E}[\mathbf{w}^\top (\mathbf{x} \mathbf{x}^\top - \bar{\mathbf{x}} \bar{\mathbf{x}}^\top) \mathbf{w}] = \frac{1}{n} \mathbf{w}^\top \boldsymbol{\Sigma}_x \mathbf{w}. \end{aligned}$$

Thirdly, for (56), we simply take our findings from (55) and pass to the expectation with respect to \mathbf{w} and obtain the claim

$$\begin{aligned} \mathbb{E}_{\mathbf{w}}[\text{Var}_{\mathbf{x}}(g(\mathbf{x}))] &= \mathbb{E}_{\mathbf{w}}[\mathbb{E}_{\mathbf{x}}[g(\mathbf{x})^2] - \mathbb{E}_{\mathbf{x}}[g(\mathbf{x})]^2] \\ &= \mathbb{E}_{\mathbf{w}}\left[\frac{1}{n} \text{Tr}(\boldsymbol{\Sigma}_x \mathbf{w} \mathbf{w}^\top)\right] = \frac{1}{n} \text{Tr}(\boldsymbol{\Sigma}_x (\boldsymbol{\Sigma}_w + \bar{\mathbf{w}} \bar{\mathbf{w}}^\top)). \end{aligned}$$

Finally, for the proof of the expression (57) for the joint variance, note that this expression can be rewritten easily as follows

$$\mathbb{E}_{\mathbf{w}, \mathbf{x}}[g(\mathbf{x})^2] - \mathbb{E}_{\mathbf{w}, \mathbf{x}}[g(\mathbf{x})]^2 = \frac{1}{n} \mathbb{E}_{\mathbf{w}, \mathbf{x}}[\mathbf{w}^\top \mathbf{x} \cdot \mathbf{w}^\top \mathbf{x}] - \frac{1}{n} (\bar{\mathbf{w}}^\top \bar{\mathbf{x}})^2 \quad (59)$$

$$= \frac{1}{n} \mathbb{E}_{\mathbf{w}, \mathbf{x}}[\mathbf{w}^\top \mathbf{x} \mathbf{x}^\top \mathbf{w}] - \frac{1}{n} \bar{\mathbf{w}}^\top \bar{\mathbf{x}} \bar{\mathbf{x}}^\top \bar{\mathbf{w}}. \quad (60)$$

Next, note that the first term on the right-hand side of (60) can, using basic trace and covariance properties, be rewritten as

$$\mathbb{E}_{\mathbf{w}, \mathbf{x}}[\mathbf{w}^\top \mathbf{x} \mathbf{x}^\top \mathbf{w}] = \text{Tr}(\mathbb{E}_{\mathbf{w}, \mathbf{x}}[\mathbf{w} \mathbf{w}^\top \mathbf{x} \mathbf{x}^\top]) = \text{Tr}((\boldsymbol{\Sigma}_w + \bar{\mathbf{w}} \bar{\mathbf{w}}^\top) (\boldsymbol{\Sigma}_x + \bar{\mathbf{x}} \bar{\mathbf{x}}^\top)).$$

Developing terms, normalizing by the factor $\frac{1}{n}$ inserting the resulting expression into (60) yields the desired result. \square

5.2 Predicting the Classification Error

After having found the class-specific means and variances of $g(\mathbf{x}) = n^{-1/2}\mathbf{w}^\top \mathbf{x}$ with the help of Proposition 5.2, we are now able to determine the theoretical classification error.

Proposition 5.3 (Classification Error and Scaling Invariance). *Let $\mathbf{w} \in \mathbb{R}^d$ be the weight vector of the linear model $g(\mathbf{x}) = n^{-1/2}\mathbf{w}^\top \mathbf{x}$ as defined in (52). Further, assume that the classification score $g(\mathbf{x})$ follows class-specific normal distributions for the two classes \mathcal{C}_1 and \mathcal{C}_2 , i.e., for $\mathbf{x} \in \mathcal{C}_\ell$,*

$$g(\mathbf{x}) \sim \mathcal{N}(\mu_\ell, \sigma_\ell^2), \quad \ell = 1, 2. \quad (61)$$

Then, the classification error can be computed as follows, and it is invariant under scaling of \mathbf{w} .

(i) *The classification error ϵ associated with any arbitrary decision threshold $\eta \in \mathbb{R}$ is given by*

$$\begin{aligned} \epsilon &\stackrel{\text{def}}{=} c_1 \cdot \mathbb{P}(\mathbf{x} \rightarrow \mathcal{C}_2 \mid \mathbf{x} \in \mathcal{C}_1) + c_2 \cdot \mathbb{P}(\mathbf{x} \rightarrow \mathcal{C}_1 \mid \mathbf{x} \in \mathcal{C}_2) \\ &= c_1 \cdot \mathbb{P}(X > \eta \mid X \sim \mathcal{N}(\mu_1, \sigma_1^2)) + c_2 \cdot \mathbb{P}(Y < \eta \mid Y \sim \mathcal{N}(\mu_2, \sigma_2^2)). \end{aligned} \quad (62)$$

(ii) *For any $\alpha \neq 0$, the scaled classifier $g_\alpha(\mathbf{x}) = \alpha \cdot g(\mathbf{x})$ yields the same classification error ϵ . The distribution of the corresponding classification score is given by $g_\alpha(\mathbf{x}) \sim \mathcal{N}(\alpha\mu_\ell, \alpha^2\sigma_\ell^2)$ for $\ell = 1, 2$, and the optimal threshold is $\eta_\alpha^* = \alpha\eta^*$, when η^* is optimal for g itself.*

Proof. The formula for ϵ in (62) follows directly from the classification rule (52) and the Gaussian assumptions (61). Regarding the scaling invariance, the distributions of $g_\alpha(\mathbf{x})$ are obtained from the basic property that $X \sim \mathcal{N}(\mu, \sigma^2)$ implies $\alpha X \sim \mathcal{N}(\alpha\mu, \alpha^2\sigma^2)$. Furthermore, for any decision threshold $\eta > 0$ and its scaled counterpart $\eta_\alpha = \alpha\eta$, the inequalities defining the classification rule are preserved, as

$$\mathbb{P}(g_\alpha(\mathbf{x}) \geq \eta_\alpha) = \mathbb{P}(\alpha g(\mathbf{x}) \geq \alpha\eta) = \mathbb{P}(g(\mathbf{x}) \geq \eta).$$

Thus, the misclassification probability remains invariant for any threshold, which implies the result holds in particular for the optimal threshold η^* (where $\eta_\alpha^* = \alpha\eta^*$). \square

Remark 5.4 (Classification Accuracy of PatternCAV and FastCAV). A consequence of this results is that by the findings in Sec. 2, in particular by the scaling (6) between \mathbf{w}_{pat} from (1) and \mathbf{w}_{fast} from (3), *FastCAV* and *PatternCAV* have the same classification accuracy, assuming normally distributed classification scores.

The two terms constituting the misclassification error ϵ in (62) correspond to the colored areas in Figure 10. Notably, the classification accuracy is determined solely by the scalars $\mu_1, \mu_2, \sigma_1^2, \sigma_2^2$, allowing ϵ to be computed via numerical integration of the normal distribution’s cumulative distribution function (CDF). To obtain these scalars, one must estimate both the data statistics and the model’s weight distribution. While data means and covariances are typically estimated empirically, deriving the distribution induced over \mathbf{w} is more involved and will be discussed in detail in Section 2.

The assumption of normally distributed scores $g(\mathbf{x})$ is highly realistic under Assumption B.3 and is frequently observed in practice. This phenomenon is supported by [Seddik et al., 2021, Theorem 3.2], as well as versions of the Central Limit Theorem for concentrated random vectors [Klartag, 2007, Fleury et al., 2007]. Finally, per Proposition 5.3, the classification performance is invariant to the scaling of \mathbf{w} by a constant factor—a property that facilitates the subsequent comparison between the *PatternCAV* and *FastCAV*.

The following result, Lemma 5.5, characterizes the intersections of normal distributions to determine optimal decision thresholds. Although these findings are elementary and similarly results have been used before (sometimes without explicitly mentioning), we provide a formal statement to ensure the paper is self-contained and provide an easy future reference. While the analysis of density function intersections in Lemma 5.5(i) follows an online discussion on *stats.stackexchange* [StackExchange Community, 2017], we complement this with parts (ii) and (iii). These sections provide a rigorous analysis of intersection locations and establish the formal link to optimal decision thresholds in binary classification settings with normally distributed scores. We also refer to [Das and Geisler, 2021] for related topics. As a technical preparation for the following result, let us briefly recall the distribution function f_{μ, σ^2} of a normally distributed random variable $X \sim \mathcal{N}(\mu, \sigma^2)$ with mean $\mu \in \mathbb{R}$ and standard deviation $\sigma > 0$, together with its derivative f'_{μ, σ^2} and its logarithm (note that the density is positive everywhere),

$$f_{\mu, \sigma^2}(x) = \frac{1}{\sqrt{2\pi\sigma^2}} \exp\left(-\frac{(x-\mu)^2}{2\sigma^2}\right), \quad (63)$$

$$f'_{\mu, \sigma^2}(x) = -\frac{(x-\mu)}{\sigma^2} \cdot \frac{1}{\sqrt{2\pi\sigma^2}} \exp\left(-\frac{(x-\mu)^2}{2\sigma^2}\right) = -\frac{x-\mu}{\sigma^2} f_{\mu, \sigma^2}(x), \quad (64)$$

$$\log(f_{\mu, \sigma^2}(x)) = -\frac{1}{2} \log(2\pi\sigma^2) - \frac{(x-\mu)^2}{2\sigma^2}. \quad (65)$$

Now we are ready to state and prove the following result.

Lemma 5.5. *Consider two univariate normal distributions with the density functions f_{μ_1, σ_1^2} and f_{μ_2, σ_2^2} (let us just write shortly f_1 and f_2), with their characterizing means $\mu_1, \mu_2 \in \mathbb{R}$ and standard deviations $\sigma_1, \sigma_2 > 0$. Then, the following hold.*

- (i) **Intersections of the density functions:** *For equal means $\mu_1 = \mu_2$ and variances $\sigma_1^2 = \sigma_2^2$, the density functions trivially coincide and every point is an intersection. Further, in the case of $\sigma_1^2 = \sigma_2^2$ but $\mu_1 \neq \mu_2$,*

$$x = \frac{\mu_1 + \mu_2}{2} \quad (66)$$

is the unique intersection, i.e., the only $x \in \mathbb{R}$ with $f_1(x) = f_2(x)$. Finally, in any other case (which exactly consists of the two cases of either $\mu_1 = \mu_2$ but $\sigma_1^2 \neq \sigma_2^2$, or when both $\mu_1 \neq \mu_2$ and $\sigma_1^2 \neq \sigma_2^2$), there always exist the two intersections $x_1, x_2 \in \mathbb{R}$ given by

$$x_{1,2} = \frac{-b \pm \sqrt{b^2 - 4ac}}{2a}, \quad (67)$$

which can be found as the solutions of the quadratic equation $ax^2 + bx + c = 0$, with a, b and c given by

$$a = 1/\sigma_2^2 - 1/\sigma_1^2, \quad (68)$$

$$b = 2(\mu_1/\sigma_1^2 - \mu_2/\sigma_2^2), \quad (69)$$

$$c = \log(\sigma_2^2/\sigma_1^2) + \mu_2^2/\sigma_2^2 - \mu_1^2/\sigma_1^2. \quad (70)$$

- (ii) **Location of the intersections:** *Let us assume that both the means and the variances are different, i.e., we consider $\mu_1 \neq \mu_2$ and $\sigma_1^2 \neq \sigma_2^2$. In this case, the two distinct solutions x_1, x_2 from (67) both exist. W.l.o.g. we assume $\mu_1 < \mu_2$. Then, we have either $\mu_1 < x_1 < \mu_2$ or $\mu_1 < x_2 < \mu_2$, while in each case the remaining second solution lies outside of the interval $[\mu_1, \mu_2]$.*
- (iii) **Optimizing the decision threshold:** *In the situation of part (ii), and denoting the argument of the intersection in-between the means by $\eta^* \in (\mu_1, \mu_2)$, it holds that $\eta^* = \arg \min_{\eta \in \mathbb{R}} h(\eta)$, where $h: \mathbb{R} \rightarrow \mathbb{R}$ is given by*

$$h(\eta) := \mathbb{P}(X_1 > \eta | X_1 \sim \mathcal{N}(\mu_1, \sigma_1^2)) + \mathbb{P}(X_2 < \eta | X_2 \sim \mathcal{N}(\mu_2, \sigma_2^2)). \quad (71)$$

In binary classification via (52), this gives the optimal threshold η^ minimizing the misclassification probability (62) for balanced classes (omitting the factors $c_1 = c_2 = \frac{1}{2}$ in h); see Proposition 5.3 and Figure 10.*

Let us proceed with the proof of Lemma 5.5. Note that this is a basic result and we do not claim any originality of this work; partly we follow [StackExchange Community, 2017]; see also [Das and Geisler, 2021] as a major reference in this regard. Still, we provide the following proof for completeness and easy future reference, as we are not aware of an easily citable reference.

Proof of Lemma 5.5. Even though the proof is elementary, let us point out once more that for the proof of part (i) we follow [StackExchange Community, 2017]. Towards finding the intersections of f_1 and f_2 , recall they are positive everywhere (i.e., $f_1(x) > 0$ and $f_2(x) > 0$ for all $x \in \mathbb{R}$), so that

$$f_1(x) = f_2(x) \iff \log(f_1(x)) - \log(f_2(x)) = 0. \quad (72)$$

We solve the equation on the right hand side of (72). Multiplying by 2 and inserting (65) twice,

$$\begin{aligned}
0 &= -\log(2\pi\sigma_1^2) - \frac{(x-\mu_1)^2}{\sigma_1^2} + \log(2\pi\sigma_2^2) + \frac{(x-\mu_2)^2}{\sigma_2^2} \\
&= \log\left(\frac{\sigma_2^2}{\sigma_1^2}\right) + \frac{x^2 - 2x\mu_2 + \mu_2^2}{\sigma_2^2} - \frac{x^2 - 2x\mu_1 + \mu_1^2}{\sigma_1^2} \\
&= ax^2 + bx + c,
\end{aligned}$$

we have arrived at a quadratic equation characterized by the factors a, b, c which depend on the different means and variances,

$$\begin{aligned}
a &= 1/\sigma_2^2 - 1/\sigma_1^2, \\
b &= 2(\mu_1/\sigma_1^2 - \mu_2/\sigma_2^2), \\
c &= \log(\sigma_2^2/\sigma_1^2) + \mu_2^2/\sigma_2^2 - \mu_1^2/\sigma_1^2.
\end{aligned}$$

For $a = 0$, in case of $\sigma_1^2 = \sigma_2^2$, the (unique!) solution when $\mu_1 \neq \mu_2$ (if $\mu_1 = \mu_2$, the distributions and density functions trivially coincide) is simply given by $x = -c/b$, and a straightforward calculation indeed yields (66). Finally, let us consider the general case $\sigma_1^2 \neq \sigma_2^2$, such that $a \neq 0$, when the general solution formula is given by (67). We show that indeed always the two solutions exist. For the discriminant, *i.e.*, the expression under the square root in (67), a simple computation yields

$$\begin{aligned}
\Delta &= b^2 - 4ac \\
&= 4(\mu_1/\sigma_1^2 - \mu_2/\sigma_2^2)^2 - 4(1/\sigma_2^2 - 1/\sigma_1^2)(\log(\sigma_2^2/\sigma_1^2) + \mu_2^2/\sigma_2^2 - \mu_1^2/\sigma_1^2) \\
&= 4\left[\mu_1^2/\sigma_1^4 - 2\mu_1\mu_2/\sigma_1^2\sigma_2^2 + \mu_2^2/\sigma_2^4 - (1/\sigma_2^2 - 1/\sigma_1^2)\log(\sigma_2^2/\sigma_1^2) \right. \\
&\quad \left. - \mu_2^2/\sigma_2^4 + \mu_1^2/\sigma_1^2\sigma_2^2 + \mu_2^2/\sigma_1^2\sigma_2^2 - \mu_1^2/\sigma_1^4\right] \\
&= 4\left[(\mu_1 - \mu_2)^2/\sigma_1^2\sigma_2^2 + (\sigma_1^2 - \sigma_2^2)/\sigma_1^2\sigma_2^2 \log(\sigma_1^2/\sigma_2^2)\right] \\
&= \frac{4}{\sigma_1^2\sigma_2^2} \left[(\mu_1 - \mu_2)^2 + (\sigma_1^2 - \sigma_2^2)\log(\sigma_1^2/\sigma_2^2)\right].
\end{aligned}$$

Now note that $(\sigma_1^2 - \sigma_2^2)$ and $\log(\sigma_1^2/\sigma_2^2)$ always have the same sign, making their product and thus the entire expression of Δ non-negative, *i.e.*, $\Delta \geq 0$; further $\Delta = 0$ holds if and only if $\mu_1 = \mu_2$ and $\sigma_1^2 = \sigma_2^2$ with infinitely many solutions, as remarked above. In every other case, there are always two solutions which can be found by (67).

Next, let us move to the proof of part (ii). Recall that w.l.o.g. we assumed that $\mu_1 < \mu_2$; further let us remark that a point of intersection, *i.e.*, some $x \in \mathbb{R}$ with $f_1(x) = f_2(x)$ is equivalent to a root point of the function g defined as the difference of the functions $g(x) = f_1(x) - f_2(x)$. Now, in case of $\sigma_1^2 < \sigma_2^2$ (or $\sigma_1^2 > \sigma_2^2$), the function g is strictly monotonically decreasing (increasing) $g(\mu_1) > 0$ and $g(\mu_2) < 0$ (or vice versa, *i.e.*, $g(\mu_1) < 0$ and $g(\mu_2) > 0$). By the mean value theorem and strict monotonicity, it follows that g has a unique root point in (μ_1, μ_2) , which is the unique point of intersection of the functions f_1 and f_2 within this interval. The remaining intersection lies in either of the intervals $(-\infty, \mu_1)$ or (μ_2, ∞) . More precisely (still assuming $\mu_1 < \mu_2$; otherwise, just switch the roles of f_1 and f_2) and distinguishing between the cases $\sigma_1^2 < \sigma_2^2$ and $\sigma_1^2 > \sigma_2^2$, by comparing the derivatives of the density function we clearly find for the solutions $x_{1,2}$ of (67) that

$$\sigma_1^2 < \sigma_2^2 \implies x_1 < \mu_1 < x_2 < \mu_2, \quad (73)$$

$$\sigma_2^2 < \sigma_1^2 \implies \mu_1 < x_1 < \mu_2 < x_2. \quad (74)$$

Finally, let us turn to part (iii). By elementary properties of the normal distribution, we have for the function h from (71) that

$$\begin{aligned}
h(\eta) &= \mathbb{P}(X_1 > \eta | X_1 \sim \mathcal{N}(\mu_1, \sigma_1^2)) + \mathbb{P}(X_2 < \eta | X_2 \sim \mathcal{N}(\mu_2, \sigma_2^2)) \\
&= \frac{1}{\sqrt{2\pi\sigma_1^2}} \int_{\eta}^{\infty} \exp\left(-\frac{(x-\mu_1)^2}{2\sigma_1^2}\right) dx + \frac{1}{\sqrt{2\pi\sigma_2^2}} \int_{-\infty}^{\eta} \exp\left(-\frac{(x-\mu_2)^2}{2\sigma_2^2}\right) dx \\
&= 1 - \frac{1}{\sqrt{2\pi\sigma_1^2}} \int_{-\infty}^{\eta} \exp\left(-\frac{(x-\mu_1)^2}{2\sigma_1^2}\right) dx + \frac{1}{\sqrt{2\pi\sigma_2^2}} \int_{-\infty}^{\eta} \exp\left(-\frac{(x-\mu_2)^2}{2\sigma_2^2}\right) dx.
\end{aligned}$$

Next, by the fundamental theorem of calculus, computing the derivative of h and putting $h'(\eta) = -f_1(\eta) + f_2(\eta) = 0$ simply leads to the equation $f_1(\eta) = f_2(\eta)$, or any of its equivalent formulations that we have already seen in (72) and solved above with the two solutions $\eta = x_1$ and $\eta = x_2$. We still have to show that the one solution that falls into the interval (μ_1, μ_2) is indeed the minimizer of h . Therefore, we compute the second derivative h'' , and with the help of (64) we obtain

$$\begin{aligned} h''(\eta) &= -f_1'(\eta) + f_2'(\eta) \\ &= \frac{(\eta - \mu_1)}{\sigma_1^2} \cdot \frac{1}{\sqrt{2\pi\sigma_1^2}} \exp\left(-\frac{(\eta - \mu_1)^2}{2\sigma_1^2}\right) - \frac{(\eta - \mu_2)}{\sigma_2^2} \cdot \frac{1}{\sqrt{2\pi\sigma_2^2}} \exp\left(-\frac{(\eta - \mu_2)^2}{2\sigma_2^2}\right). \end{aligned}$$

Evaluating h'' at η^* (which may be either x_1 or x_2) from part (ii), and just letting $f(\eta^*) := f_{\mu_1, \sigma_1^2}(\eta^*) = f_{\mu_2, \sigma_2^2}(\eta^*)$, yields

$$\begin{aligned} h''(\eta^*) &= \frac{(\eta^* - \mu_1)}{\sigma_1^2} f_{\mu_1, \sigma_1^2}(\eta^*) - \frac{(\eta^* - \mu_2)}{\sigma_2^2} f_{\mu_2, \sigma_2^2}(\eta^*) \\ &= \left[\frac{(\eta^* - \mu_1)}{\sigma_1^2} - \frac{(\eta^* - \mu_2)}{\sigma_2^2} \right] f(\eta^*) \\ &> 0, \end{aligned}$$

since $\mu_1 < \eta^* < \mu_2$ and $f(\eta^*) > 0$. As $h''(\eta^*) > 0$, we conclude that h has a strict local minimum in η^* . To finish the proof, we need to argue that this is the only minimum and the remaining point of intersection cannot be a minimum. Indeed, note that $\lim_{\eta \rightarrow \pm\infty} h(\eta) = 1$; therefore, if the remaining critical point would be a local minimum as well, the function h would need to have a local maximum, too. However, this cannot be the case as only two critical points of h exist, namely at the two intersections of the densities f_1 and f_2 . Therefore, the minimum of h attained in η^* must be a global minimum. \square

Remark 5.6. Note that changing the roles of f_1 and f_2 only changes the signs of the coefficients a, b, c from (68), (69) and (70). Geometrically, if the original parabola $ax^2 + bx + c$ opened upward, the new parabola opens downward (and vice versa), but has exactly the same roots $x_{1,2}$ as given in (67).

5.3 Numerical Experiments

We provide numerical experiments both for synthetic data (Fig. 11) and real data (Fig. 12), illustrating the above approach to predict the classification accuracy.

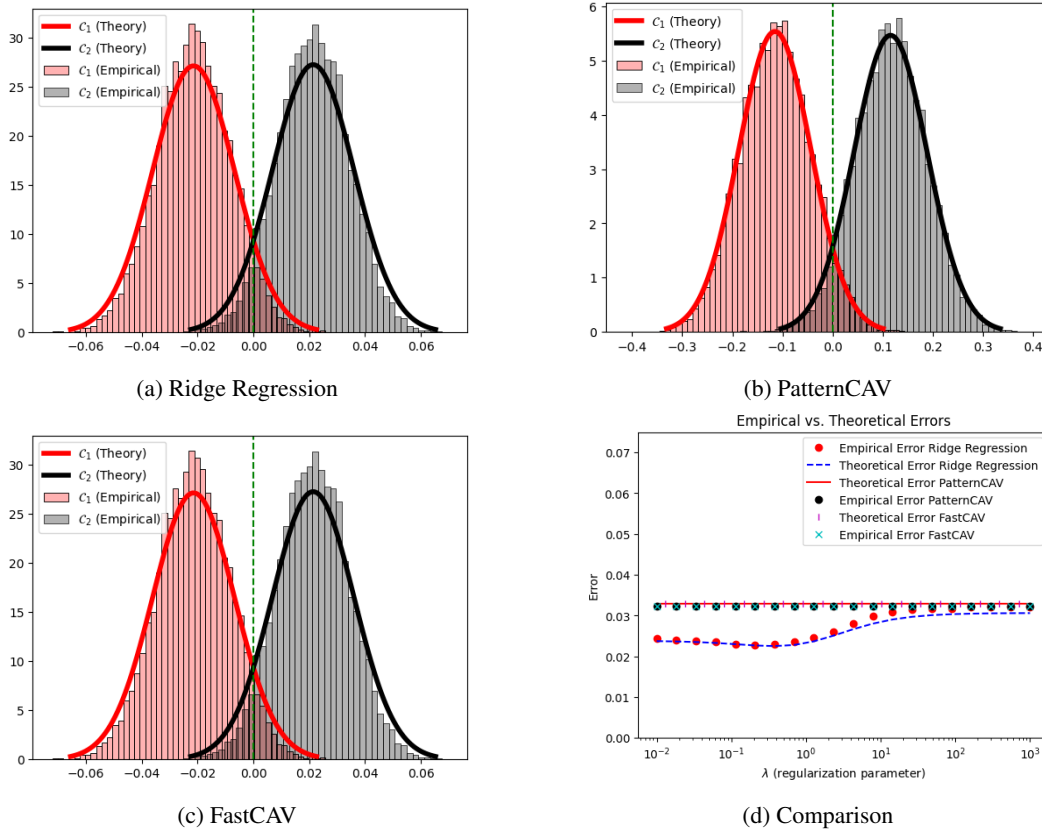


Figure 11: Comparison of theoretical prediction and histogram of empirical simulation of the classification score $g(x) = w_{\text{CAV}}^T x$, for ridge regression 11a, *PatternCAV* 11b, *FastCAV* 11c, and comparison of the classification error over different values of λ for the ridge regression (while simply repeating the values for the ridge *PatternCAV* and *FastCAV*) in (11d), showing the quality of the theoretical prediction, the agreement between *PatternCAV* and *FastCAV* (and also ridge regression for sufficiently large λ). The data follows a multivariate normal distribution for two classes with randomly generated $\mu_1 \in \mathbb{R}^d$ and $\mu_2 = -\mu_1$. The covariances Σ_1, Σ_2 are Toeplitz matrices, defined by $(\Sigma_k)_{i,j} = \alpha_k^{|i-j|}$ with the parameters $\alpha_1 = 0.2$ and $\alpha_2 = 0.4$. The experiments have been performed in *GoogleColab*.

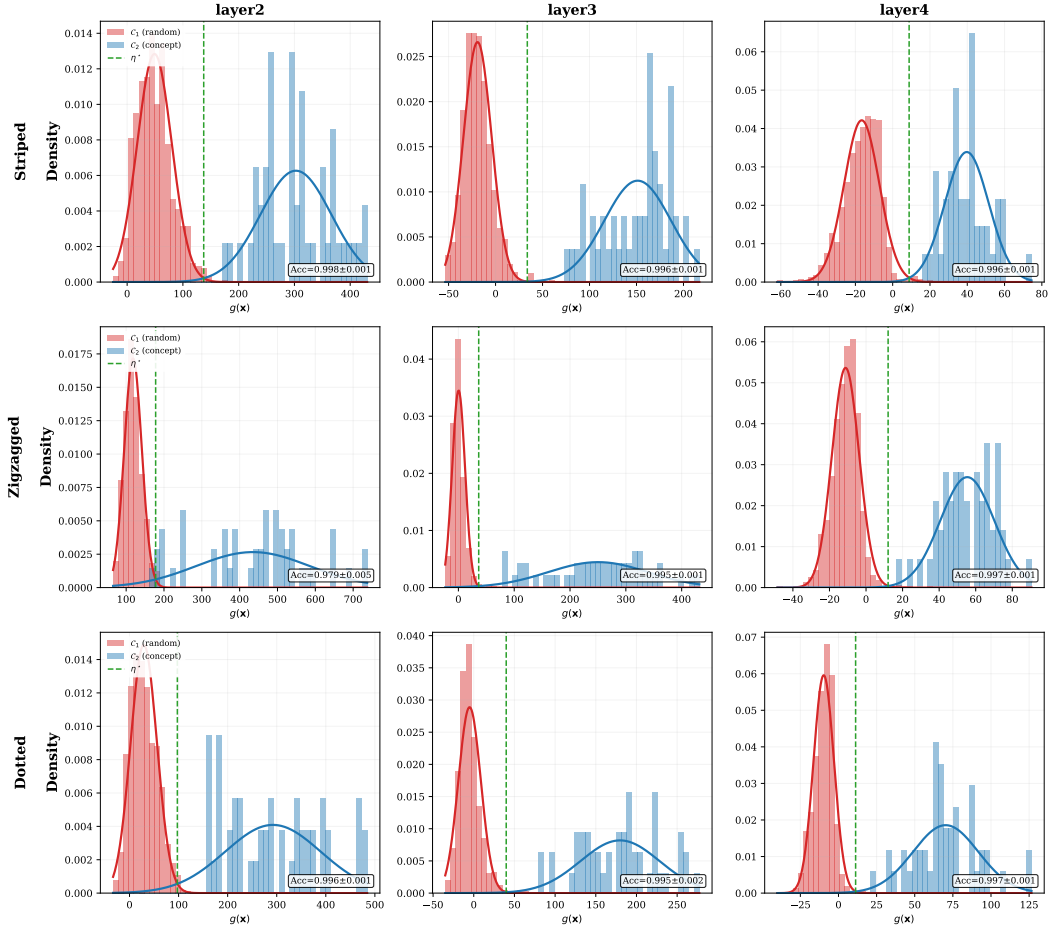


Figure 12: Classification score distributions of *PatternCAV* on *ResNet-50* (**rows:** the concepts *striped*, *zigzagged* and *dotted*; **columns:** layer2 to layer4). Histograms show the empirical density of $g(\mathbf{x}) = \mathbf{w}_{\text{CAV}} \mathbf{x}$, where \mathbf{x} denotes the laten activation of either *non-concept* (\mathcal{C}_1 , red, 1000 samples) or *concept* (\mathcal{C}_2 , blue, 50 samples) classes; solid curves are *fitted Gaussians* (theoretical prediction in advance — like in Fig. 11 — is difficult to to the very large dimension of the layers, e.g. regarding reliable covariance estimation). The dashed green line is the optimal threshold η^* from the general quadratic formula of Lemma 5.5. The accuracy averaged over 20 runs (0.979–0.998) confirms reliable concept encoding across all layers. While we observe by visual inspection a close match of the *non-concept* (red) data histogram to the fitted Gaussian curve, the Gaussian behavior is clearly less pronounced for the *concept* data (blue), likely due to the much lower sample size.

Acknowledgement. This work was supported by the German Research Foundation (DFG) as research unit DeSbi [KI-FOR 5363] (459422098), by the Research Council of Finland (Decision #363624) as *A Mathematical Theory of Trustworthy Federated Learning (MATHFUL)*, by the Jane and Aatos Erkko Foundation (Decision #A835) as *A Mathematical Theory of Federated Learning (TRUST-FELT)*, and by Business Finland as *Forward-Looking AI Governance in Banking & Insurance (FLAIG)*.

References

- Karen Simonyan, Andrea Vedaldi, and Andrew Zisserman. Deep inside convolutional networks: Visualising image classification models and saliency maps. *arXiv preprint arXiv:1312.6034*, 2013.
- Ramprasaath R Selvaraju, Michael Cogswell, Abhishek Das, Ramakrishna Vedantam, Devi Parikh, and Dhruv Batra. Grad-cam: Visual explanations from deep networks via gradient-based localization. In *Proceedings of the IEEE international conference on computer vision*, pages 618–626, 2017.
- Mukund Sundararajan, Ankur Taly, and Qiqi Yan. Axiomatic attribution for deep networks. In *International conference on machine learning*, pages 3319–3328. PMLR, 2017.
- Been Kim, Martin Wattenberg, Justin Gilmer, Carrie Cai, James Wexler, Fernanda Viegas, et al. Interpretability beyond feature attribution: Quantitative testing with concept activation vectors (tcav). In *International conference on machine learning*, pages 2668–2677. PMLR, 2018.
- Amirata Ghorbani, James Wexler, James Y Zou, and Been Kim. Towards automatic concept-based explanations. *Advances in neural information processing systems*, 32, 2019.
- Reduan Achtibat, Maximilian Dreyer, Ilona Eisenbraun, Sebastian Bosse, Thomas Wiegand, Wojciech Samek, and Sebastian Lapuschkin. From attribution maps to human-understandable explanations through concept relevance propagation. *Nature Machine Intelligence*, 5(9):1006–1019, 2023.
- Sebastian Bach, Alexander Binder, Grégoire Montavon, Frederick Klauschen, Klaus-Robert Müller, and Wojciech Samek. On pixel-wise explanations for non-linear classifier decisions by layer-wise relevance propagation. *PloS one*, 10(7):e0130140, 2015.
- Halil Ibrahim Aysel, Xiaohao Cai, and Adam Prugel-Bennett. Concept-based explainable artificial intelligence: Metrics and benchmarks. *arXiv preprint arXiv:2501.19271*, 2025.
- Eleonora Poeta, Gabriele Ciravegna, Eliana Pastor, Tania Cerquitelli, and Elena Baralis. Concept-based explainable artificial intelligence: A survey. *ACM Computing Surveys*, 2023.
- Maximilian Dreyer, Frederik Pahde, Christopher J Anders, Wojciech Samek, and Sebastian Lapuschkin. From hope to safety: Unlearning biases of deep models via gradient penalization in latent space. In *Proceedings of the AAAI Conference on Artificial Intelligence*, volume 38, pages 21046–21054, 2024.
- Frederik Pahde, Maximilian Dreyer, Moritz Weckbecker, Leander Weber, Christopher J. Anders, Thomas Wiegand, Wojciech Samek, and Sebastian Lapuschkin. Navigating neural space: Revisiting concept activation vectors to overcome directional divergence. In *International Conference on Learning Representations*, 2022. URL <https://api.semanticscholar.org/CorpusID:246652506>.
- Stefan Haufe, Frank Meinecke, Kai Görden, Sven Dähne, John-Dylan Haynes, Benjamin Blankertz, and Felix Bießmann. On the interpretation of weight vectors of linear models in multivariate neuroimaging. *Neuroimage*, 87:96–110, 2014.
- Tyler Martin and Adrian Weller. Interpretable machine learning. *M. Phil. diss., Dept. of Engineering, University of Cambridge*, 2(3):5, 2019.
- Laines Schmalwasser, Niklas Penzel, Joachim Denzler, and Julia Niebling. Fastcav: Efficient computation of concept activation vectors for explaining deep neural networks. In *Proceedings of the 42nd International Conference on Machine Learning (ICML)*, 2025.
- Aðalsteinn Pálsson and Yngvi Björnsson. Unveiling concepts learned by a world-class chess-playing agent. In *IJCAI*, pages 4864–4872, 2023.
- Thomas McGrath, Andrei Kapishnikov, Nenad Tomašev, Adam Pearce, Martin Wattenberg, Demis Hassabis, Been Kim, Ulrich Paquet, and Vladimir Kramnik. Acquisition of chess knowledge in alphazero. *Proceedings of the National Academy of Sciences*, 119(47):e2206625119, 2022.
- Lisa Schut, Nenad Tomasev, Tom McGrath, Demis Hassabis, Ulrich Paquet, and Been Kim. Bridging the human-ai knowledge gap: Concept discovery and transfer in alphazero. *CoRR*, 2023.

- Pang Wei Koh, Thao Nguyen, Yew Siang Tang, Stephen Mussmann, Emma Pierson, Been Kim, and Percy Liang. Concept bottleneck models. In *International conference on machine learning*, pages 5338–5348. PMLR, 2020.
- Mert Yuksekogonul, Maggie Wang, and James Zou. Post-hoc concept bottleneck models. *arXiv preprint arXiv:2205.15480*, 2022.
- Antonio De Santis, Riccardo Campi, Matteo Bianchi, and Marco Brambilla. Visual-tcav: Concept-based attribution and saliency maps for post-hoc explainability in image classification. *arXiv preprint arXiv:2411.05698*, 2024.
- Jonathan Crabbé and Mihaela van der Schaar. Concept activation regions: A generalized framework for concept-based explanations. *Advances in Neural Information Processing Systems*, 35:2590–2607, 2022.
- Haiyan Zhao, Xuansheng Wu, Fan Yang, Bo Shen, Ninghao Liu, and Mengnan Du. Denoising concept vectors with sparse autoencoders for improved language model steering. In *Findings of the Association for Computational Linguistics: EACL 2026*, pages 797–808, 2026.
- Hanyu Zhang, Xiting Wang, Chengao Li, Xiang Ao, and Qing He. Controlling large language models through concept activation vectors. In *Proceedings of the AAAI Conference on Artificial Intelligence*, volume 39, pages 25851–25859, 2025.
- Chung-En Sun, Tuomas Oikarinen, Berk Ustun, and Tsui-Wei Weng. Concept bottleneck large language models. *arXiv preprint arXiv:2412.07992*, 2024.
- Joris Postmus and Steven Abreu. Steering large language models using conceptors: Improving addition-based activation engineering. *arXiv preprint arXiv:2410.16314*, 2024.
- Thomas Fel, Augustin Picard, Louis Bethune, Thibaut Boissin, Julien Colin, Spyros Gidaris, and Thomas Serre. A holistic approach to unifying automatic concept extraction and concept importance estimation. In *Advances in Neural Information Processing Systems*, volume 36, 2023.
- Arjun Akula, Shuai Wang, and Song-Chun Zhu. Cocox: Generating conceptual and counterfactual explanations via fault-lines. In *Proceedings of the AAAI conference on artificial intelligence*, volume 34, pages 2594–2601, 2020.
- David Alvarez Melis and Tommi Jaakkola. Towards robust interpretability with self-explaining neural networks. *Advances in neural information processing systems*, 31, 2018.
- Satyapriya Krishna, Tessa Han, Alex Gu, Javin Pombra, Shahin Jabbari, Steven Wu, and Himabindu Lakkaraju. The disagreement problem in explainable machine learning: A practitioner’s perspective. *Trans. Mach. Learn. Res.*, 2024, 2022. URL <https://api.semanticscholar.org/CorpusID:246485817>.
- Julia Wenkmann and Damien Garreau. On the variability of concept activation vectors. *arXiv preprint arXiv:2509.24058*, 2025.
- Ekkehard Schnoor, Malik Tiomoko, Jawher Said, Alex Jung, and Wojciech Samek. Concept activation vectors: a unifying view and adversarial attacks. In *ICASSP 2026-2026 IEEE International Conference on Acoustics, Speech and Signal Processing (ICASSP)*, pages 3481–3485. IEEE, 2026.
- Jarl Waldemar Lindeberg. Eine neue herleitung des exponentialgesetzes in der wahrscheinlichkeit-srechnung. *Mathematische Zeitschrift*, 15(1):211–225, 1922.
- Roman Vershynin. A friendly proof of the berry-esseen theorem. *arXiv preprint arXiv:2602.06234*, 2026.
- Charles Stein. A bound for the error in the normal approximation to the distribution of a sum of dependent random variables. In *Proceedings of the sixth Berkeley symposium on mathematical statistics and probability, volume 2: Probability theory*, volume 6, pages 583–603. University of California Press, 1972.
- Damien Garreau and Ulrike Luxburg. Explaining the explainer: A first theoretical analysis of lime. In *International conference on artificial intelligence and statistics*, pages 1287–1296. PMLR, 2020.

- Damien Garreau and Ulrike von Luxburg. Looking deeper into tabular lime. *arXiv preprint arXiv:2008.11092*, 2020.
- Marco Tulio Ribeiro, Sameer Singh, and Carlos Guestrin. " why should i trust you?" explaining the predictions of any classifier. In *Proceedings of the 22nd ACM SIGKDD international conference on knowledge discovery and data mining*, pages 1135–1144, 2016.
- Tyler Chen, Akshay Seshadri, Mattia J Villani, Pradeep Niroula, Shouvanik Chakrabarti, Archan Ray, Pranav Deshpande, Romina Yalovetzky, Marco Pistoia, and Niraj Kumar. A unified framework for provably efficient algorithms to estimate shapley values. *arXiv preprint arXiv:2506.05216*, 2025.
- Lloyd S Shapley et al. A value for n-person games. 1953.
- Scott M Lundberg and Su-In Lee. A unified approach to interpreting model predictions. *Advances in neural information processing systems*, 30, 2017.
- Angus Nicolson, Lisa Schut, Alison Noble, and Yarin Gal. Explaining explainability: Recommendations for effective use of concept activation vectors. *Transactions on Machine Learning Research*.
- Art B Owen. Infinitely imbalanced logistic regression. *Journal of Machine Learning Research*, 8(4), 2007.
- Haibo He and Edwardo A Garcia. Learning from imbalanced data. *IEEE Transactions on knowledge and data engineering*, 21(9):1263–1284, 2009.
- Mateusz Buda, Atsuto Maki, and Maciej A Mazurowski. A systematic study of the class imbalance problem in convolutional neural networks. *Neural networks*, 106:249–259, 2018.
- Malik Tiomoko. *Advanced Random Matrix Methods for Machine Learning*. PhD thesis, Université Paris-Saclay, 2021.
- Hamza Cherkaoui, Malik Tiomoko, Mohamed El Amine Seddik, Cosme Louart, Ekkehard Schnoor, and Balázs Kégl. High-dimensional analysis of bootstrap ensemble classifiers. In *The 29th International Conference on Artificial Intelligence and Statistics*.
- Norman L Johnson. Systems of frequency curves generated by methods of translation. *Biometrika*, 36(1/2):149–176, 1949.
- Tiberiu Popoviciu. Sur les équations algébriques ayant toutes leurs racines réelles. *Mathematica*, 9 (129-145):20, 1935.
- Andrew Gelman, {John B.} Carlin, {Hal S.} Stern, {David B.} Dunson, Aki Vehtari, and {Donald B.} Rubin. *Bayesian Data Analysis*. CreateSpace, United States, 3rd ed edition, 2013. ISBN 9781439840955.
- Kaiming He, Xiangyu Zhang, Shaoqing Ren, and Jian Sun. Deep residual learning for image recognition. In *CVPR*, pages 770–778, 2016.
- Mircea Cimpoi, Subhansu Maji, Iasonas Kokkinos, Sammy Mohamed, and Andrea Vedaldi. Describing textures in the wild. In *CVPR*, pages 3606–3613, 2014.
- Jia Deng, Wei Dong, Richard Socher, Li-Jia Li, Kai Li, and Li Fei-Fei. ImageNet: A large-scale hierarchical image database. In *CVPR*, pages 248–255, 2009.
- Bo'az Klartag. A central limit theorem for convex sets. *Inventiones mathematicae*, 168(1):91–131, 2007.
- Bruno Fleury, Olivier Guédon, and Grigoris Paouris. A stability result for mean width of lp-centroid bodies. *Advances in Mathematics*, 214(2):865–877, 2007.
- Mohamed El Amine Seddik, Cosme Louart, Romain Couillet, and Mohamed Tamaazousti. The unexpected deterministic and universal behavior of large softmax classifiers. In *International Conference on Artificial Intelligence and Statistics*, pages 1045–1053. PMLR, 2021.

- StackExchange Community. How to find the point where two normal distributions intersect? Cross Validated, 2017. <https://stats.stackexchange.com/questions/311592/how-to-find-the-point-where-two-normal-distributions-intersect>, Accessed: 2025-07-28.
- Abhranil Das and Wilson S Geisler. A method to integrate and classify normal distributions. *Journal of Vision*, 21(10):1–1, 2021.
- David JC MacKay. The evidence framework applied to classification networks. *Neural computation*, 4(5):720–736, 1992.
- Christopher M Bishop and Nasser M Nasrabadi. *Pattern recognition and machine learning*, volume 4. Springer, 2006.
- David J Spiegelhalter and Steffen L Lauritzen. Sequential updating of conditional probabilities on directed graphical structures. *Networks*, 20(5):579–605, 1990.
- Agustinus Kristiadi, Matthias Hein, and Philipp Hennig. Being bayesian, even just a bit, fixes overconfidence in relu networks. In *International conference on machine learning*, pages 5436–5446. PMLR, 2020.
- Agustinus Kristiadi, Matthias Hein, and Philipp Hennig. An infinite-feature extension for bayesian relu nets that fixes their asymptotic overconfidence. *Advances in Neural Information Processing Systems*, 34:18789–18800, 2021.
- Jean Daunizeau. Semi-analytical approximations to statistical moments of sigmoid and softmax mappings of normal variables, 2017. URL <https://arxiv.org/abs/1703.00091>.
- Jean Daunizeau, Vincent Adam, and Lionel Rigoux. Vba: a probabilistic treatment of nonlinear models for neurobiological and behavioural data. *PLoS computational biology*, 10(1):e1003441, 2014.
- A. W. van der Vaart. *Asymptotic Statistics*. Cambridge Series in Statistical and Probabilistic Mathematics. Cambridge University Press, 1998.
- Malik Tiomoko, Romain Couillet, and Hafiz Tiomoko. Large dimensional analysis and improvement of multi task learning. *arXiv preprint arXiv:2009.01591*, 2020.
- Malik Tiomoko, Ekkehard Schnoor, Mohamed El Amine Seddik, Igor Colin, and Aladin Virmaux. Deciphering lasso-based classification through a large dimensional analysis of the iterative soft-thresholding algorithm. In *International Conference on Machine Learning*, pages 21449–21477. PMLR, 2022.
- Malik Tiomoko and Ekkehard Schnoor. Incorporating priors in learning: A random matrix study under a teacher–student framework. In *ICASSP 2026-2026 IEEE International Conference on Acoustics, Speech and Signal Processing (ICASSP)*, pages 22547–22551. IEEE, 2026.
- Michel Ledoux and Michel Talagrand. *Probability in Banach spaces: isoperimetry and processes*. Classics in mathematics. Springer, Berlin ; London, 2011. ISBN 978-3-642-20211-7 978-3-642-20212-4.
- Michel Ledoux. *The Concentration of Measure Phenomenon*, volume 89 of *Mathematical Surveys and Monographs*. American Mathematical Society, Providence, RI, 2001.
- Mohamed El Amine Seddik, Cosme Louart, Mohamed Tamaazousti, and Romain Couillet. Random matrix theory proves that deep learning representations of gan-data behave as gaussian mixtures. In *International Conference on Machine Learning*, pages 8573–8582. PMLR, 2020.
- Romain Couillet and Zhenyu Liao. *Random matrix methods for machine learning*. Cambridge University Press, 2022.
- Cosme Louart and Romain Couillet. Concentration of measure and large random matrices with an application to sample covariance matrices. *arXiv preprint arXiv:1805.08295*, 2018.
- Cosme Louart, Zhenyu Liao, and Romain Couillet. A random matrix approach to neural networks. *The Annals of Applied Probability*, 28(2):1190–1248, 2018.

Chiheb Yaakoubi, Cosme Louart, Malik Tiomoko, and Zhenyu Liao. Characterization of gaussian universality breakdown in high-dimensional empirical risk minimization. *arXiv preprint arXiv:2604.03146*, 2026.

MAI Xiaoyi and Zhenyu Liao. The breakdown of gaussian universality in classification of high-dimensional linear factor mixtures. In *The Thirteenth International Conference on Learning Representations*, 2025.

Supplementary Material

A Mathematical Preliminaries

The supplementary material is structured as follows. Sec. A collects useful mathematical preliminaries on the sigmoid function and from probability theory. Sec. B provides the technical details and proofs supporting the results of Sec. 2; in particular, we derive the distributions of the CAVs obtained from *FastCAV* and *PatternCAV*, give a detailed treatment of the *ridge regression* case, and discuss related topics such as the asymptotic normality of sensitivity scores and the variability of CAVs.

A.1 The Sigmoid Function

Definition and Convergence. The logistic sigmoid function $s : \mathbb{R} \rightarrow (0, 1)$, along with its generalized scaled variant $s_\alpha : \mathbb{R} \rightarrow (0, 1)$ which incorporates a positive scaling parameter $\alpha > 0$ to control the steepness, are defined as follows by (recall also Figure 2)

$$s(x) = \frac{1}{1 + \exp(-x)}, \quad \text{and} \quad s_\alpha(x) = s(\alpha \cdot x) = \frac{1}{1 + \exp(-\alpha x)}. \quad (\text{A.1})$$

With this convention, we have $s_1 = s$. The scaled sigmoid function s_α converges pointwise to

$$\lim_{\alpha \rightarrow \infty} s_\alpha(x) = s_\infty(x) := \begin{cases} 1 & \text{if } x > 0 \\ 0.5 & \text{if } x = 0 \\ 0 & \text{if } x < 0, \end{cases} \quad (\text{A.2})$$

the so-called *Heaviside step function*. This convergence justifies the use of the scaled sigmoid s_α as a smooth approximation for the indicator function $\mathbb{1}_{\{x>0\}}$.

Derivatives and Boundedness. The derivatives of the (scaled) sigmoid function can be expressed in terms of the functions,

$$s'(x) = s(x)(1 - s(x)), \quad \text{and} \quad s'_\alpha(x) = \alpha \cdot s_\alpha(x)(1 - s_\alpha(x)). \quad (\text{A.3})$$

Note that the maximum range of s_α is the interval $(0, 1)$, such that the derivative $\alpha \cdot s_\alpha(x)(1 - s_\alpha(x))$ is bounded. Therefore,

$$\sup_{x \in \mathbb{R}} |s'_\alpha(x)| = \alpha \cdot \max_{z \in [0,1]} z(1 - z) = \frac{\alpha}{4}, \quad \text{and} \quad \sup_{x \in \mathbb{R}} |s(x)| = \frac{1}{4}. \quad (\text{A.4})$$

Consequently, s_α is $\frac{\alpha}{4}$ -Lipschitz-continuous; in particular, $s = s_1$ is $\frac{1}{4}$ -Lipschitz-continuous.

A.2 Basic and Advanced Tools from Probability Theory

Variations of Averages of Random Variables. Let us briefly recall the following very basic fact for the variance of the average of i.i.d. random variables, which turns out useful e.g. in the context of Multi-TCAV in Sec. 3.1 as it describes the decay of variances with increasing sample size.

Lemma A.1. Consider a real-valued random variable $X : \Omega \rightarrow \mathbb{R}$ on a probability space $(\Omega, \mathcal{E}, \mathbb{P})$ with finite variance $\text{Var}(X) < \infty$. Let X_1, X_2, \dots, X_N be N i.i.d. copies of X . We assume $\mathbb{P}(X = 0) = 0$. Let S_N be the empirical average

$$S_N = \frac{1}{N} \sum_{i=1}^N X_i. \quad (\text{A.5})$$

Then, we also shortly write for the variance of the average S_N in (A.5) that it satisfies $\text{Var}(S_N) = \text{Var}(X)/N = \mathcal{O}(1/N)$.

Proof. For completeness let us provide the proof, which is elementary and can be found in many textbooks. By the properties of the variance and due to the independence of the random variables

X_1, X_2, \dots, X_N , we have

$$\begin{aligned}\text{Var}(S_N) &= \text{Var}\left(\frac{1}{N} \sum_{i=1}^N X_i\right) = \frac{1}{N^2} \text{Var}\left(\sum_{i=1}^N X_i\right) \\ &= \frac{1}{N^2} \sum_{i=1}^N \text{Var}(X_i) = \frac{1}{N^2} (N \cdot \text{Var}(X)) = \frac{\text{Var}(X)}{N}.\end{aligned}$$

The final equality follows from the fact that all X_i are identically distributed, implying $\text{Var}(X_i) = \text{Var}(X)$ for all i . \square

Let us furthermore recall the classical *Popoviciu's Inequality* [Popoviciu, 1935] from probability theory, which provides a general upper bound for the variance of bounded random variables.

Theorem A.2 (Popoviciu's Inequality). *Let X be an (essentially) bounded random variable with $a \leq X \leq b$ almost surely for some $a, b \in \mathbb{R}$. Then, the variance of X is bounded as follows by*

$$\text{Var}(X) \leq \frac{1}{4}(b-a)^2. \quad (\text{A.6})$$

Equality in (A.6) holds if and only if $\mathbb{P}(X = a) = \mathbb{P}(X = b) = \frac{1}{2}$, i.e., when the probability mass is evenly distributed between the extreme values.

If $[a, b] = [0, 1]$, the upper bound is $\frac{1}{4}$, and it is attained for a symmetric Bernoulli distribution; see Figure 4. Therefore, this is trivially also the generic upper bound (21) for the variance of any TCAV score, understood as random variable taking values in $[0, 1]$.

The Logit-Normal Distribution. For a Gaussian random variable $X \sim \mathcal{N}(\mu, \sigma^2)$, consider $s_\alpha(X)$, the (scaled, by $\alpha > 0$) so-called *logit-normal distribution* of X passed through a (scaled) logistic sigmoid function (A.1), which naturally appears in the context of α -TCAV in this paper. Note that $s_\alpha(X) = s(\alpha \cdot X) = s(Y)$ with $Y \sim \mathcal{N}(\alpha\mu, \alpha^2\sigma^2)$, such that essentially it is sufficient to consider the standard sigmoid function σ , but we explicitly use α as an additional parameter. While it is known that none of its moments has a closed-form solution [MacKay, 1992, Section 2], good approximations have been provided in the literature. We use the following approximations to compute the expectations $\mathbb{E}[s_\alpha(X)]$ and $\mathbb{E}[s_\alpha^2(X)]$ (and thus, obtain an approximation for the variance as well which we state for convenience).

$$\mathbb{E}_{X \sim \mathcal{N}(\mu, \sigma^2)} [s_\alpha(X)] \approx s\left(\frac{\alpha\mu}{\sqrt{1 + \tau_1\alpha^2\sigma^2}}\right) =: m(\mu, \sigma^2, \alpha) =: m, \quad (\text{A.7})$$

$$\mathbb{E}_{X \sim \mathcal{N}(\mu, \sigma^2)} [s_\alpha^2(X)] \approx m^2 + m(1-m) \left(1 - \frac{1}{\sqrt{1 + \tau_2\alpha^2\sigma^2}}\right), \quad (\text{A.8})$$

$$\text{Var}_{X \sim \mathcal{N}(\mu, \sigma^2)} [s_\alpha(X)] \approx m(1-m) \left(1 - \frac{1}{\sqrt{1 + \tau_2\alpha^2\sigma^2}}\right), \quad (\text{A.9})$$

that have been provided in the literature, where the two constants τ_1 in (A.7) and τ_2 both in (A.8) and in (A.9) are given by

$$\tau_1 = \frac{\pi}{8}, \quad \text{and} \quad \tau_2 = 0.358. \quad (\text{A.10})$$

The approximation of the mean (A.7) and the constant τ_1 in (A.10) are due to [MacKay, 1992, Section 2]; see also [Bishop and Nasrabadi, 2006, Section 4.5.2], and [Spiegelhalter and Lauritzen, 1990] for an earlier discussion of the problem, and [Kristiadi et al., 2020, 2021] for more recent applications in Bayesian deep learning. For the second moment (A.8) and the variance (A.9), and the constant τ_2 appearing there, we rely on [Daunizeau, 2017, eq. (23)]; see also [Daunizeau et al., 2014]. Let us comment on a few observations; we begin by analyzing the influence of σ^2 , while assuming μ and α to be fixed.

- As $\sigma^2 \rightarrow \infty$, the mean approximation (A.7) converges to $s(0) = \frac{1}{2}$, as the density function of the normal distribution *flattens out* (independently of μ and α).
- The second moment (A.8) collapses to $s^2(\alpha\mu)$ as $\sigma^2 \rightarrow 0$, and as $\sigma^2 \rightarrow \infty$, it converges to $\frac{1}{2}$.

- As pointed out by [Daunizeau, 2017, p. 15], the variance approximation (A.9) is a monotonically increasing function of σ^2 . It is lower-bounded by 0 (in the limit $\sigma^2 \rightarrow 0$), and upper-bounded by $\frac{1}{4}$ in the limit $\sigma^2 \rightarrow \infty$ (when becoming Bernoulli-like), aligned with classical *Popoviciu's inequality* [Popoviciu, 1935] which we recall in Theorem A.2.

In the context of this paper, we are especially interested in the behavior with regard to $\alpha > 0$ and fixed mean μ and variance σ^2 . In the limit $\alpha \rightarrow \infty$, s_α converges to the *Heaviside step function* s_∞ from (A.2), which differs from the $\mathbb{1}_{\{x>0\}}$ only in the origin. We show that the above estimates of first and second moment are highly consistent when taking the limit $\alpha \rightarrow \infty$.

- In this limiting case, the expectation corresponds to the Gaussian tail probability $\mathbb{P}(X > 0) = \Phi(\mu/\sigma)$, where Φ denotes the cdf of the standard normal distribution, since, by standardizing to $\mathcal{N}(0, 1)$ in the final steps,

$$\begin{aligned} \mathbb{E}_{X \sim \mathcal{N}(\mu, \sigma^2)} [\mathbb{1}_{X>0}] &= \mathbb{E}_{X \sim \mathcal{N}(\mu, \sigma^2)} [s_\infty(X)] \\ &= \mathbb{P}(X > 0) = \mathbb{P}\left(\frac{X - \mu}{\sigma} > \frac{-\mu}{\sigma}\right) = \Phi\left(\frac{\mu}{\sigma}\right). \end{aligned} \quad (\text{A.11})$$

Our mean approximation (A.7) is consistent in this limit. Due to the continuity of the sigmoid function s from (A.1),

$$\lim_{\alpha \rightarrow \infty} m(\mu, \sigma^2, \alpha) = s\left(\frac{\mu}{\sigma\sqrt{\tau_1}}\right) = s\left(\frac{\mu}{\sigma}\sqrt{8/\pi}\right) \approx \Phi\left(\frac{\mu}{\sigma}\right), \quad (\text{A.12})$$

employing the following common highly accurate approximation of the sigmoid function s by Φ , the cumulative distribution function of the standard normal distribution, which is given by

$$s(z) \approx \Phi(\sqrt{\tau_1} \cdot z), \quad \text{where} \quad \tau_1 = \pi/8, \quad z \in \mathbb{R}. \quad (\text{A.13})$$

The constant $\tau_1 = \pi/8$ is motivated by matching the derivatives of s and Φ at the origin. Since $s'(0) = 1/4$ and $\frac{d}{dz}\Phi(\lambda z)|_{z=0} = \lambda/\sqrt{2\pi}$, setting these equal yields $\lambda^2 = \pi/8$, which is precisely the scaling factor τ_1 that moderates the variance in our approximation. For more details, we again refer the reader to [MacKay, 1992, Section 2] and [Bishop and Nasrabadi, 2006, Section 4.5.2].

- Regarding the (approximation of the) variance (or the second moment), let us point out that $\mathbb{E}[\mathbb{1}_{X>0}] = \mathbb{E}[\mathbb{1}_{X>0}^2]$, as $\mathbb{1}_{X>0}$ is a Bernoulli random variable. As they differ only in a point of measure zero for $X \sim \mathcal{N}(\mu, \sigma^2)$, we also have $\mathbb{E}[\mathbb{1}_{X>0}^2] = \mathbb{E}[s_\infty^2(X)]$. By general properties of the Bernoulli distribution and similar as seen in (A.11),

$$\begin{aligned} \text{Var}(\mathbb{1}_{X>0}) &= \mathbb{E}[\mathbb{1}_{X>0}^2] - \mathbb{E}[\mathbb{1}_{X>0}]^2 \\ &= \mathbb{E}[\mathbb{1}_{X>0}] - \mathbb{E}[\mathbb{1}_{X>0}]^2 \\ &= \mathbb{P}(X > 0) (1 - \mathbb{P}(X > 0)) \\ &= \Phi\left(\frac{\mu}{\sigma}\right) \left(1 - \Phi\left(\frac{\mu}{\sigma}\right)\right). \end{aligned}$$

Once again, this is consistent with variance approximation in (A.9). Taking the limit $\alpha \rightarrow \infty$, we obtain with (A.12) that

$$\begin{aligned} &\lim_{\alpha \rightarrow \infty} m(\mu, \sigma^2, \alpha) (1 - m(\mu, \sigma^2, \alpha)) \left(1 - \frac{1}{\sqrt{1 + \tau_2 \alpha^2 \sigma^2}}\right) \\ &= \lim_{\alpha \rightarrow \infty} m(\mu, \sigma^2, \alpha) (1 - m(\mu, \sigma^2, \alpha)) \\ &\approx \Phi\left(\frac{\mu}{\sigma}\right) \left(1 - \Phi\left(\frac{\mu}{\sigma}\right)\right). \end{aligned}$$

B Distributions of Concept Activation Vectors

B.1 FastCAV and PatternCAV

Proof of Proposition 2.2. The mean (4) is obvious, and (5) follows from the following computation starting from (1).

$$\begin{aligned}
\Sigma_{\mathbf{w}_{\text{pat}}} &= \mathbb{E} [\mathbf{w}_{\text{pat}} \mathbf{w}_{\text{pat}}^\top] - (\boldsymbol{\mu}_2 - \boldsymbol{\mu}_1)(\boldsymbol{\mu}_2 - \boldsymbol{\mu}_1)^\top \\
&= \mathbb{E} \left[\left(\frac{1}{n_1} \sum_{i=1}^{n_1} \mathbf{x}_i^{(1)} - \frac{1}{n_2} \sum_{i=1}^{n_2} \mathbf{x}_i^{(2)} \right) \left(\frac{1}{n_1} \sum_{i=1}^{n_1} \mathbf{x}_i^{(1)\top} - \frac{1}{n_2} \sum_{i=1}^{n_2} \mathbf{x}_i^{(2)\top} \right) \right] \\
&\quad - \boldsymbol{\mu}_2 \boldsymbol{\mu}_2^\top + \boldsymbol{\mu}_2 \boldsymbol{\mu}_1^\top + \boldsymbol{\mu}_1 \boldsymbol{\mu}_2^\top - \boldsymbol{\mu}_1 \boldsymbol{\mu}_1^\top \\
&= \mathbb{E} \left[\frac{1}{n_1^2} \sum_{i=1}^{n_1} \mathbf{x}_i^{(1)} \mathbf{x}_i^{(1)\top} \right] + \frac{n_1 - 1}{n_1} \boldsymbol{\mu}_1 \boldsymbol{\mu}_1^\top - \boldsymbol{\mu}_1 \boldsymbol{\mu}_2^\top - \boldsymbol{\mu}_2 \boldsymbol{\mu}_1^\top + \mathbb{E} \left[\frac{1}{n_2^2} \sum_{i=1}^{n_2} \mathbf{x}_i^{(2)} \mathbf{x}_i^{(2)\top} \right] \\
&\quad + \frac{n_2 - 1}{n_2} \boldsymbol{\mu}_2 \boldsymbol{\mu}_2^\top - \boldsymbol{\mu}_2 \boldsymbol{\mu}_2^\top + \boldsymbol{\mu}_2 \boldsymbol{\mu}_1^\top + \boldsymbol{\mu}_1 \boldsymbol{\mu}_2^\top - \boldsymbol{\mu}_1 \boldsymbol{\mu}_1^\top \\
&= \frac{1}{n_1} \mathbb{E} \left[\frac{1}{n_1} \sum_{i=1}^{n_1} \mathbf{x}_i^{(1)} \mathbf{x}_i^{(1)\top} \right] - \frac{1}{n_1} \boldsymbol{\mu}_1 \boldsymbol{\mu}_1^\top + \frac{1}{n_2} \mathbb{E} \left[\frac{1}{n_2} \sum_{i=1}^{n_2} \mathbf{x}_i^{(2)} \mathbf{x}_i^{(2)\top} \right] - \frac{1}{n_2} \boldsymbol{\mu}_2 \boldsymbol{\mu}_2^\top \\
&= \frac{1}{n_1} \Sigma_1 + \frac{1}{n_2} \Sigma_2.
\end{aligned}$$

For this derivation, we used the following straightforward straightforward computations for the first term in the second line

$$\begin{aligned}
&\mathbb{E} \left[\left(\frac{1}{n_1} \sum_{i=1}^{n_1} \mathbf{x}_i^{(1)} - \frac{1}{n_2} \sum_{i=1}^{n_2} \mathbf{x}_i^{(2)} \right) \left(\frac{1}{n_1} \sum_{i=1}^{n_1} \mathbf{x}_i^{(1)\top} - \frac{1}{n_2} \sum_{i=1}^{n_2} \mathbf{x}_i^{(2)\top} \right) \right] \\
&= \mathbb{E} \left[\frac{1}{n_1^2} \sum_{i,j=1}^{n_1} \mathbf{x}_i^{(1)} \mathbf{x}_j^{(1)\top} \right] - \boldsymbol{\mu}_1 \boldsymbol{\mu}_2^\top - \boldsymbol{\mu}_2 \boldsymbol{\mu}_1^\top + \mathbb{E} \left[\frac{1}{n_2^2} \sum_{i,j=1}^{n_2} \mathbf{x}_i^{(2)} \mathbf{x}_j^{(2)\top} \right],
\end{aligned}$$

where for the first term we obtain (similar for the last term for the second class \mathcal{C}_2), using independence for the second term,

$$\begin{aligned}
\mathbb{E} \left[\frac{1}{n_1^2} \sum_{i,j=1}^{n_1} \mathbf{x}_i^{(1)} \mathbf{x}_j^{(1)\top} \right] &= \mathbb{E} \left[\frac{1}{n_1^2} \sum_{i=1}^{n_1} \mathbf{x}_i^{(1)} \mathbf{x}_i^{(1)\top} + \frac{1}{n_1^2} \sum_{i \neq j} \mathbf{x}_i^{(1)} \mathbf{x}_j^{(1)\top} \right] \\
&= \frac{1}{n_1} \mathbb{E} \left[\frac{1}{n_1} \sum_{i=1}^{n_1} \mathbf{x}_i^{(1)} \mathbf{x}_i^{(1)\top} \right] + \frac{n_1(n_1 - 1)}{n_1^2} \sum_{i \neq j} \boldsymbol{\mu}_1 \boldsymbol{\mu}_1^\top \\
&= \frac{1}{n_1} \mathbb{E} \left[\frac{1}{n_1} \sum_{i=1}^{n_1} \mathbf{x}_i^{(1)} \mathbf{x}_i^{(1)\top} \right] + \frac{n_1 - 1}{n_1} \boldsymbol{\mu}_1 \boldsymbol{\mu}_1^\top. \tag{A.14}
\end{aligned}$$

Next, let us turn to the *FastCAV* \mathbf{w}_{fast} . Recalling its definition from (3), and also (2), we easily obtain that

$$\begin{aligned}
\mathbf{w}_{\text{fast}} &= \frac{1}{n_2} \sum_{i=1}^{n_2} \mathbf{x}_i^{(2)} - \frac{1}{n_1 + n_2} \sum_{\ell=1}^2 \sum_{i=1}^{n_\ell} \mathbf{x}_i^{(\ell)} \\
&= \frac{1}{n_2} \sum_{i=1}^{n_2} \mathbf{x}_i^{(2)} - \frac{1}{n_1 + n_2} \sum_{i=1}^{n_1} \mathbf{x}_i^{(1)} - \frac{1}{n_1 + n_2} \sum_{i=1}^{n_2} \mathbf{x}_i^{(2)} \\
&= \left(\frac{1}{n_2} - \frac{1}{n_1 + n_2} \right) \sum_{i=1}^{n_2} \mathbf{x}_i^{(2)} - \frac{1}{n_1 + n_2} \sum_{i=1}^{n_1} \mathbf{x}_i^{(1)} \\
&= \frac{n_1}{n_2} \cdot \frac{1}{n_1 + n_2} \sum_{i=1}^{n_2} \mathbf{x}_i^{(2)} - \frac{1}{n_1 + n_2} \sum_{i=1}^{n_1} \mathbf{x}_i^{(1)} \\
&= \frac{n_1}{n_1 + n_2} \left(\frac{1}{n_2} \sum_{i=1}^{n_2} \mathbf{x}_i^{(2)} - \frac{1}{n_1} \sum_{i=1}^{n_1} \mathbf{x}_i^{(1)} \right) = \frac{n_1}{n_1 + n_2} \mathbf{w}_{\text{pat}},
\end{aligned}$$

i.e., the relation from (6). This directly yields (7) and (8), while the balanced case $n_1 = n_2$ leads to Corollary 2.3. \square

Note that both Corollary 2.3 (with $n_1 = n_2$) and Corollary 2.4 (with fixed n_1 and $n_2 \rightarrow \infty$) are an immediate consequence of Proposition 2.2. After characterizing the distributions of CAVs \mathbf{w}_{CAV} , we next investigate inner products $\langle \mathbf{z}, \mathbf{w}_{\text{CAV}} \rangle$, as they appear in the the sensitivity scores $S_{C,k,l}(\mathbf{x}) = \langle \nabla h_{l,k}(f_l(\mathbf{x})), \mathbf{v}_C^l \rangle$ in (14). We next prove Lemma B.1 for $\mathbf{w}_{\text{CAV}} = \mathbf{w}_{\text{pat}}$, which also complements [Wenkmann and Garreau, 2025, Corollary 1] considering the *logistic regression*.

Lemma B.1 (Distribution of $\langle \mathbf{z}, \mathbf{w}_{\text{pat}} \rangle$). *For any fixed deterministic vector $\mathbf{z} \in \mathbb{R}^d$, mean and variance of its projection $\langle \mathbf{z}, \mathbf{w}_{\text{pat}} \rangle$ on \mathbf{w}_{pat} from (1) are given by (any $n_1, n_2 \in \mathbb{N}$)*

$$\mathbb{E}[\langle \mathbf{z}, \mathbf{w}_{\text{pat}} \rangle] = \langle \mathbf{z}, \boldsymbol{\mu}_2 - \boldsymbol{\mu}_1 \rangle, \quad (\text{A.15})$$

$$\text{Var}(\langle \mathbf{z}, \mathbf{w}_{\text{pat}} \rangle) = \frac{1}{n_1} \mathbf{z}^\top \boldsymbol{\Sigma}_1 \mathbf{z} + \frac{1}{n_2} \mathbf{z}^\top \boldsymbol{\Sigma}_2 \mathbf{z}. \quad (\text{A.16})$$

As $n_1, n_2 \rightarrow \infty$ with $n_1/n \rightarrow \zeta \in (0, 1)$, i.e., $n_2/n \rightarrow 1 - \zeta \in (0, 1)$, the scaled error is asymptotically Gaussian; denoting convergence in distribution (or weakly) by \xrightarrow{d} , it holds that

$$\sqrt{n}(\langle \mathbf{z}, \mathbf{w}_{\text{pat}} \rangle - \langle \mathbf{z}, \boldsymbol{\mu}_2 - \boldsymbol{\mu}_1 \rangle) \xrightarrow{d} \mathcal{N}\left(0, \frac{\mathbf{z}^\top \boldsymbol{\Sigma}_1 \mathbf{z}}{\zeta} + \frac{\mathbf{z}^\top \boldsymbol{\Sigma}_2 \mathbf{z}}{1 - \zeta}\right). \quad (\text{A.17})$$

Note that using the results in Sec. 2, it is straightforward to obtain further results, e.g. for the *FastCAV* \mathbf{w}_{fast} from (3). Furthermore, note that for deterministic *concept* data and only $n_1 \rightarrow \infty$, and further, if $\mathbf{z} = \nabla h_{l,k}(f_l(\mathbf{x}))$ as in the definition of $S_{C,k,l}(\mathbf{x})$ in (14), then the limiting normal distribution (A.17) reads as

$$\mathcal{N}\left(0, \nabla h_{l,k}(f_l(\mathbf{x}))^\top \boldsymbol{\Sigma}_1 \nabla h_{l,k}(f_l(\mathbf{x}))\right), \quad (\text{A.18})$$

which resembles the variance $V(\mathbf{x})$ given in [Wenkmann and Garreau, 2025, eq. (9)] for the case of the *logistic regression*, up to the different expression for the covariance $\boldsymbol{\Sigma}_1$. Let us prove the above result.

Proof of Lemma B.1. We first derive the moments for any $n_1, n_2 \in \mathbb{N}$. By linearity of the inner product and the expectation,

$$\mathbb{E}[\langle \mathbf{z}, \mathbf{w}_{\text{pat}} \rangle] = \frac{1}{n_2} \sum_{i=1}^{n_2} \mathbf{z}^\top \mathbb{E}[\mathbf{x}_i^{(2)}] - \frac{1}{n_1} \sum_{j=1}^{n_1} \mathbf{z}^\top \mathbb{E}[\mathbf{x}_j^{(1)}] = \mathbf{z}^\top \boldsymbol{\mu}_2 - \mathbf{z}^\top \boldsymbol{\mu}_1 = \langle \mathbf{z}, \boldsymbol{\mu}_2 - \boldsymbol{\mu}_1 \rangle,$$

by the definition of \mathbf{w}_{pat} from (1), which gives (A.15). For the variance in (A.16), we apply *Bienaymé's identity*: by independence between classes and between samples within each class, the variance of

the sum is the sum of the variances. Thus, we obtain

$$\begin{aligned}\text{Var}(\langle \mathbf{z}, \mathbf{w}_{\text{pat}} \rangle) &= \frac{1}{n_2^2} \sum_{i=1}^{n_2} \text{Var} \left(\mathbf{z}^\top \mathbf{x}_i^{(2)} \right) + \frac{1}{n_1^2} \sum_{j=1}^{n_1} \text{Var} \left(\mathbf{z}^\top \mathbf{x}_j^{(1)} \right) \\ &= \frac{1}{n_2^2} (n_2 \mathbf{z}^\top \Sigma_2 \mathbf{z}) + \frac{1}{n_1^2} (n_1 \mathbf{z}^\top \Sigma_1 \mathbf{z}) = \frac{\mathbf{z}^\top \Sigma_2 \mathbf{z}}{n_2} + \frac{\mathbf{z}^\top \Sigma_1 \mathbf{z}}{n_1}.\end{aligned}$$

To establish asymptotic normality, we observe that $\langle \mathbf{z}, \mathbf{w}_{\text{pat}} \rangle$ is a sum of independent random variables. By the Multivariate Central Limit Theorem [Vaart, 1998, Chapter 2.1], the sample means satisfy $\sqrt{n_\ell} \left(\frac{1}{n_\ell} \sum_{i=1}^{n_\ell} \mathbf{x}_i^{(\ell)} - \boldsymbol{\mu}_\ell \right) \xrightarrow{d} \mathcal{N}(\mathbf{0}, \Sigma_\ell)$ (convergence in distribution, or weakly). By the *Cramér-Wold theorem* or (*Cramér-Wold device*) [Vaart, 1998, p. 16], any linear combination of these means converges to a normal distribution. \square

B.2 Ridge Regression

Assumptions and Deterministic Equivalents. Next, let us turn to the case of the *ridge regression* (A.20), which is considerably more challenging compared to the *FastCAV* and the *PatternCAV*. We rely on the aforementioned work of [Tiomoko, 2021, Chapter 2.3] and [Tiomoko et al., 2020, p. 42-50]; see also [Cherkaoui et al.]. As a technical assumption we require the notion of *concentrated random vectors* that we will introduce below and that is well-established in various works analysing machine learning with the help of random matrix theory [Tiomoko et al., 2022, Tiomoko and Schnoor, 2026]. Before we lay out the technical assumptions, let us introduce some notation required specifically for this section. We write $\mathbf{0}_d$ for the zero vector in \mathbb{R}^d , and similar $\mathbb{1}_d$ for the all-ones vector in \mathbb{R}^d . We denote the diagonal matrix of \mathbf{v} as \mathcal{D}_v . Norms are denoted by $\|\cdot\|_p$ for ℓ_p -norms, $\|\cdot\|_{2 \rightarrow 2}$ for spectral, and $\|\cdot\|_F$ for Frobenius. Vertical concatenation is written as $[\mathbf{v}_1, \mathbf{v}_2]^\top \in \mathbb{R}^{2d}$, while $[\mathbf{v}_1 | \mathbf{v}_2] \in \mathbb{R}^{d \times 2}$ denotes horizontal concatenation. Next, we make more specific assumptions on the data to be *concentrated*, meaning that any Lipschitz-continuous scalar observations are tightly concentrated around their mean. We will first state the precise definition of the notion of *concentrated random vectors* just below in Definition B.2, together with additional comments and motivation.

Definition B.2 (*q-exponential concentration; observable diameter*). Let $(\mathcal{X}, \|\cdot\|_{\mathcal{X}})$ be a normed vector space and $q > 0$. A random vector $\mathbf{x} \in \mathcal{X}$ is said to be *q-exponentially concentrated* if for any 1-Lipschitz continuous (with respect to $\|\cdot\|_{\mathcal{X}}$) real-valued function $\varphi : \mathcal{X} \rightarrow \mathbb{R}$ there exists $C \geq 0$ independent of $\dim(\mathcal{X})$ and $\sigma > 0$ such that, for all $t \geq 0$,

$$\mathbb{P}(|\varphi(\mathbf{x}) - \mathbb{E}\varphi(\mathbf{x})| \geq t) \leq C e^{-(t/\sigma)^q}. \quad (\text{A.19})$$

This is denoted as $\mathbf{x} \propto \mathcal{E}_q(\sigma | \mathcal{X}, \|\cdot\|_{\mathcal{X}})$, where σ is called the *observable diameter*. If σ does not depend on $\dim(\mathcal{X})$, we write $\mathbf{x} \propto \mathcal{E}_q(1 | \mathcal{X}, \|\cdot\|_{\mathcal{X}})$.

The most fundamental example for a random vector with the concentration property from B.2 is the isotropic Gaussian random vector $\mathbf{x} \sim \mathcal{N}(\mathbf{0}, \mathbf{I})$ in \mathbb{R}^d , for which $\mathbf{x} \propto \mathcal{E}_2(1 | \mathbb{R}^d, \|\cdot\|_2)$ by the classical *Gaussian concentration inequality* [Ledoux and Talagrand, 2011, Ledoux, 2001]. While similar notions of the concentration property described in B.2 exist, such as linear and convex concentration, Lipschitz concentration turned out to be particularly useful by being both a mathematically convenient assumption, and a model for realistic data such as natural images. This is due to a fundamental property of its *stability under Lipschitz transforms*: if $f : \mathcal{Z} \rightarrow \mathcal{X}$ (for $(\mathcal{Z}, \|\cdot\|_{\mathcal{Z}})$ being another normed space) is a K -Lipschitz function and $\mathbf{x} \in \mathcal{X}$ with $\mathbf{x} \propto \mathcal{E}_q(\sigma | \mathcal{X}, \|\cdot\|_{\mathcal{X}})$, then $f(\mathbf{x}) \propto \mathcal{E}_q(K \cdot \sigma | \mathcal{Z}, \|\cdot\|_{\mathcal{Z}})$, where K might depend on $\dim(\mathcal{X})$. As neural networks represent Lipschitz continuous mappings, generative adversarial networks are Lipschitz continuous transforms of (isotropic) Gaussian random vectors and can therefore be modeled using concentration properties as provided in Definition B.2, thus making them a model for realistic data [Seddik et al., 2020]. Lipschitzness of neural networks has been studied in a variety of works; [Seddik et al., 2020] also provides a short overview providing Lipschitz constants of various parts of neural networks (fully connected and convolutional layers, pooling layers and activation functions, residual connections, batch normalization layers etc.). Due to the nested structure of Lipschitz-continuous functions, any of their concatenations is Lipschitz-continuous, notably also parts of network outputting hidden-layer activations, making this approach highly suitable regarding concept activation vectors. We make the following assumptions on the data concentration, as well as large-dimensional asymptotics.

Assumption B.3 (Distribution of \mathbf{X} and \mathbf{x}). The data matrix $\mathbf{X} \in \mathbb{R}^{d \times n}$, and all its columns $\mathbf{x} \in \mathbb{R}^d$ (no matter which class), are assumed to follow the following q -exponential concentration under Lipschitz-continuous observations.

$$\mathbf{x} \propto \mathcal{E}_2(1 | \mathbb{R}^d, \|\cdot\|_2), \quad \mathbf{X} \propto \mathcal{E}_2(1 | \mathbb{R}^{d \times n}, \|\cdot\|_F).$$

Assumption B.4 (Large n , large d). We assume $n > d$ and, as $n_\ell, n, d \rightarrow \infty$, asymptotically $d/n \rightarrow c_0 \in (0, 1)$ and $n_\ell/n \rightarrow c_\ell > 0$ for $\ell = 1, 2$.

Next, let us recall the *ridge regression* problem, i.e., the following ℓ_2 -regularized least-squares problem with a normalized data matrix $\mathbf{X} \in \mathbb{R}^{d \times n}$,

$$\mathbf{w}_{\text{ridge}} = \arg \min_{\mathbf{w} \in \mathbb{R}^d} \left\| \mathbf{y} - \frac{1}{\sqrt{n}} \mathbf{X}^\top \mathbf{w} \right\|_2^2 + \lambda \|\mathbf{w}\|_2^2. \quad (\text{A.20})$$

Next, note that the gradient of the objective function in (A.20) vanishes if and only if the following equation is satisfied,

$$\frac{1}{n} \mathbf{X} \mathbf{X}^\top \mathbf{w} - \frac{\mathbf{X}}{\sqrt{n}} \mathbf{y} - \lambda \mathbf{w} = \mathbf{0}.$$

Rearranging for \mathbf{w} provides an explicit solution depending on \mathbf{X} , which is (assuming the inverse matrix exists) given by

$$\mathbf{w}_{\text{ridge}} = \left(\frac{1}{n} \mathbf{X} \mathbf{X}^\top + \lambda \mathbf{I}_p \right)^{-1} \frac{\mathbf{X}}{\sqrt{n}} \mathbf{y}. \quad (\text{A.21})$$

With a view toward our results on the classification accuracy of CAVs (notably Propositions 5.2 and 5.3), and the variance of of CAVs from Definition (2.5), we are interested in determining mean and covariance of $\mathbf{w}_{\text{ridge}}$. While $\mathbb{E}[\mathbf{w}_{\text{ridge}}]$ and $\text{Cov}(\mathbf{w}_{\text{ridge}})$ may be difficult to compute explicitly, we may instead take the approach of *deterministic equivalents* [Couillet and Liao, 2022, Definition 4] from random matrix theory. For a random vector $\mathbf{w} \in \mathbb{R}^d$, we aim to find some deterministic vector $\bar{\mathbf{w}} \in \mathbb{R}^d$ (a deterministic equivalent of \mathbf{w} ; note that it is generally not unique), such that it holds

$$\mathbb{E}[\mathbf{w}^\top \mathbf{v}] = \mathbb{E}[\mathbf{w}]^\top \mathbf{v} = \bar{\mathbf{w}}^\top \mathbf{v} \quad \forall \mathbf{v} \in \mathbb{R}^d. \quad (\text{A.22})$$

The deterministic equivalent $\bar{\mathbf{w}}$ can be regarded as a generalization of the mean $\mathbb{E}[\mathbf{w}]$; however, instead of finding the mean we only require to find any deterministic vector that behaves the same under taking inner products. Recalling the covariance

$$\text{Cov}(\mathbf{w}) = \mathbb{E}[(\mathbf{w} - \mathbb{E}[\mathbf{w}])(\mathbf{w} - \mathbb{E}[\mathbf{w}])^\top] = \mathbb{E}[\mathbf{w} \mathbf{w}^\top] - \mathbb{E}[\mathbf{w}]\mathbb{E}[\mathbf{w}]^\top, \quad (\text{A.23})$$

a similar approach can be taken here. Note that we may replace $\mathbb{E}[\mathbf{w}]$ by $\bar{\mathbf{w}}$, but it may be hard to explicitly compute $\mathbb{E}[\mathbf{w} \mathbf{w}^\top]$, the first summand in (A.23). Furthermore, in some applications, we may not require knowledge of the entire covariance matrix (A.23), but we are only interested in some scalar observation of it - like the trace as in Definition (2.5), that is

$$\text{Tr}(\text{Cov}(\mathbf{w})) = \text{Tr}(\mathbb{E}[\mathbf{w} \mathbf{w}^\top]) - \text{Tr}(\mathbb{E}[\mathbf{w}]\mathbb{E}[\mathbf{w}]^\top) = \mathbb{E}[\text{Tr}(\mathbf{w} \mathbf{w}^\top)] - \text{Tr}(\mathbb{E}[\mathbf{w}]\mathbb{E}[\mathbf{w}]^\top). \quad (\text{A.24})$$

Again, to treat the summand $\mathbb{E}[\text{Tr}(\mathbf{w} \mathbf{w}^\top)]$, we may consider the random matrix $\mathbf{M} = \mathbf{w} \mathbf{w}^\top \in \mathbb{R}^{d \times d}$ and make the *ansatz*

$$\mathbb{E}[\text{Tr}(\mathbf{B} \mathbf{M})] = \text{Tr}(\mathbb{E}[\mathbf{B} \mathbf{M}]) = \text{Tr}(\mathbf{B} \bar{\mathbf{M}}) \quad \forall \mathbf{B} \in \mathbb{R}^{d \times d}, \quad \mathbf{M} = \mathbf{w} \mathbf{w}^\top \in \mathbb{R}^{d \times d}, \quad (\text{A.25})$$

such that we can read off a deterministic equivalent $\bar{\mathbf{M}}$. However, it turns out difficult to precisely derive the form given in (A.25), and we restrict ourselves to the more modest goal of only $\mathbb{E}[\text{Tr}(\mathbf{B} \mathbf{M})]$ for any matrix \mathbf{B} (such as $\mathbf{B} = \mathbf{I}$ having Definition (2.5) in mind) without explicitly bringing it into the form $\text{Tr}(\mathbf{B} \bar{\mathbf{M}})$ where we can read off a deterministic equivalent. Therefore, our goal in Theorem B.6 below is to compute firstly a deterministic equivalent $\bar{\mathbf{w}}_{\text{ridge}}$ in the sense of (A.21), and secondly compute the expression $\mathbb{E}[\text{Tr}(\mathbf{B} \mathbf{M})]$ for any matrix \mathbf{B} . Before we proceed with this result, let us further recall the following theorem providing a deterministic equivalent of the resolvent of the random matrix $\frac{1}{n} \mathbf{X} \mathbf{X}^\top$ which will be used for Theorem B.6 below.

Theorem B.5 ([Louart and Couillet, 2018]). Consider $\mathbf{Q} = \mathbf{Q}(\lambda) = \left(\frac{1}{n} \mathbf{X} \mathbf{X}^\top + \lambda \mathbf{I}_p \right)^{-1}$, i.e., the resolvent of the random matrix $\frac{1}{n} \mathbf{X} \mathbf{X}^\top$, which is defined for any $\lambda \in \mathbb{C}$ such that $\frac{1}{n} \mathbf{X} \mathbf{X}^\top + \lambda \mathbf{I}_p$ is

invertible. Then, under the aforementioned assumptions and with high probability, a deterministic equivalent $\bar{\mathbf{Q}} = \bar{\mathbf{Q}}(\lambda)$ of $\mathbf{Q}(\lambda)$ is given as the unique solution of the fixed point equation in $\bar{\mathbf{Q}}$,

$$\bar{\mathbf{Q}}(\lambda) = \left(\sum_{\ell=1}^2 \frac{n_\ell}{n} \frac{\mathbf{C}_\ell}{1 + \delta_\ell} + \lambda \mathbf{I}_d \right)^{-1} \in \mathbb{R}^{d \times d}, \quad \delta_\ell = \frac{1}{n} \text{Tr}(\mathbf{C}_\ell \bar{\mathbf{Q}}) \in \mathbb{R}, \quad \ell = 1, 2. \quad (\text{A.26})$$

Proof. [Louart and Couillet, 2018] □

Theorem B.6. Under the aforementioned assumptions, the deterministic equivalent $\overline{\mathbf{w}_{\text{ridge}}}$ of the solution $\mathbf{w}_{\text{ridge}}$ of the regression problem given in (A.20) as well as the expression $\mathbb{E} \text{Tr}(\mathbf{B} \mathbf{w}_{\text{ridge}} \mathbf{w}_{\text{ridge}}^\top)$ for any matrix $\mathbf{B} \in \mathbb{R}^{d \times d}$ (of asymptotically uniformly bounded norm) are provided as follows.

$$\overline{\mathbf{w}_{\text{ridge}}} = \frac{1}{\sqrt{n}} \mathbf{y}^\top \mathbf{J} \mathbf{M}_\delta^\top \bar{\mathbf{Q}} \quad (\text{A.27})$$

$$\mathbb{E} \text{Tr}(\mathbf{B} \mathbf{w}_{\text{ridge}} \mathbf{w}_{\text{ridge}}^\top) = \frac{1}{n} (\mathbf{y}^\top \mathbf{J} \mathbf{M}_\delta^\top \mathbf{K} \mathbf{M}_\delta \mathbf{J}^\top \mathbf{y} + \mathbf{y}^\top \mathbf{V} \mathbf{y} - 2 \mathbf{y}^\top \mathbf{J} \mathbf{M}_\delta^\top \bar{\mathbf{Q}} \mathbf{M}_\delta \mathbf{J}^\top \mathbf{y}), \quad (\text{A.28})$$

where, in (A.27), by $\bar{\mathbf{Q}} = \bar{\mathbf{Q}}(\lambda)$ we denote a deterministic equivalent of the random matrix $\mathbf{Q} = \mathbf{Q}(\lambda) = \left(\frac{1}{n} \mathbf{X} \mathbf{X}^\top + \lambda \mathbf{I}_p \right)^{-1}$, the resolvent² of random matrix $\frac{1}{n} \mathbf{X} \mathbf{X}^\top$. It is obtained as the unique solution of the following fixed-point equation

$$\bar{\mathbf{Q}} = \left(\sum_{\ell=1}^2 \frac{n_\ell}{n} \frac{\mathbf{C}_\ell}{1 + \delta_\ell} + \lambda \mathbf{I}_d \right)^{-1} \in \mathbb{R}^{d \times d}, \quad \delta_\ell = \frac{1}{n} \text{Tr}(\mathbf{C}_\ell \bar{\mathbf{Q}}) \in \mathbb{R}, \quad \boldsymbol{\delta} = (\delta_1, \delta_2). \quad (\text{A.29})$$

Further, still in (A.27) regarding the deterministic equivalent $\bar{\mathbf{w}}_{\text{ridge}}$, the matrices $\mathbf{J} \in \mathbb{R}^{n \times 2}$ and $\mathbf{M}_\delta \in \mathbb{R}^{d \times 2}$ are given by

$$\mathbf{J} = \begin{pmatrix} \mathbf{1}_{n_1} & \mathbf{0}_{n_1} \\ \mathbf{0}_{n_2} & \mathbf{1}_{n_2} \end{pmatrix} \in \mathbb{R}^{n \times 2}, \quad \mathbf{M}_\delta = \left[\frac{1}{1 + \delta_1} \boldsymbol{\mu}_1 \mid \frac{1}{1 + \delta_2} \boldsymbol{\mu}_2 \right] \in \mathbb{R}^{d \times 2}. \quad (\text{A.30})$$

Finally, all the remaining expressions (apart from $\bar{\mathbf{Q}}$ and δ_ℓ , $\ell = 1, 2$ already given in (A.29)) in the deterministic equivalent (A.28) are defined in the following equations below by

$$\tilde{\mathbf{V}} = \frac{1}{n} \begin{pmatrix} \text{Tr}(\boldsymbol{\Sigma}_1 \bar{\mathbf{Q}} \boldsymbol{\Sigma}_1 \bar{\mathbf{Q}}) & \text{Tr}(\boldsymbol{\Sigma}_1 \bar{\mathbf{Q}} \boldsymbol{\Sigma}_2 \bar{\mathbf{Q}}) \\ \text{Tr}(\boldsymbol{\Sigma}_2 \bar{\mathbf{Q}} \boldsymbol{\Sigma}_1 \bar{\mathbf{Q}}) & \text{Tr}(\boldsymbol{\Sigma}_2 \bar{\mathbf{Q}} \boldsymbol{\Sigma}_2 \bar{\mathbf{Q}}) \end{pmatrix} \in \mathbb{R}^{2 \times 2}, \quad (\text{A.31})$$

$$\tilde{\mathbf{A}} = \frac{1}{n} \begin{pmatrix} \frac{n_1}{(1 + \delta_1)^2} & 0 \\ 0 & \frac{n_2}{(1 + \delta_2)^2} \end{pmatrix} \in \mathbb{R}^{2 \times 2}, \quad (\text{A.32})$$

$$\bar{\mathbf{t}}^{(\ell)} = \frac{1}{n} [\text{Tr}(\mathbf{B} \bar{\mathbf{Q}} \boldsymbol{\Sigma}_1 \bar{\mathbf{Q}}), \text{Tr}(\mathbf{B} \bar{\mathbf{Q}} \boldsymbol{\Sigma}_2 \bar{\mathbf{Q}})]^\top \in \mathbb{R}^2, \quad (\text{A.33})$$

$$\mathbf{d}^{(\ell)} = [d_1^{(\ell)}, d_2^{(\ell)}]^\top = \left(\mathbf{I}_2 - \tilde{\mathbf{V}} \tilde{\mathbf{A}} \right)^{-1} \bar{\mathbf{t}}^{(\ell)} \in \mathbb{R}^2, \quad (\text{A.34})$$

$$\mathbf{K} = \bar{\mathbf{Q}} \mathbf{B} \bar{\mathbf{Q}} + \sum_{\ell'=1}^2 \frac{n_{\ell'}}{n} \frac{d_{\ell'}^{(\ell)}}{(1 + \delta_{\ell'})^2} \bar{\mathbf{Q}} \mathbf{C}_{\ell'} \bar{\mathbf{Q}}, \in \mathbb{R}^{d \times d}, \quad (\text{A.35})$$

$$\mathbf{V} = \mathcal{D}_{\mathbf{v}} \in \mathbb{R}^{n \times n}, \quad \mathbf{v} = \left[\frac{\text{Tr}(\boldsymbol{\Sigma}_1 \mathbf{K})}{(1 + \delta_1)^2} \mathbf{1}_{n_1}, \frac{\text{Tr}(\boldsymbol{\Sigma}_2 \mathbf{K})}{(1 + \delta_2)^2} \mathbf{1}_{n_2} \right] \in \mathbb{R}^n, \quad (\text{A.36})$$

$$\boldsymbol{\delta}' = (\delta'_1, \delta'_2) = \left(\frac{1}{n} \text{Tr}(\boldsymbol{\Sigma}_1 \mathbf{K}), \frac{1}{n} \text{Tr}(\boldsymbol{\Sigma}_2 \mathbf{K}) \right), \quad (\text{A.37})$$

$$\mathbf{M}_{\boldsymbol{\delta}'} = \left[\frac{\delta'_1}{(1 + \delta_1)^2} \boldsymbol{\mu}_1 \mid \frac{\delta'_2}{(1 + \delta_2)^2} \boldsymbol{\mu}_2 \right] \in \mathbb{R}^{d \times 2}. \quad (\text{A.38})$$

Note that while the variance computation uses the output of the fixed point iteration performed for the computation of the means μ_1 and μ_2 , namely $\bar{\mathbf{Q}} \in \mathbb{R}^{d \times d}$ and $\boldsymbol{\delta} = (\delta_1, \delta_2)$, the expressions

²The resolvent is defined for any $\lambda \in \mathbb{C}$ such that $\frac{1}{n} \mathbf{X} \mathbf{X}^\top + \lambda \mathbf{I}_p$ is invertible

from (A.27) and (A.28) are explicit, and similarly, all the terms from (A.31) to (A.38) required for the computation of (A.28) can be evaluated directly, provided $\bar{\mathbf{Q}} \in \mathbb{R}^{d \times d}$ and $\delta = (\delta_1, \delta_2)$ and the data statistics $\boldsymbol{\mu}_1, \boldsymbol{\mu}_2 \in \mathbb{R}^d$ as well as $\boldsymbol{\Sigma}_1, \boldsymbol{\Sigma}_2 \in \mathbb{R}^{d \times d}$. Let us point out that the matrix \mathbf{B} appears implicitly in the expressions (A.33) and (A.35); as discussed above, it is therefore difficult to rewrite the solution as $\mathbb{E}[\text{Tr}(\mathbf{B}\mathbf{M})] = \text{Tr}(\mathbf{B}\bar{\mathbf{M}})$, *i.e.*, it seems intractable to factorize the overall expression as $\mathbf{B}\bar{\mathbf{M}}$ in a way that we could read off the deterministic equivalent $\bar{\mathbf{M}}$.

Proof sketch. We obtain the deterministic equivalent (A.27) of $\mathbf{w}_{\text{ridge}}$ as follows (see also [Tiomoko et al., 2020, p. 42-50])

$$\begin{aligned} \mathbb{E}[\mathbf{w}_{\text{ridge}}^\top \mathbf{v}] &= \mathbb{E}\left[\mathbf{y}^\top \frac{\mathbf{X}^\top}{\sqrt{n}} \left(\frac{1}{n} \mathbf{X} \mathbf{X}^\top + \lambda \mathbf{I}_p\right)^{-1} \mathbf{v}\right] \\ &= \frac{1}{\sqrt{n}} \mathbb{E}_{\mathbf{X}} \left[\mathbf{y}^\top \mathbf{X}^\top \left(\frac{1}{n} \mathbf{X} \mathbf{X}^\top + \lambda \mathbf{I}_d\right)^{-1} \mathbf{v}\right] \\ &= \frac{1}{\sqrt{n}} \mathbb{E}_{\mathbf{X}} [\mathbf{y}^\top \mathbf{X}^\top \mathbf{Q} \mathbf{v}] \\ &= \frac{1}{\sqrt{n}} \mathbf{y}^\top \mathbf{J} \mathbf{M}_\delta^\top \bar{\mathbf{Q}} \mathbf{v}. \end{aligned}$$

Note that $\mathbf{y} = [-1, \dots, -1, 1, \dots, 1]^\top$ is simply considered a deterministic label vector. We can deduce that a deterministic equivalent for $\mathbf{w}_{\text{ridge}}$ is $\bar{\mathbf{w}}_{\text{ridge}} = \frac{1}{\sqrt{n}} \bar{\mathbf{Q}} \mathbf{M}_\delta \mathbf{J}^\top \mathbf{y}$. We compute

$$\begin{aligned} \mathbb{E} \text{Tr}[\mathbf{B} \mathbf{w}_{\text{ridge}} \mathbf{w}_{\text{ridge}}^\top] &= \frac{1}{n} \mathbb{E} \text{Tr} \left[\mathbf{B} \left(\frac{1}{n} \mathbf{X} \mathbf{X}^\top + \lambda \mathbf{I}_p\right)^{-1} \mathbf{X} \mathbf{y} \mathbf{y}^\top \mathbf{X}^\top \left(\frac{1}{n} \mathbf{X} \mathbf{X}^\top + \lambda \mathbf{I}_p\right)^{-1} \right] \\ &= \frac{1}{n} \mathbb{E} \mathbf{y}^\top \mathbf{X}^\top \left(\frac{1}{n} \mathbf{X} \mathbf{X}^\top + \lambda \mathbf{I}_p\right)^{-1} \mathbf{B} \left(\frac{1}{n} \mathbf{X} \mathbf{X}^\top + \lambda \mathbf{I}_p\right)^{-1} \mathbf{X} \mathbf{y} \\ &= \frac{1}{n} \mathbb{E} \mathbf{y}^\top \mathbf{X}^\top \mathbf{Q} \mathbf{B} \mathbf{Q} \mathbf{X} \mathbf{y} \\ &= \underbrace{\frac{1}{n} \mathbf{y}^\top \mathbf{J} \mathbf{M}_\delta^\top \mathbf{K} \mathbf{M}_\delta \mathbf{J}^\top \mathbf{y}}_{T_1} + \underbrace{\frac{1}{n} \mathbf{y}^\top \mathbf{V} \mathbf{y}}_{T_2} - 2 \underbrace{\frac{1}{n} \mathbf{y}^\top \mathbf{J} \mathbf{M}_\delta^\top \bar{\mathbf{Q}} \mathbf{M}_\delta \mathbf{J}^\top \mathbf{y}}_{T_3}, \quad (\text{A.39}) \end{aligned}$$

and refer to [Louart et al., 2018] as well as [Louart and Couillet, 2018] and [Tiomoko et al., 2020, p. 42-50] for more details. \square

In the context of CAVs, this result has two major applications in the context of our paper. Firstly, it allows to study the distribution of classification scores and the prediction of the classification accuracies as explained in Sec. 5. Secondly, it allows to study the variance (decay) of CAVs based on the *ridge regression* in the sense of Definition (2.5). We comment on this in the next paragraph.

Variability of Ridge-Regression-CAVs. We apply Definition (2.5) to analyze the variability of CAVs based on the ridge regression, using the above Theorem B.6 with $\mathbf{B} = \mathbf{I}$. We approximate

$$\text{Tr}(\text{Cov}(\mathbf{w}_{\text{ridge}})) \approx \mathbb{E}[\text{Tr}(\mathbf{w}_{\text{ridge}} \mathbf{w}_{\text{ridge}}^\top)] - \text{Tr}(\bar{\mathbf{w}}_{\text{ridge}} \bar{\mathbf{w}}_{\text{ridge}}^\top), \quad (\text{A.40})$$

where $\bar{\mathbf{w}}_{\text{ridge}} = \frac{1}{\sqrt{n}} \bar{\mathbf{Q}} \mathbf{M}_\delta \mathbf{J}^\top \mathbf{y}$ is the deterministic equivalent (A.27). We consider the high-dimensional regime where the number of concept samples n_2 is fixed, while the number of non-concept samples $n_1 \rightarrow \infty$ and $d \rightarrow \infty$. Note that, in the case of identity covariance ($\mathbf{C}_1 = \mathbf{C}_2 = \mathbf{I}_d$), we have $\bar{\mathbf{Q}} = \bar{q} \mathbf{I}_d$ for $\bar{\mathbf{Q}}$ from (A.29), and $\delta_1 = \delta_2 = \delta$. We obtain the self-consistent equations

$$\bar{q} = \left(\frac{1}{1+\delta} + \lambda\right)^{-1}, \quad \delta = \frac{d}{n} \bar{q} \quad (\text{A.41})$$

As $n_1 \rightarrow \infty$, we have $n = n_1 + n_2 \approx n_1$. If d scales linearly with n_1 , then \bar{q} and δ converge to $\mathcal{O}(1)$ constants. For the auxiliary matrix \mathbf{K} (recall (A.35), and $\mathbf{B} = \mathbf{I}$) which captures noise propagation

$$\text{Tr}(\mathbf{K}) = \mathcal{O}\left(\frac{d}{n}\right) = \mathcal{O}\left(\frac{d}{n_1}\right). \quad (\text{A.42})$$

To find the variance, we subtract the squared deterministic mean from the second moment terms T_1, T_2, T_3 defined in (A.39). Further, assuming $\boldsymbol{\mu}_1 = -\boldsymbol{\mu}_2 = \mathbf{e}_1$, where \mathbf{e}_1 denotes the 1st standard basis vector, we analyze the scaling of the individual terms.

- *Mean Subtraction:* The term $\text{Tr}(\bar{\mathbf{w}}_{\text{ridge}} \bar{\mathbf{w}}_{\text{ridge}}^\top) = \frac{1}{n} \mathbf{y}^\top \mathbf{J} \mathbf{M}_\delta^\top \bar{\mathbf{Q}}^2 \mathbf{M}_\delta \mathbf{J}^\top \mathbf{y}$ scales as $\mathcal{O}(d/n_1)$.
- *Term T_2 :* This term $\frac{1}{n} \mathbf{y}^\top \mathbf{V} \mathbf{y}$ represents the pure variance contribution. Since $\text{Tr}(\mathbf{V})$ involves $\text{Tr}(\mathbf{K})$, it scales as $\mathcal{O}(d)$.
- *Cancellation of the terms T_1 and T_3 :* The leading $\mathcal{O}(d)$ components of the alignment terms T_1 and T_3 effectively cancel with the deterministic mean components when considering the generalized covariance, leaving the fluctuation terms as the dominant contribution.

Combining the terms T_1, T_2, T_3 in (A.39) with the leading factor $1/n$, the expression (A.40) scales as

$$\mathbb{E} \text{Tr}(\text{Cov}(\mathbf{w}_{\text{ridge}})) = \frac{1}{n} [\mathcal{O}(d)] = \mathcal{O}\left(\frac{d}{n_1}\right) \quad (\text{A.43})$$

As $n_1 \rightarrow \infty$, adding non-concept data reduces the variance of the CAV at a rate inversely proportional to the number of non-concept samples. As a connection to the classical regime, it is important to note the behavior of this result in lower dimensions. In the classical regime where the dimensionality d is fixed ($d = \mathcal{O}(1)$) and $n_1 \rightarrow \infty$, our result recovers the standard statistical convergence rate

$$\mathbb{E} \text{Tr}(\text{Cov}(\mathbf{w}_{\text{ridge}})) = \mathcal{O}\left(\frac{1}{n_1}\right) \quad (\text{A.44})$$

This confirms that the high-dimensional result $\mathcal{O}(d/n_1)$ is a natural generalization; in high dimensions, the "effective noise" grows with d , requiring a proportional increase in n_1 to maintain the same level of directional stability for the CAV.

Limitations and Gaussian Universality While our theoretical framework effectively leverages the Gaussian universality of the decision score $g(\mathbf{x})$ —providing a robust approximation that aligns well with our empirical observations (see Section C for accurate prediction of both the distribution of the decision score and the corresponding classification accuracy), we acknowledge that this property may not be exact in all high-dimensional regimes. Recent studies have characterized specific conditions under which this universality breaks down, suggesting that the score distribution may instead be better described as a convolution between a Gaussian and an auxiliary distribution. In particular, [Yaakoubi et al., 2026, Xiaoyi and Liao, 2025] highlight these nuances in the context of high-dimensional empirical risk minimization and linear factor models. Although our current Gaussian-based results provide a highly satisfactory description of the classification accuracy for the synthetic and real-world data tested, incorporating these more precise distributional results remains a valuable direction for future work to further refine the alignment between theory and experiment in edge-case scenarios.